UM-HSRI-77-39-2

WHOLE BODY RESPONSE RESEARCH PROGRAM

Appendix A: Methodology

N. M. Alem
J. B. Benson
G. L. Holstein
J. W. Melvin

FINAL REPORT
APRIL 1978

THE UNIVERSITY OF MICHIGAN
HIGHWAY SAFETY RESEARCH INSTITUTE

Technical Report Documentation Page

1. Report No.	2. Government Accession No.	3. Recipient's Catalog No.
UM-HSRI-77-39-2		

4. Title and Subtitle	5. Report Date
Whole Body Response Research Program Appendix A: Methedology	April 25, 1978
	6. Performing Organization Code
	8. Performing Organization Report No.
7. Author(s)	UM-HSRI-77-39-2
N.M. Alem, J.B. Benson, G.L. Holstein, J.W. Melvin	
9. Performing Organization Name and Address	10. Work Unit No. (TRAIS)
Highway Safety Research Institue The University of Michigan Huron Parkway and Baxter Road Ann Arbor, Michigan, 48109	320316
	11. Contract or Grant No.
	77-375-KB1
	13. Type of Report and Period Covered
12. Sponsoring Agency Name and Address	Final 7-1-73 to 8-31-77
General Motors Research Laboratories GM Tech Center 12 Mile and Mound Roads Warren, Michigan 48042	14. Sponsoring Agency Code

15. Supplementary Notes

16. Abstract

The general objective of this program was to generate data on the kinematics and response of human surrogates in a realistic automobile impact environment. The program used a test configuration consisting of an idealized hard seat representation of a car seat with a three-point harness restraint system. Three different severity levels of crash test conditions were used. The human surrogates tested in this program were fifteen male cadavers, a Hybrid II (Part 572) Anthropomorphic Test Device and a Hybrid III ATD recently developed by GM. In addition, mathematical simulations of the response and kinematics of a 50th percentile male occupant were performed at the three levels of crash severity, using the MVMA Two-Dimensional Crash Victim Simulator. The data that has been produced by this program represents one of the most comprehensive and extensive documentations of whole-body response to date. The primary utility of the data is for comparing the similarities and differences in response and kinematics of the various types of human surrogates and in pointing out areas that need improvement in both anthropomorphic test devices and mathematical models.

17. Key Words	18. Distribution Statement
Whole-Body Kinematics; Cadaver Anthropometry; 3-D Motion; X-Ray Measurements; Head Injury Criterion; Digital Filtering & Processing.	Unlimited

19. Security Classif. (of this report)	20. Security Classif. (of this page)	21. No. of Pages	22. Price
Unclassified	Unclassified	108	

(APPENDIX A)
TABLE OF CONTENTS

(APPENDIX A)
TABLE OF CONTENTS
(CONTINUED)

EXPERIMENTAL PROCEDURES

J. R. Benson & N. M. Alem

Each Whole Body Response test was conducted following certain procedures which were developed during the early phases of the program. As the program progressed, more efficient procedures and methods were established and the protocol was refined accordingly.

The following sections describe the protocol of conducting a WBR test. Though it is oriented to tests using human cadavers, this protocol applies as well to the anthropometric test devices (dummies) used in the research program. The sequence of tasks includes the design of the experiment, subject and sled preparation, conducting the test and finally, performing a post-test examination.

Design Of Experiment

The test configuration for all WBR tests is shown in Figure 1. The subject, which approximates 50th percentile male, was seated for a frontal impact in a GM-supplied test fixture and was restrained by a three-point belt system instrumented with load transducers in a driver's side configuration. Every attempt was made to comply with the requirements desribed in the diagram.

Three levels of impact severity were used in the WBR program. The low-severity tests corresponded to 16.5-mph sled velocity change, and to a 10-g constant deceleration level. The intermediate-severity tests had twice the kinetic energy of the low-severity ones, which corresponds to 23.3 mph velocity change and 10 g deceleration level. Finally, the kinetic energy of the mid-severity tests was doubled for the high-severity tests, by adjusting the velocity change to 33 mph and the sled deceleration level to 20 g's. Typical sled pulses for these three severities are given in Figure 2.

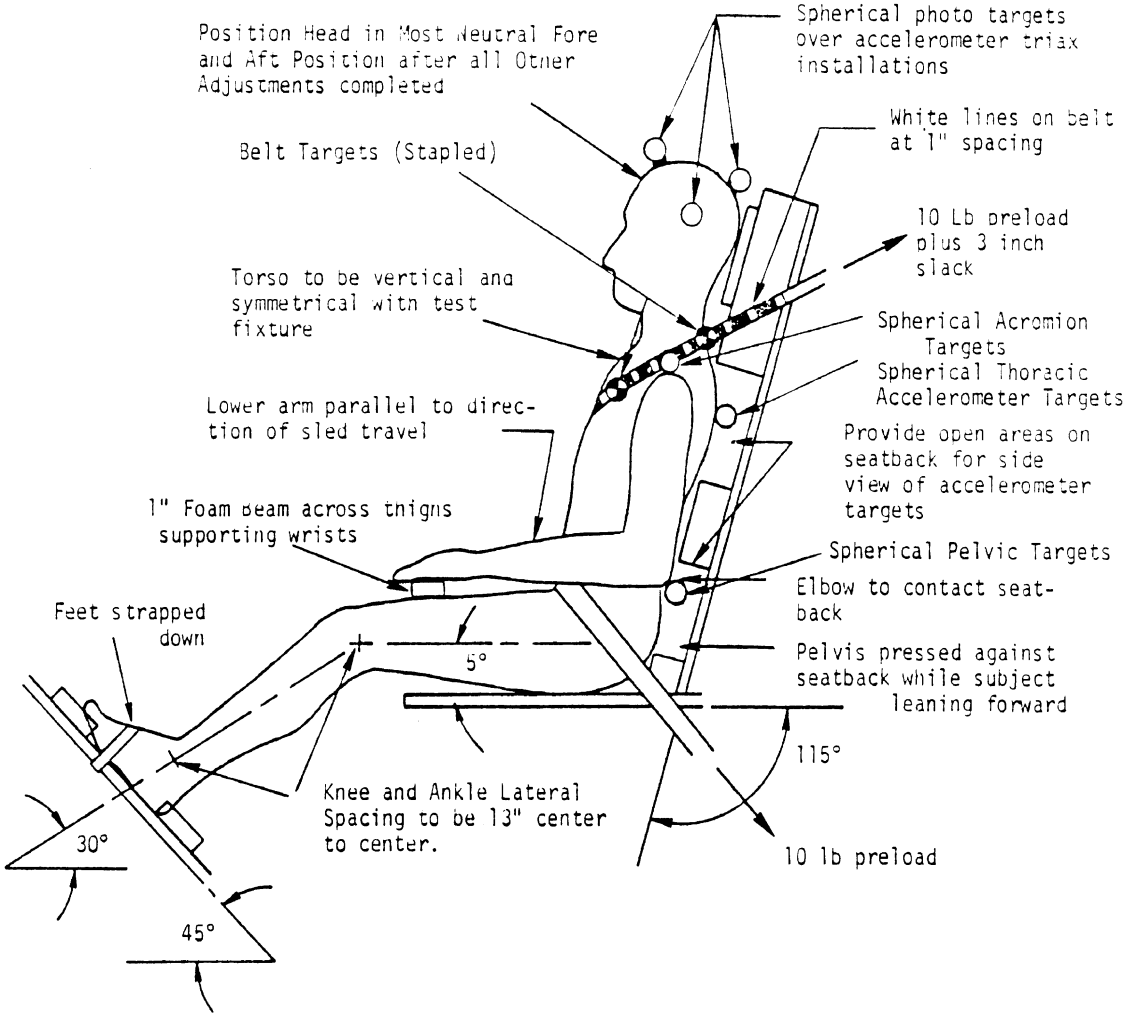

FIGURE 1. SEATING, RESTRAINTS AND TARGETING DIAGRAM FOR ALL WBR TESTS.

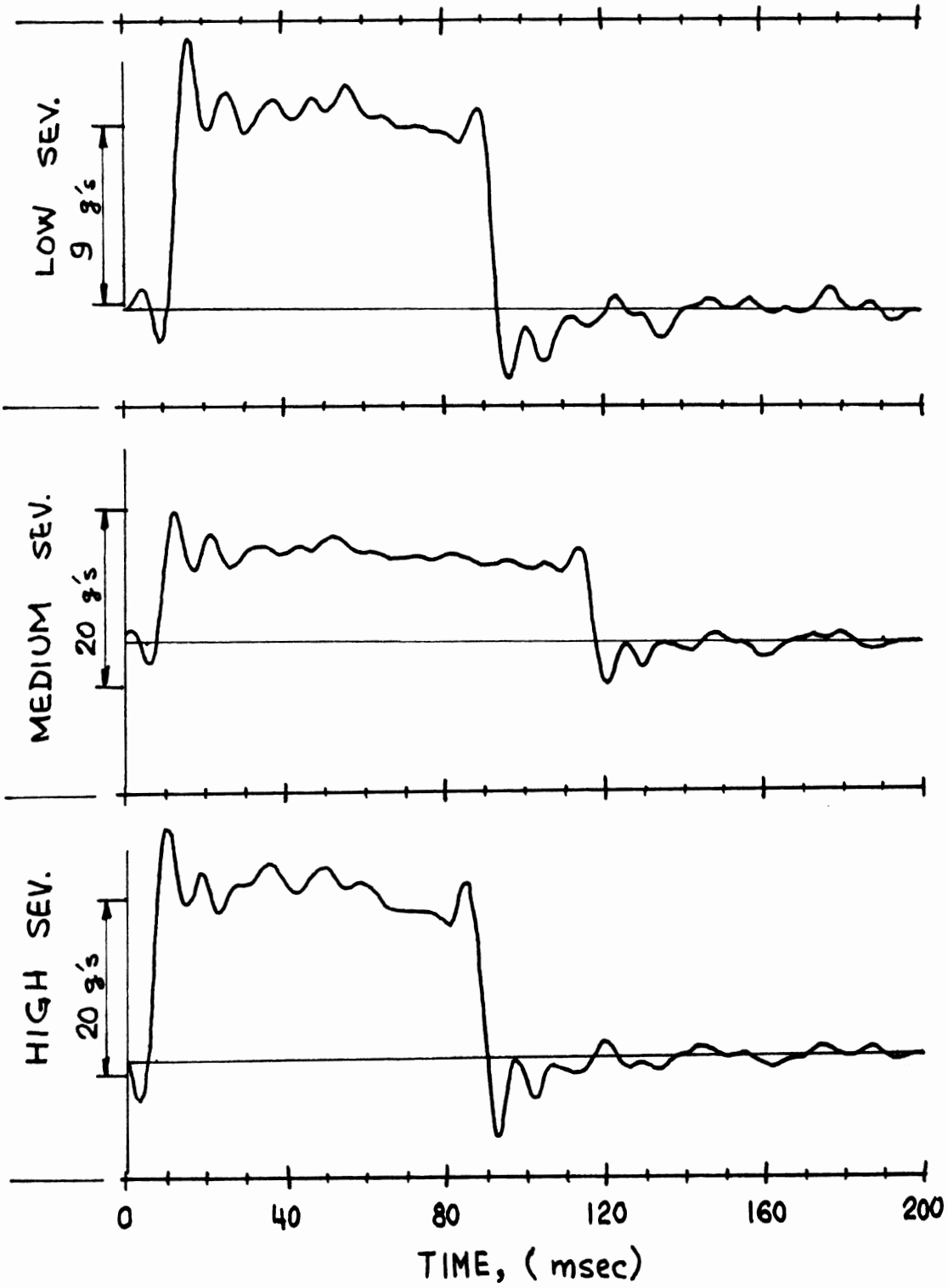

FIGURE 2. TYPICAL LOW, INTERMEDIATE AND HIGH SEVERITY SLED DECELERATION PULSES.

Once a cadaver became available from the U-M Anatomy Department, its suitability for a WBR run was investigated; thus, only subjects approximating 50th percentile male were selected, and only if the integrity of the skeletal structure would result in realistic whole body kinematic response in the 3-point belt tests being conducted. Most of the cadavers tested were unembalmed, since embalming is known to affect human tissue.

With the availabilty and suitability of a subject established, the test severity level was selected next, in consultation with GMRL Biosciences Department personnel. The purpose of this procedure was to ensure an even distribution of good data, by examining results from previous tests and considering the overall objectives of the Whole Body Response Research program.

Subject Preparation

The procedure is initiated by a call from the Anatomy Department to notify HSRI that a suitable cadaver is available. Three HSRI personnel would then bring the subject to the Biomedical Laboratory for preparation. This includes the following tasks:

- Obtain the subject medical history and current weight.
- Sanitarily prepare the cadaver by closing all body openings.
- Obtain all anthropometric measurements.
- Install 3 mounts on the skull for the 9-accelerometer package and record fixture dimensions. The fixture shown in Figure 3, is used to locate and align the three mounts shown in figure 4.
- Install thoracic and pelvic accelelerometer mounts shown in Figures 5 and 6.
- Remove head fixture when acrylic is set. Install lead pellets as x-ray targets on 3 triaxial mounts and 4 anatomical landmarks.

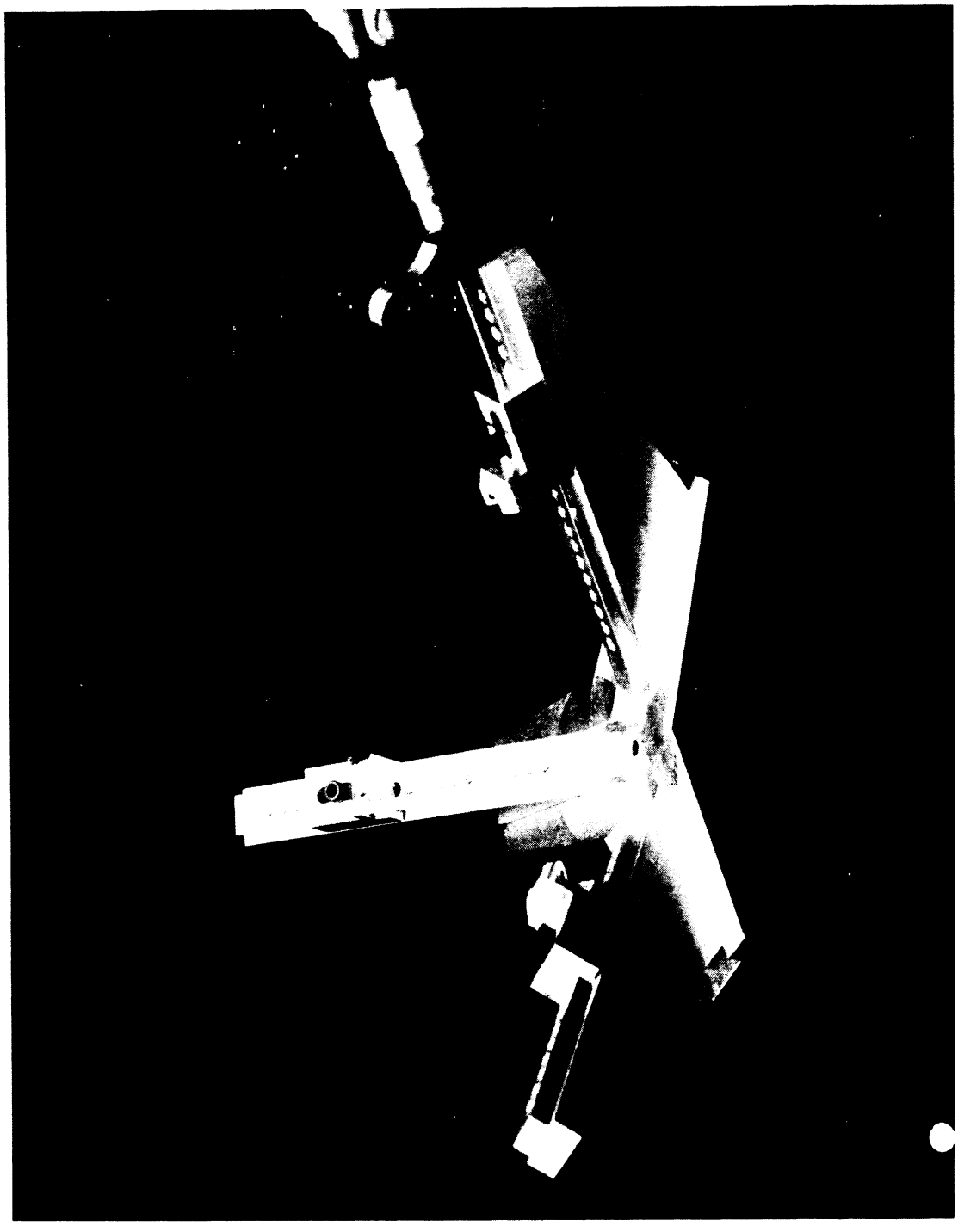

FIGURE 3. FIXTURE FOR LOCATING AND ALIGNING THE THREE HEAD TRIAXIAL MOUNTS.

FIGURE 4. THREE TRIAXIAL MOUNTS RIGIDLY ATTACHED TO THE SKULL.

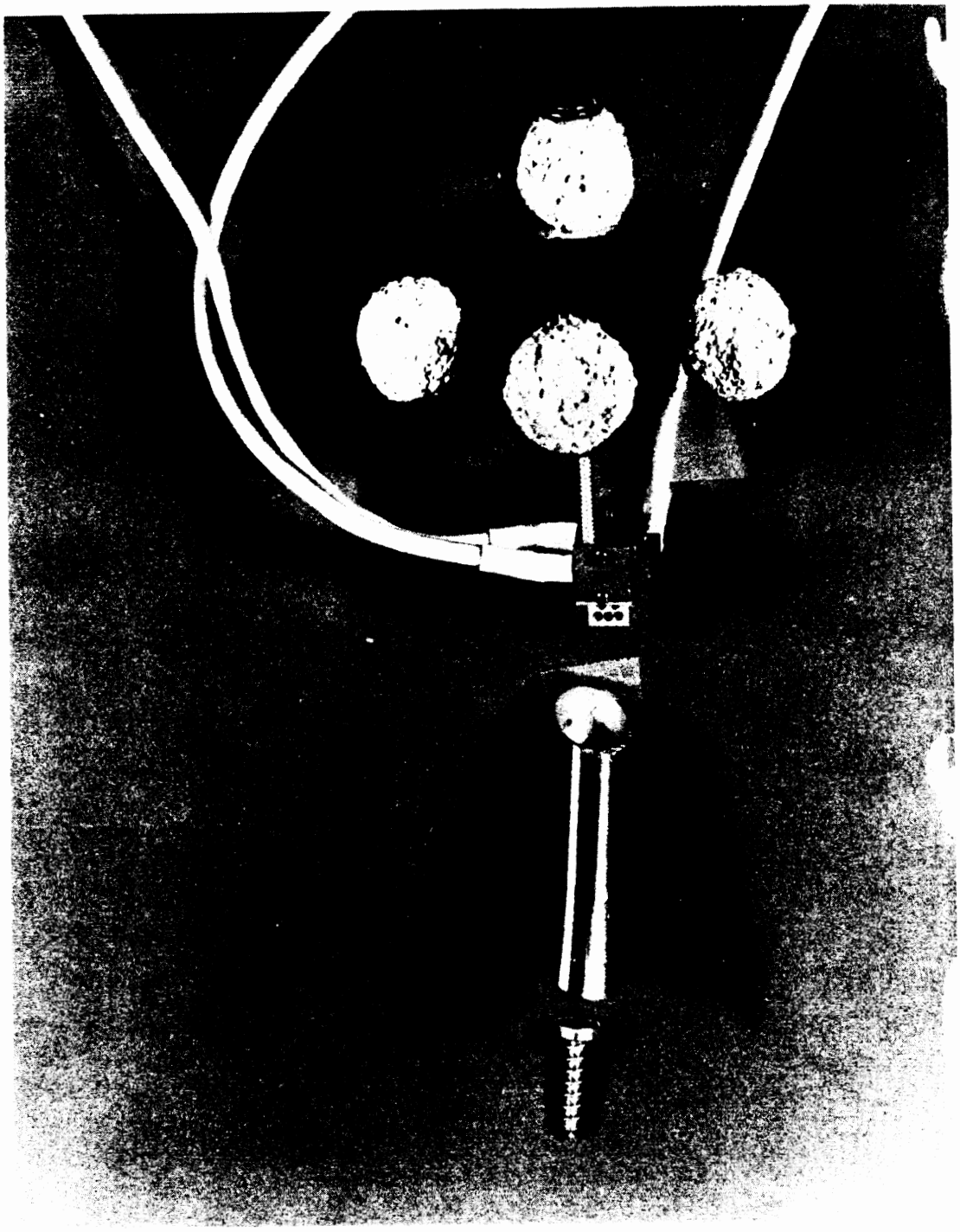

FIGURE 5. THORACIC ACCELEROMETER MOUNT.

FIGURE 6. PELVIC ACCELEROMETER MOUNT.

EXPERIMENTAL PROCEDURES

► Place cadaver in wood mock-seat for x-raying, and tape securely in position. Rotate the x-ray table to a vertical position.

► Obtain two orthogonal x-rays of the head showing seven pellets on each, and record approximate table-targets distances.

► Obtain overlaping lateral whole body x-rays in mock seat with scaling targets alongside.

► Rotate the x-ray table to a horizontal position, and place cadaver on table in prone position.

► Obtain overlaping frontal whole body x-rays with scaling ragets alongside.

► Return cadaver to cooler for overnight storage; clean surgery and x-ray areas.

► Next morning, remove cadaver from cooler and place on surgery table for final preparation.

► Dress cadaver in vinyl sweat suit then in cotton underwear. Spray areas between skin, vinyl and cotton surfaces with Scotch adhesive spray to increase friction.

► Place socks and gloves on cadaver and tape securely to underwear. Place hood over cadaver's head and stitch to underwear.

► Place prepared cadaver on gurney and take to sled lab for testing.

Sled Preparation

The preparation of the HSRI sled (Figure 7) for a WBR test is carried out simultaneously with cadaver preparation. The tasks involved are listed below in the general order in which they are accomplished:

► Place the WBR seating buck (GM-supplied) on the HSRI sled.

► Install alignment blocks on the sled and push the buck agianst them. Fasten buck securely to sled.

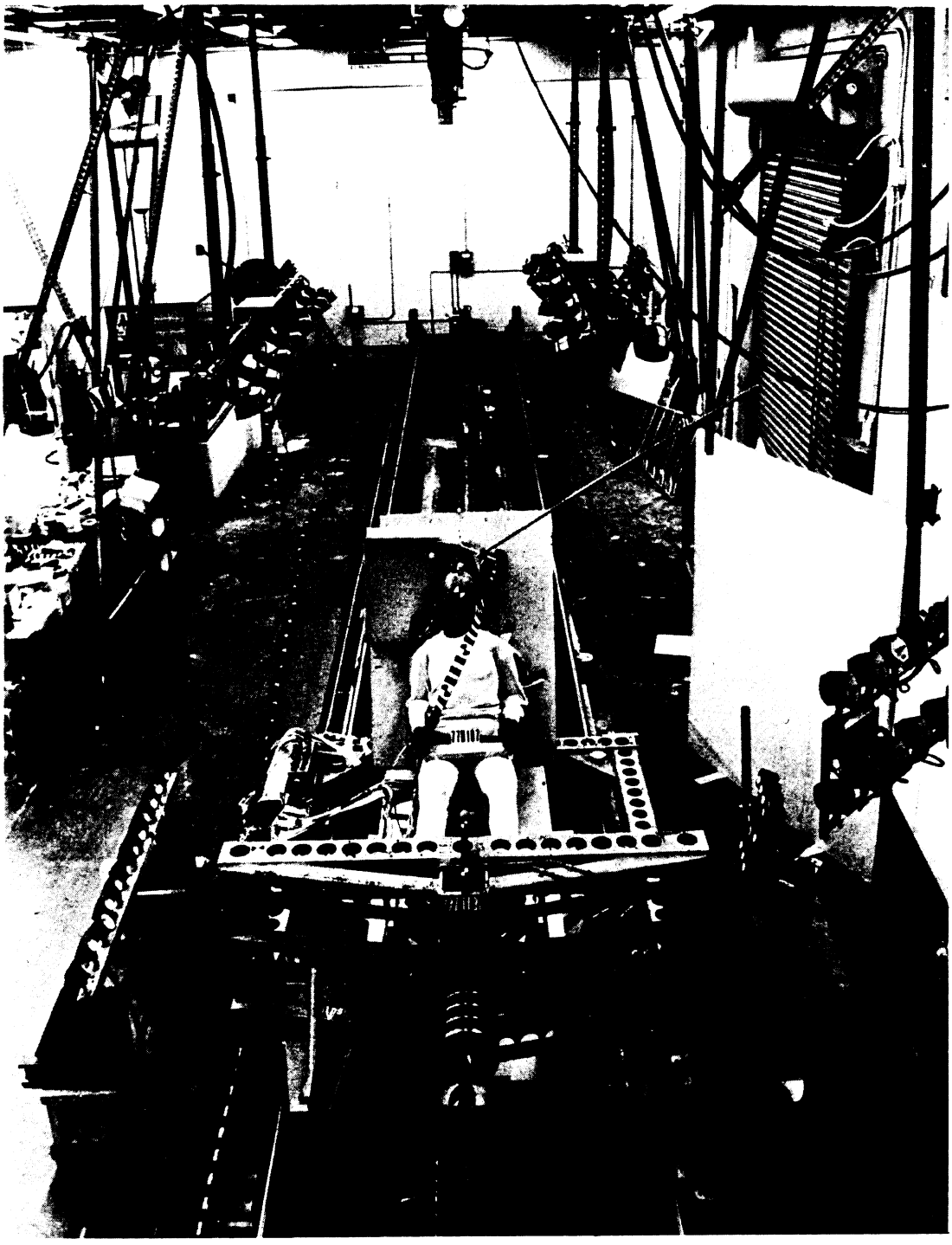

FIGURE 7. HSRI IMPACT SLED FACILITY.

EXPERIMENTAL PROCEDURES

►Prepare the belts by painting white stripes on shoulder belt, assembling the buckles, and setting the belt lengths with a 10-lb load applied. Install prepared belts on the WBR buck and anchor properly.

►Check the availability of thoracic, pelvic, acromion and femur photographic targets, and fabricate any required targets. These are shown in Figures 8, 9, 10 and 11.

►Move sled to programmer's T-zero position to check photographic coverage. Align overhead reference; position, aim and focus the high-speed cameras; install reference and scaling targets on front of sled; finally, install run identification number on front, top and sides of sled.

►Install airway pressurization tank and tubing on sled.

Instrumentation Preparation

This includes preparation of transducers, amplifiers and recording equipment to be used in the test. The tasks to be accomplished during this phase are:

►Prepare the instrumentation data sheet by assigning the variables to be recorded to specific transducers and tape channels.

►Assemble accelerometors on mounting blocks to make three head triaxial, one thoracic triaxial and one pelvic biaxial assemblies.

►Check polarities of accelerometers. Assign positive sensitivity if acceleration in a given anatomical direction produces a positive output; otherwise, assign a negative sensitivity.

►Plug all transducers into assigned channels on sled patch panel. Connect sled patch pannel to assigned amplifiers. Turn amplifiers on.

►Adjust all transducers to correct excitations. Select aplifiers correct gains. Check and adjust all transducers for zero balance.

►Connect amplifiers outputs to Visicorder. Check visually response of all transducers to input. Repair or replace defective or malfunctionning transducers.

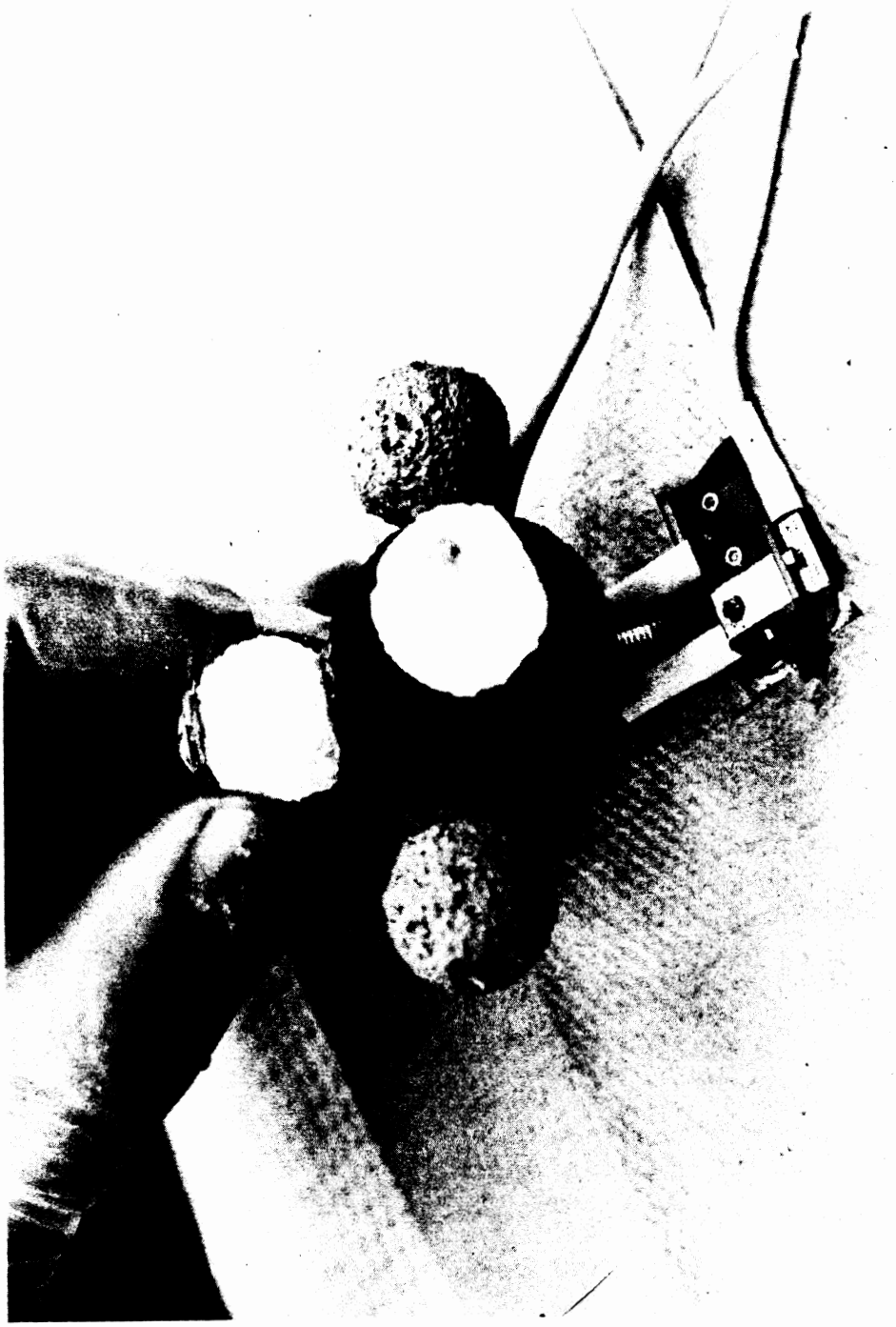

FIGURE 8. THORACIC PHOTOGRAPHIC TARGETING.

EXPERIMENTAL PROCEDURES

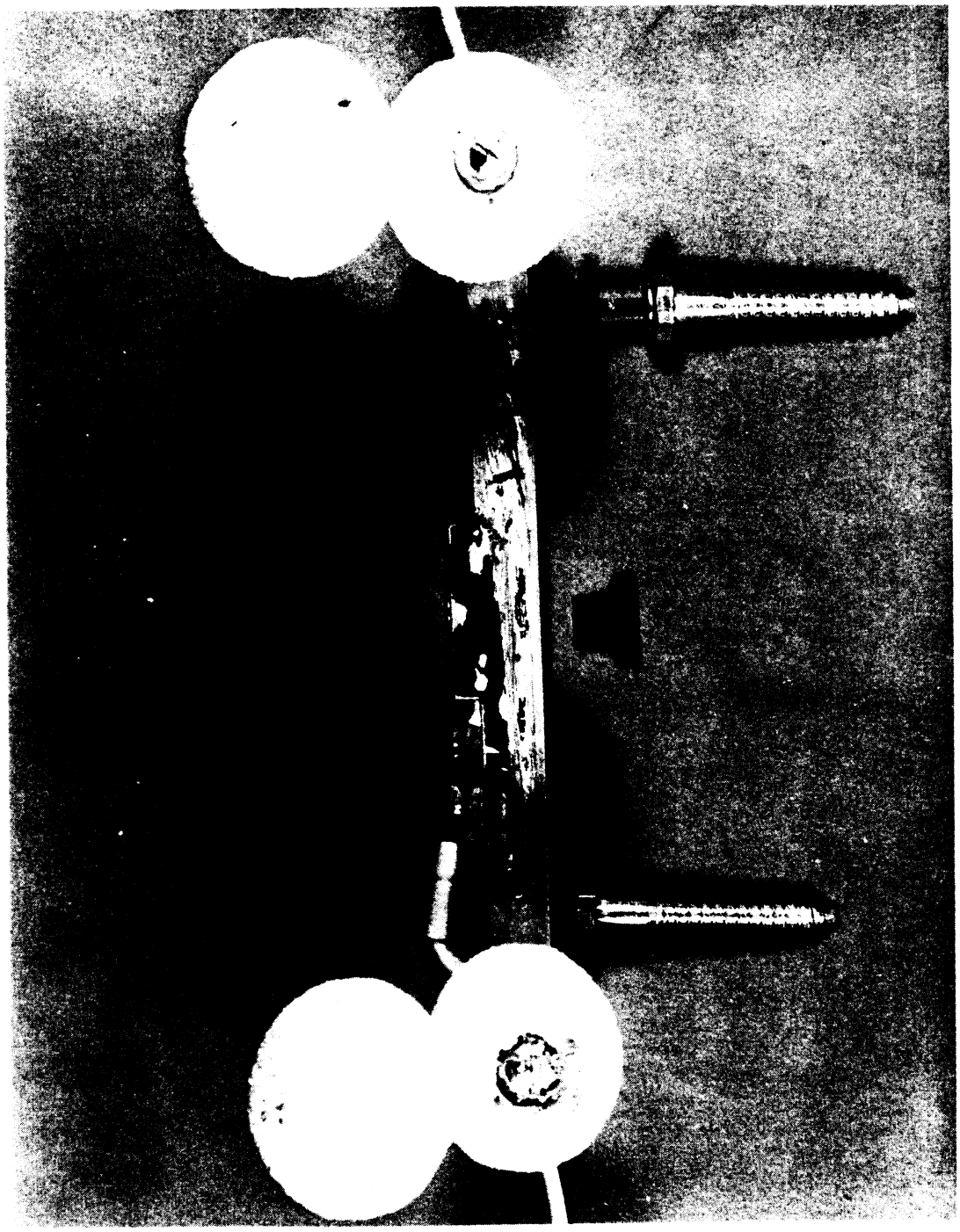

FIGURE 9. PELVIC PHOTOGRAPHIC TARGETING.

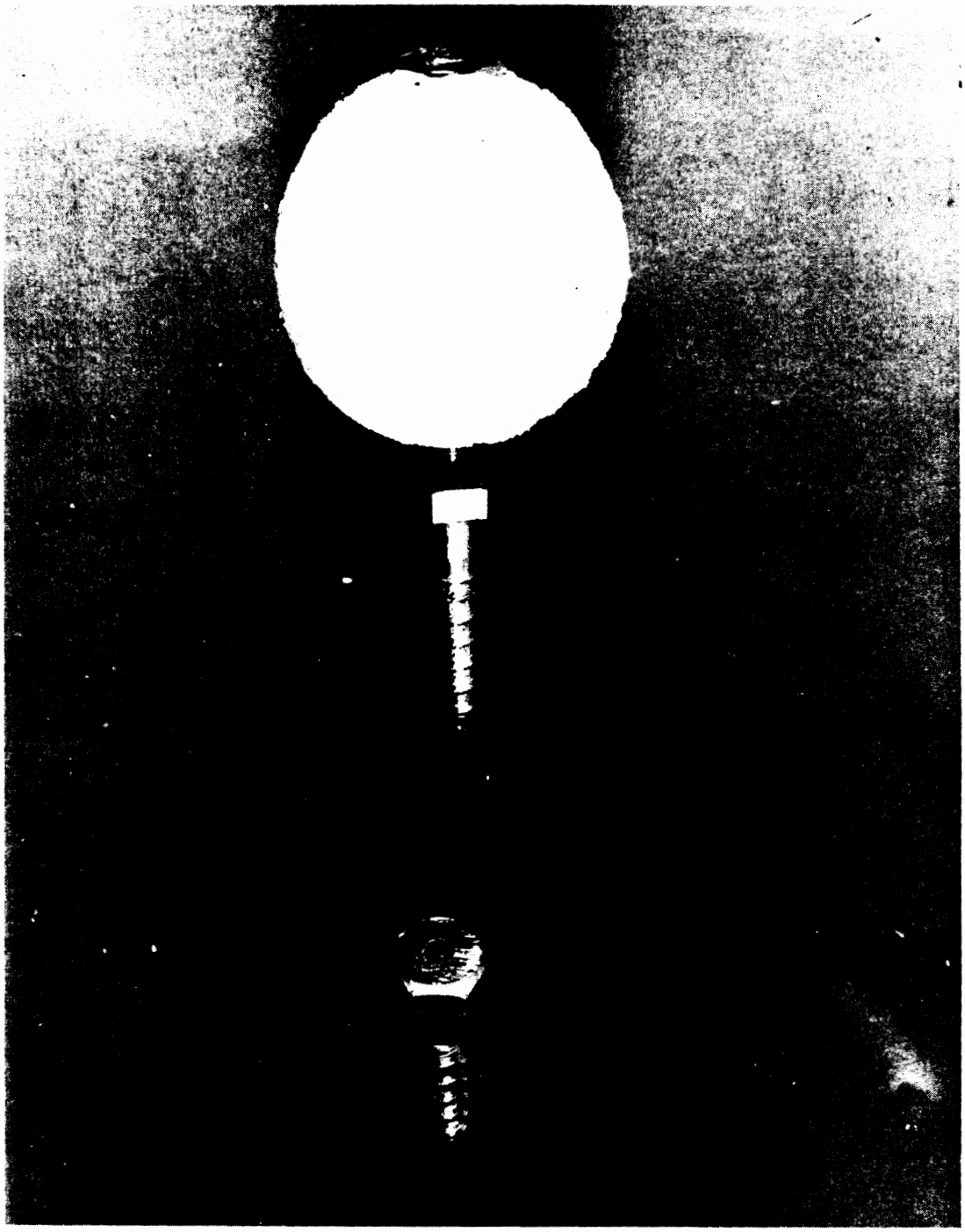

FIGURE 1Ø. COMPONENTS OF ACROMION PHOTO-TARGET.

EXPERIMENTAL PROCEDURES

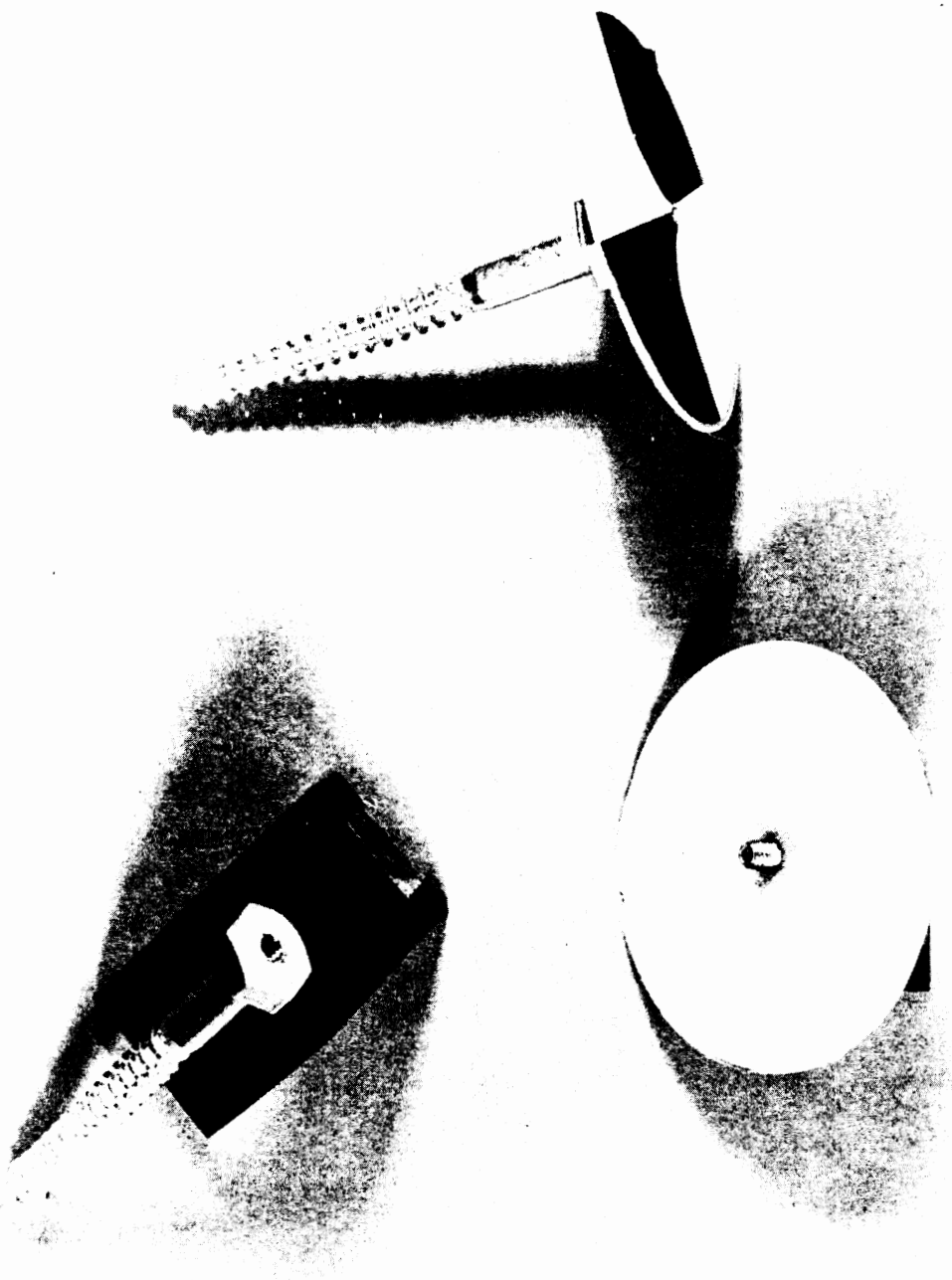

FIGURE 11. COMPONENTS OF FEMUR PHOTO-TARGET.

►Connect amplifiers, velocity transducer, digital gate and time base outputs to input ports of assigned tape channels.

►Install tape reels on recorders and index them just beyond previous test. Program digital gate to desired gate duration. Set time base frequency to 1000 Hz.

►Compute gross weight of sled. Calculate sled accelerator and programmer pressures. Determine and adjust delay settings of test sequencing control relays.

Run Sequence

Once all preparations have been concluded, the actual test may be initiated. The pre-test activities are carried out on and off the sled. The on-sled final activities are:

►Lift cadaver from gurney with overhead crane. While suspended, install thoracic and pelvic accelerometer assemblies and the corresponding photographic targets.

►Lower cadaver onto seat of WBR buck and attach lap and shoulder belts to hold him in place.

► Install three head triaxial accelerometers at their assigned mounts. Route and strain-relieve transducer cables.

► Install acromion and femur targets. Loop a string around legs to maintain a 13-inch separation between centers of knees. Staple 3 photo-targets to upper striped section of shoulder belt. Attach head accelerometer photo-targets, if specified.

►Tension lap belt to 10-lb preload. Adjust back support to clear thoracic transducer mount. Push cadaver against back support. Tension soulder belt to 10 lbs preload. Carefully position cadaver in position against seat back using two single strips of 1/2-inch masking tape, one across chest and one across head. Place 1/2-inch thich styrofoam board on top of cadaver's thighs to support wrists.

►Recheck the 10-lb preloads on lap and shoulder belts. Measure and record anchor orientations.

► Push sled to programmer's T-zero position for final check. Final focus and aim cameras. Take pre-test setup photographs.

► Push sled down to accelerator. Adjust programmer to specified pressure from nitrogen tanks.

►Using duct tape, secure shoulder belt tensionning rod in tensionned postion. Introduce slack in shoulder belt by backing off tensionning nut a 3-inch distance along the rod. Place small cut in the tape to facilitate release of shoulder belt slack under impact.

► Using a paper punch, punch a round hole in each strip of masking tape holding cadaver head and chest to seat back. Recheck the cadaver positionning and inspect sled to ensure all tools and loose items have been removed.

This completes the on-sled activities, after which the test setup is not disturbed until impact time. The final steps taken before the actual firing of the sled consist of the following off-sled activities:

►Check, and adjust if necessary, amplifiers settings and zero balances. Record about one minute of zero-level signals on analog tape. Turn sled patch panel switch to "CAL" position, and tape-record about 1 minute of transducer calibration signals. Return patch panel switch to "RUN" position. Turn on the time base unit.

►Charge sled brake system to specified pressure. Attach winch cable to sled. Engage sled to accelerator piston. Open accelerator piston air bleed valve. Winch sled back into launch position. Remove winch cable from sled. Install trip wires.

►Finally, close accelerator piston bleed valve. Check programmer and accelerator pressures. Initiate launch sequence.

After the sled comes to a complete stop, the test crew examines all transducers and their cables for apparent damages. Post-test photographs are then taken. Using the visicorder, a quick look is taken at the recorded signals to note any failures. Finally, all cables and transducers are disengaged from thhe cadaver, which is then taken to the surgery room for autopsy and x-rays.

The cadaver post-test examination concludes the actual test, and the job of analyzing all test records begins.

DIGITAL SIGNAL PROCESSING

N. M. Alem

Introduction

The complexity of experimental measurements in biomechanics research has become so great, that an equally sophisticated signal processing system is required to handle the resulting analog signals.

With the availability of digital computers, this task is greatly simplified. First, analog signals are converted to digital ones, which are then digitally filtered and prepared for presentation and/or analysis.

The HSRI signal processing package is described in the following pages. It comprises two seperate phases: the analog-to-digital (A-D) conversion phase, and the digital filtering phase. Currently, the HSRI system is capable of A-D sampling rates from 400 to 25600 Hertz, and of lowpass digital filtering cutoff frequencies from 20 to 9120 Hertz. With this operating range, a wide variety of signals can be handled, from impact data lasting few milliseconds and containing frequencies as high as several kHz, to non-impact data lasting several hundred milliseconds, and in which only frequencies as low as 50 Hz would be kept.

Analog-to-Digital Conversion

The first operation in signal processing is to convert all analog signals into digital form. In general, the electrical transducer signals are tape-recorded , and the A-D process is carried out after the test has been conducted by playing the tape back into the A-D unit, which is cont-

rolled by a digital computer.

It is necessary, therefore, to study carefully the parameters of the test in order to define the recording and playback tape speeds that will results in the desired frequency contents and sampling rates. Since the analog signals contain, in general, frequencies higher than the sampling rate, aliasing errors may result. To eliminate these errors, the analog signals are electronically filtered before they are digitized, by passing them through lowpass analog filters, designed specifically for this purpose.

The Sampling Process

The operation of sampling may be viewed as a form of impulse modulation. Accordingly, if an analog signal x(t) is sampled at equal time intervals of T seconds, then, the sampled signal $x^*(t)$ may be represented as a train of impulses, given by

$$x^*(t) = T \sum_{n=0}^{\infty} x(nt)\delta(t-nT)$$

where

$$x(t) = 0 \quad \text{for } t < 0$$

$$\delta(t) = \begin{cases} 1 & \text{for } t = nT \\ 0 & \text{for } t \neq nT \end{cases}$$

The digital signal $x^*(t)$ is not continuous in time, but a sequence of numbers taken as the values of x(t) at t=nT. The inverse of the sampling interval, 1/T, is called the sampling rate, usually given in Hertz.

To recover the original continuous x(t), the digital signal $x^*(t)$ is passed through an ideal lowpass filter of bandwidth equal to half the sampling rate. The recovery is exact if, and only if, the Fourier transform of the continuous x(t) is identically zero outside the central strip of plus or minus half the sampling rate. This band is known as the Nyquist band, and half the sampling rate is known as the Nyquist frequency.

The exact recovery is guaranteed by the sampling theorem, which states that as long as the sampling rate is

at least twice the highest frequency contained in the continuous signal, its recovery from the digitized signal will be exact. The implication of this theorem is that if we sample at the rate 1/T, sufficiently higher than the Nyquist frequency, then we can retrieve the original signal by using the ideal interpolation operator, which has the impulse response

$$p(t,n) = \frac{\sin\left[\frac{\pi}{T}(t-nT)\right]}{\frac{\pi}{T}(t-nT)}$$

Then, the recovered signal $x^{\circ}(t)$ is given by

$$x^{\circ}(t) = \sum_{n=0}^{\infty} x^{*}(nT)\, p(t,n)$$

Again, $x^{\circ}(t)$ will be identical to $x(t)$ if the analog signal is band-limited to the Nyquist band. To guarantee this, the analog signal must be electronically filtered, prior to the A-D process, to eliminate all frequencies above the Nyquist rate. If pre-conversion filters were not used, aliased frequencies may be contained in the digitized signals, and the recovery would not be exact.

The A-D conversion unit at HSRI digitizes 14 channels simultaneously, with 10-bit full scale resolution. Thus, a 5-volt signal is converted to the number 1024 or 2^{10}, which corresponds to about 5 millivolts resolution of the analog signal. It is felt that the resulting accuracy is sufficient, since most transducers and amplifiers cannot be adjusted to better than this amount.

Anti-Aliasing Filters

The sampling rates, required in biomechanics research, vary with the types of signals being generated. To provide full flexibility in a signal processing system, variable-rate A-D units and variable analog filters must be used for anti-aliasing.

The same flexibilty is provided by time-expansion of the recorded analog signals, that is, by recording the signals at one tape speed, and playing them back at another. Thus the desired sampling rate is obtained by manipulating the tape speeds, while using a fixed-rate A-D sampling and

fixed-frequency anaolg filters.

The tape speeds on most IRIG tape recorders range from 1-7/8 to 120 inches per second (IPS), allowing time expansions and reductions of 2, 4, 8, 16, 32 and 64 times the original signals. The fixed sampling rate of the HSRI A-D conversion unit was selected at 400 Hz, so that time expansions would result in equivalent sampling rates of 800, 1600, 3200, 6400, 12800 and 25600 Hz.

Since the sampling rate of the A-D unit is fixed at 400 Hz, the anti-aliasing analog filters must also have fixed cutoff frequencies, so that all frequencies above the Nyquist rate of 200 Hz are practically eliminated. The design of these active low-pass filters must therefore be based on the 200 Hz, and must take into account the slow rolloff of the gain at the corner, which is typical of all analog filters.

The anti-aliasing filter chosen at HSRI is the Burr-Brown 5707-LP4L-1000 low-pass active filter. This a linear phase (Bessel), 4-pole (-24 dB/octave) filter, with corner frequency at 100 Hz. The log-magnitude versus frequency response curve for this filter is shown in Figure 1. The choice of a Bessel filter was based on the desire to have a linear relationship between the phases of the input and output signals. Furthermore, the corner frequency of 100 Hz, which corresponds, in a 4-pole Bessel filter, to an attenuation of 24 dB at the desired Nyquist rate of 200 Hz, also corresponds to an attenuation of 3 dB at 67 Hz, with flat response (0.5 dB) up to only 33 Hz. This means that, for this filter, the acceptable passband is 0-33 hz and the stopband's low edge is 200 Hz, with a transition band of 33-200 Hz. Sharp-corner digital filters may be used to eliminate frequencies in the transition band. The result is an effective digitizing and filtering scheme.

A bank of 14 of these Burr-Brown filters are used at HSRI as anti-aliasing filters. The 14-channel tape output is passed through this bank before it is transmitted to the A-D unit. Tape speed reductions are used to time-expand the signals, thereby increasing the sampling rate and the corresponding passband. With the use of these filters, the digital signals are guaranteed to have no significant aliasing errors.

The A-D conversion computer program, developped at HSRI, digitizes 14 channels simultaneously, and produces a file on digital tape which contains all 14 channels in raw

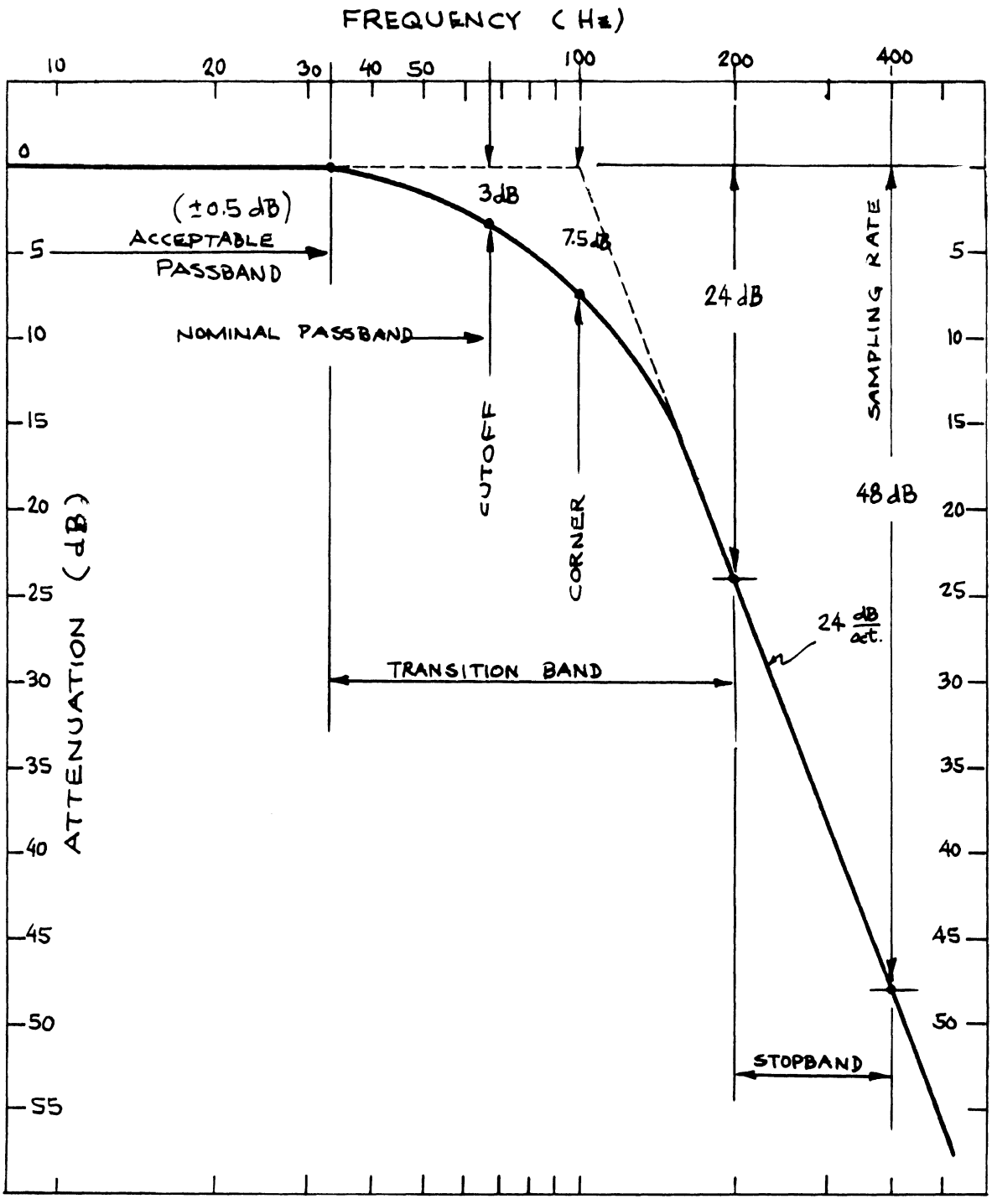

FIGURE 1. GAIN-FREQUENCY RESPONSE OF THE BURR-BROWN 5707-LP4L-1000 LOWPASS ACTIVE FILTER.

form. The actual sampling process is started and stopped with two 50-microsecond electrical pulses transmitted to the A-D unit on seperate channels to indicate the beginning and end of the useful data. To generate these two pulses, the normal procedure is to record on one tape-channel a square "gate", which is initiated mechanically (by a switch) just before the test is about to take place. The duration of the gate is controlled by a programmable electronic circuit built at HSRI. During playback, this gate is passed through a differentiator-discriminator circuit, also built at HSRI, to produce the first pulse at the beginning of the gate on one channel, and the second pulse on another channel at the end of the gate.

Once all the desired tests are converted and saved on seperate files, another program is run to sort out the channels, perform digital filtering and convert the data to physical units.

DIGITAL FILTERING

Until recently, filtering of recorded signals has typically been carried out using analog filters. With the development of digital computers, a shift from the traditional approach to signal processing has been taking place. Because of their flexibility and versatility, digital computers were often used to simulate analog processing systems for the purpose of studying the characteristics of these systems before commiting them to hardware.

Thus, early work on digital filtering was concerned with the ways analog filters could be approximated on digital computers. This work invited researchers to experiment with increasingly sophisticated algorithms, which had no apparent practical applications, but required the evaluation of the Fourier transform of the input as well as the inverse transformation of the logarithm of the transformed output.

In 1965, an efficient algorithm for computing the Fourier transform was disclosed, and became known as the Fast Fourier Transform or FFT. The FFT allowed implementation of algorithms which were otherwise time-consuming, even on the fast digital computers. Since the FFT is inherently a discrete-time concept, it was used to process discrete-time signals and involved properties that were

exact in the discrete-time domain; thus, the FFT was not merely an approximation of the continuous-time Fourier transform, but had its own mathematics and properties.

As a consequence of the FFT, many signal processing concepts had to be reformulated to conform to the exact mathematics of digital signals. Among these conceptual changes was the realization that digital filters were no longer mere approximations of the well developed analog filters. For instance, it was not practical to talk of the slope of the magintude response (e.g., -20 dB/decade) of a filter; instead, one talks of the attenuation of a stopband, a ripple in the gain of the passband, and of the transition width of the band between pass and stop bands.

The implication of these conceptual changes is that many industry and government standards cannot be intelligently applied to digital filters. An example is Society of Automotive Engineers instrumentation guideline SAE-J211a, which specifies the "channel class" filters to be used on transducers signals in the impact of anthropometric dummies. The recommended practice in SAE-J211a is to use filters which have a passband ripple of 0.5 dB, a common tolerance in commercial analog filters, which can be reduced easily to 0.01 dB in a digital filter. Another recommended practice, also based on analog filters, is to allow the -3 dB point (corner frequency) to be as much as 1.65 the cutoff frequency. In digital filters, the corner frequency can be made as low as 1.05 the cutoff frequency; thus, the gain of Channel Class 1000, which has a cutoff frequency of 1000 Hz, is allowed to be above -3 dB until a corner frequency of 1650 Hz, while in digital filter, the gain can drop below -3 dB at the "corner frequency" of 1125 Hz.

Currently, there is no "standard" for digital filters for biomechanics applications, similar to SAE-J211a. Until such standard or guideline is established, HSRI will follow a practice that it has developed for design and implementation of digital filters, based on its experience in biomechanics instrumentation. The following sections discuss in general terms some of the principals involved in digital filtering, and describe the practice currently followed at HSRI.

Basic Concepts

A linear time-invariant system which transforms an input signal into an output may be viewed as a filter. A digital filter is a system which operates on a digital signal, given as a sequence of numbers, usually derived from an analog signal by periodic sampling. Since a digital filter is a discrete-time system, the z-transform may be used to describe its transfer function, defined as the ratio of the output to the input

$$H^*(z) = \frac{\sum_{j=0}^{N-1} a_j z^{-j}}{1 + \sum_{j=1}^{N} b_j z^{-j}}$$

In the discrete-time domain, this relationship may be written as a difference equation relating the output sequence to the input one

$$y(kT) = \sum_{j=0}^{N-1} a_j x(kT-jT) - \sum_{j=1}^{N} b_j y(kT-jT)$$

It is clear from this relation that the output y(n) depends on the delayed input x(n-k), as well as the delayed output y(n-k). If the feedback elements, characterized by the b-coefficients, are all zero, the output may then be written as a weighted sum of delayed input

$$y(kT) = \sum_{j=0}^{N-1} a_j x(kT-jT)$$

Such a system would be called a non-recursive one, since the output does not depend on previous values of the resulting output itself.

The response of a digital filter to a unit-impulse, which defines the filter coefficients, may have a finite duration, in which case the filter is called a finite-inpulse response (FIR) filter. If the impulse response is of infinite duration, as in analog systems, the digital filter would then be called an infinite-duration impulse response (IIR) one. The duration, or length, of the digital filter is determined by the number N of coefficients used to describe its impulse response. In practical applications, one must deal with a finite number of constants to describe either system. An IIR filter must therefore be expressed as a rational function, while an FIR filter may be represented

by a polynomial.

Consider a periodic sequence x(n), with period N, so that x(n)=x(n+kN) for any integer k. A distinction should be made between periodic and aperiodic sequences. In general, most signal processing systems deal with a section of an aperiodic signal. This portion may be considered as one period of a periodic signal, with period equal to the duration of the available portion. Since the z-transform of the periodic function does not exist, one may use the Fourier transform to deal with it. It is possible to consider the coefficients of the Fourier series representing one period as a periodic sequence, sampled in the frequency domain. The duality between the equations defining the coefficients in terms of the input signal, and those permitting reconstruction of the signal from its Fourier coefficients, leads to the definition of a transform-pair known as the discrete Fourier transform or DFT.

Given an input sequence of finite duration, it is possible then to represent it as one period of a periodic sequence. The DFT of such finite N-duration sequence corresponds to N equally spaced samples of the unit circle in the z-domain. This assertion allows dealing with "strips" of of aperiodic signals., and the use of the DFT for designing and implementing digital filters, using powerful techniques that have been recently developed.

Specification Of Digital Filters

Most of the filters used in biomechanics research are lowpass filters, with a desired cutoff frequency. A lowpass digital filter approximates an ideal response which cannot be physically achieved. Thus, such a filter is specified by giving tolerance limits as shown in Figure 2.

A lowpass digital filter is therefore specified by giving tolerance on the passband ripple, in which the magnitude of the response must be unity (zero dB) within an error of D1, by giving the stopband in which the magnitude of the response must be zero within an error D2, and by giving the upper limit of the passband and the lower limit of the stopband. This defines a transition band in which the gain drops smoothly from unity to zero. Any filter whose magnitude response falls within these limits would then meet the specifications. Since digital signals contain no frequencies higher than half the sampling rate,

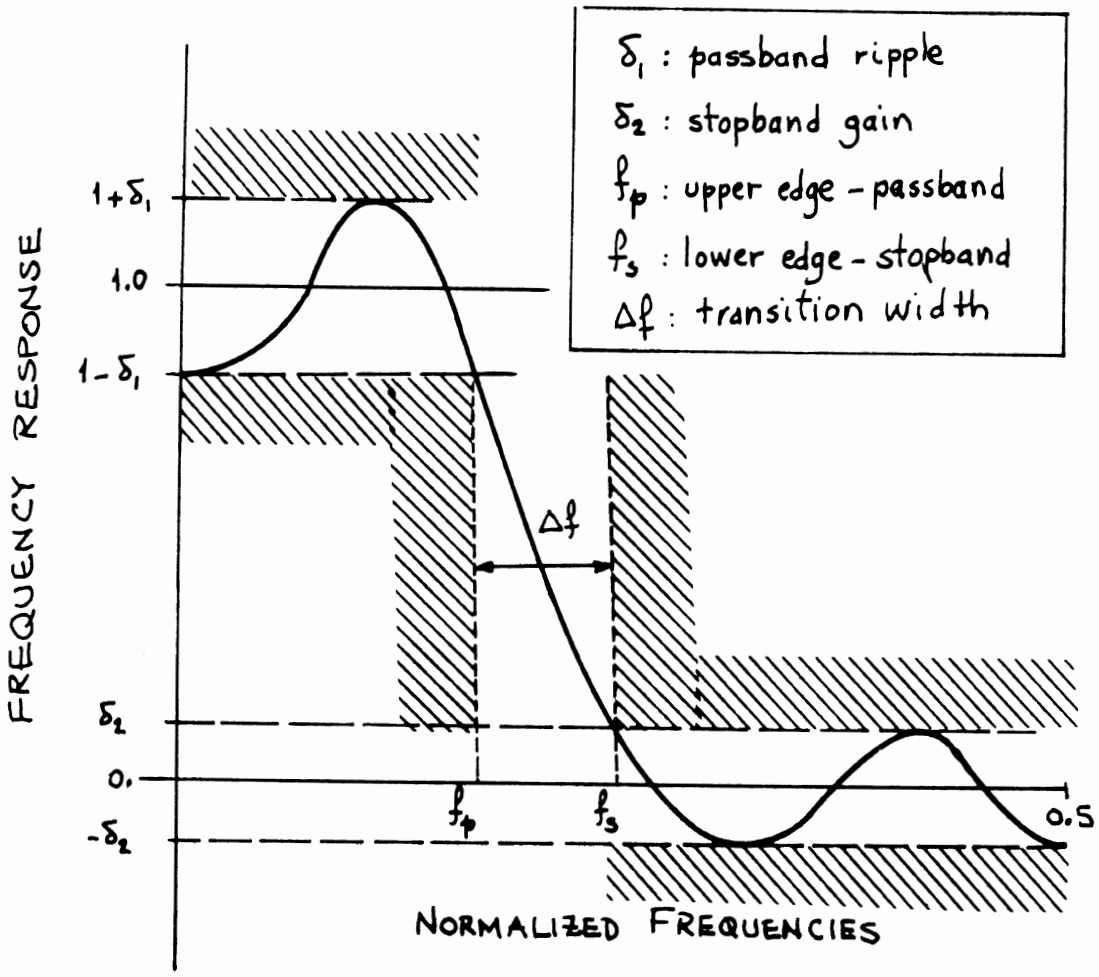

FIGURE 2. DIGITAL FILTER SPECIFICATIONS

specification of the edges of the transition band may be done in frequencies normalized to the sampling rate, so that they range from 0. to 0.5. Furthermore, the tolerances may be specified in gains so that instead of unity, the passband will be 0 dB within D1 dB, and the stopband gain will typically be -100 dB.

IIR Versus FIR Filters

The problem of designing a digital filter whose magnitude falls within the prescribed limits starts by selecting the type of filter, IIR or FIR, on which the design procedure would depend. Each type has its advantages

and shortcomings. The infinite inpulse response filter is usually derived from analog filters, for which design methods and procedures are well developed, and most of which are based on simple closed-form formulas. Thus, design of IIR digital filters can achieve excellent magnitude response at the expense of non-linear phase response.

In most biomechanics applications, the phase relationship between various signals is of great importance. It is therefore desirable to have a simple phase response, such as the linear phase of FIR filters. Furthermore, FIR filters design techniques, suitable for digital computer applications, are now available and widely used, and result in optimum filter responses in magnitude and phase.

Most of FIR filter design techniques are iterative in nature, since cosed-form design formulas do not exist. However, the wide availability of digital computers and the existence of a theorem to find an optimal filter, make the iteration procedure a practical matter.

The choice was made at HSRI to use FIR filters. The flexibility and desired response of these filters was not sufficiently offset by the simplicity of the IIR filters. The development of a signal processing system at HSRI includes therefore filter design and implementation phases. The design method is based on an algorithm published by Parks and McClellan in 1972. The realization of the filter uses the Fast Fourier Transform (FFT) and results in a phase-transparent algorithm.

Optimum FIR Filter Design

The design of an FIR filter is a problem of approximation; that is, given an ideal frequency response, the problem is to find the best approximation to that response.

An FIR filter may be described either by its frequency response or by its impulse response. Although many methods exist to design such filters, only one will be discussed.

This design method is based on approximating the ideal magnitude frequency response with one that has specified magnitudes at selected frequencies. Thus a lowpass FIR filter with duration N, is specified by (N-1)/2 points equally spaced in the frequency domain, with room for

adjustment between samples. The response between samples is obtained by the ideal interpolation operator. The impulse response is obtained by using the inverse discrete Fourier transform (IDFT). The procedure is to compare the frequency response of the designed filter to the ideal response, then iterate until the error is satisfactory.

It may be shown that the magnitude response of the designed filter contains ripples in the passband and stopband, which may have "peaks" of various magnitudes. An equiripple design uses a set of weights to force these peaks to be equal in the two bands of the lowpass filter. These weights are derived from the specifications of D1 and D2. Then, the points where the peaks occur (minimax) would no longer be equally spaced in the frequency domain.

In 1972, Parks and McClellan reformulated a theorem of approximation theory to show that a unique optimum FIR filter exits. The filter is optimum in the sense that the errors are the lowest possible maximum errors in the passband and stopband. Subsequently, McClellan and Parks published in 1973 "A Computer Program for Designing Optimum FIR Linear Phase Digital Filters," in which they presented a general algorithm for the design of a large class of these filters. The design program at HSRI is largely based on this algorithm, but was written to interact with the user and simplify the input of specifications and decision-making on the acceptance of the resulting filter. Furthermore, most applications at HSRI require the use of lowpass filters, hence the short HSRI version which limits the design to this class.

The availabilty at HSRI of permanent computer files and their immediate access, allows the storage of the various designed filters on a master file containing their impulse responses. When a digital filter with certain frequency response is needed, a search of the master file is made to determine if it has already been designed. If the desired response is not met by an existing filter, a new one is designed and stored on the master file for later reference.

Currently, the data processing requirements at HSRI are met by a "bank" of 18 lowpass FIR digital filters. The normalized cutoff frequency ranges from 0.05 to 0.356, so that, for a 3200-Hz sampling rate, the lowest frequency-cutoff would be 160 Hz, and the highest would be 1140 Hz. If filters with cutoff frequencies outside this range are desired, then appropriate sampling rates are selected to allow filtering as low as 20 Hz and as high as 9120 Hz.

TABLE 1. CUTOFF FREQUENCIES OF 18 DIGITAL FILTERS AT THE 7 POSSIBLE SAMPLING RATES.

		SAMPLING RATES (HZ)						
	NORM. CUTOFF	400	800	1600	3200	6400	12800	25600
#1	0.050000	20	40	80	160	320	640	1280
#2	0.056123	22	45	90	180	359	718	1437
#3	0.062996	25	50	101	202	403	806	1613
#4	0.070711	28	57	113	226	453	905	1810
#5	0.079370	32	63	127	254	508	1016	2032
#6	0.089090	36	71	143	285	570	1140	2281
#7	0.100000	40	80	160	320	640	1280	2560
#8	0.112246	45	90	180	359	718	1437	2874
#9	0.125992	50	101	202	403	806	1613	3225
#10	0.141421	57	113	226	453	905	1810	3620
#11	0.158740	63	127	254	508	1016	2032	4064
#12	0.178180	71	143	285	570	1140	2281	4561
#13	0.200000	80	160	320	640	1280	2560	5120
#14	0.224492	90	180	359	718	1437	2874	5747
#15	0.251984	101	202	403	806	1613	3225	6451
#16	0.282843	113	226	453	905	1810	3620	7241
#17	0.317480	127	254	508	1016	2032	4064	8127
#18	0.356359	143	285	570	1140	2281	4561	9123

The analog signals are initially digitized at the sampling rate which accomodates the highest cutoff frequency. The sampling rate is subsequently reduced for those signals which must be filtered at lower frequencies than allowed by the initial sampling. This is done by selecting every 2nd or every 4th point. Since this is another form of sampling, it will be associated with a new Nyquist rate, which is 1/2 or 1/4 the original Nyquist rate. Therefore, prior to "skipping" points, the digital signal is filtered to eliminate all frequencies above the new Nyquist rate. Two anti-aliasing digital filters were designed for this purpose: one to be used for sampling every other point, the other for sampling every fourth point. By cascading

these filters, a very flexible scheme for digital filtering is achieved.

The 18 digital filters were designed in the normalized frequency domain, and therefore, the edges of their transition bands, in Hertz, will depend on the sampling rate. Most of the design effort went into obtaining consistent response for all filters, while maintaining a medium-length impulse. The cutoff frequencies were spread uniformly over the spectrum of interest. Bandpass ripple was maintained at about 0.05 dB, and stopband attenuation was designed at 100 dB. This required varying the width of the transition band from 2 to 1.25 times the cutoff frequency, and resulting in "corner" frequencies (-3 dB) varying from 1.25 to 1.05 times the cutoff frequency. The log magnitude versus frequency curves for three typical filters are shown in Figures 3, 4 and 5. The full range of available filters is given in Table 1, which gives the cutoff frequencies of the 18 filters at the 7 possible sampling rates.

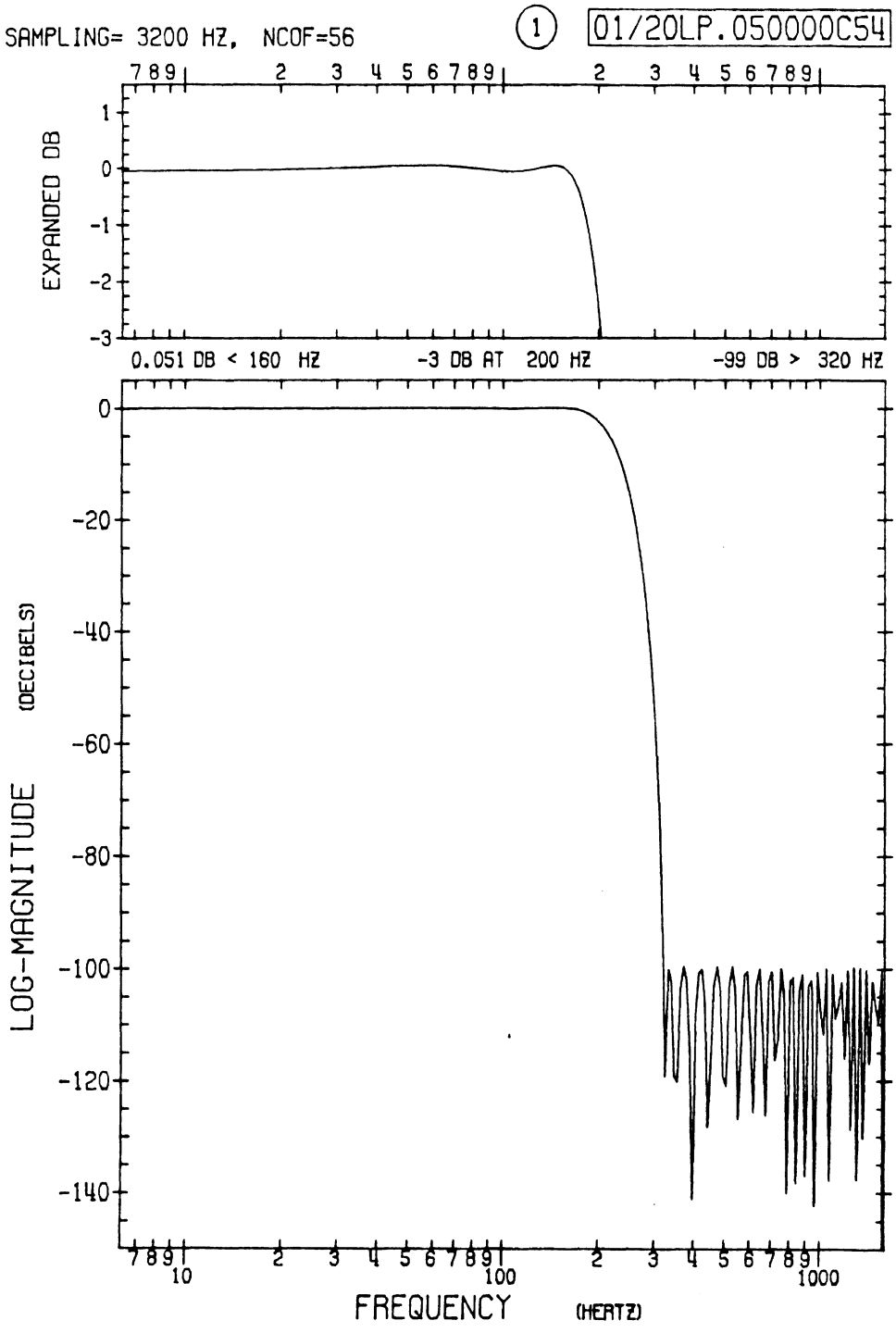

FIGURE 3. FREQUENCY RESPONSE OF FILTER #1 FOR 3200-HZ SAMPLING RATE.

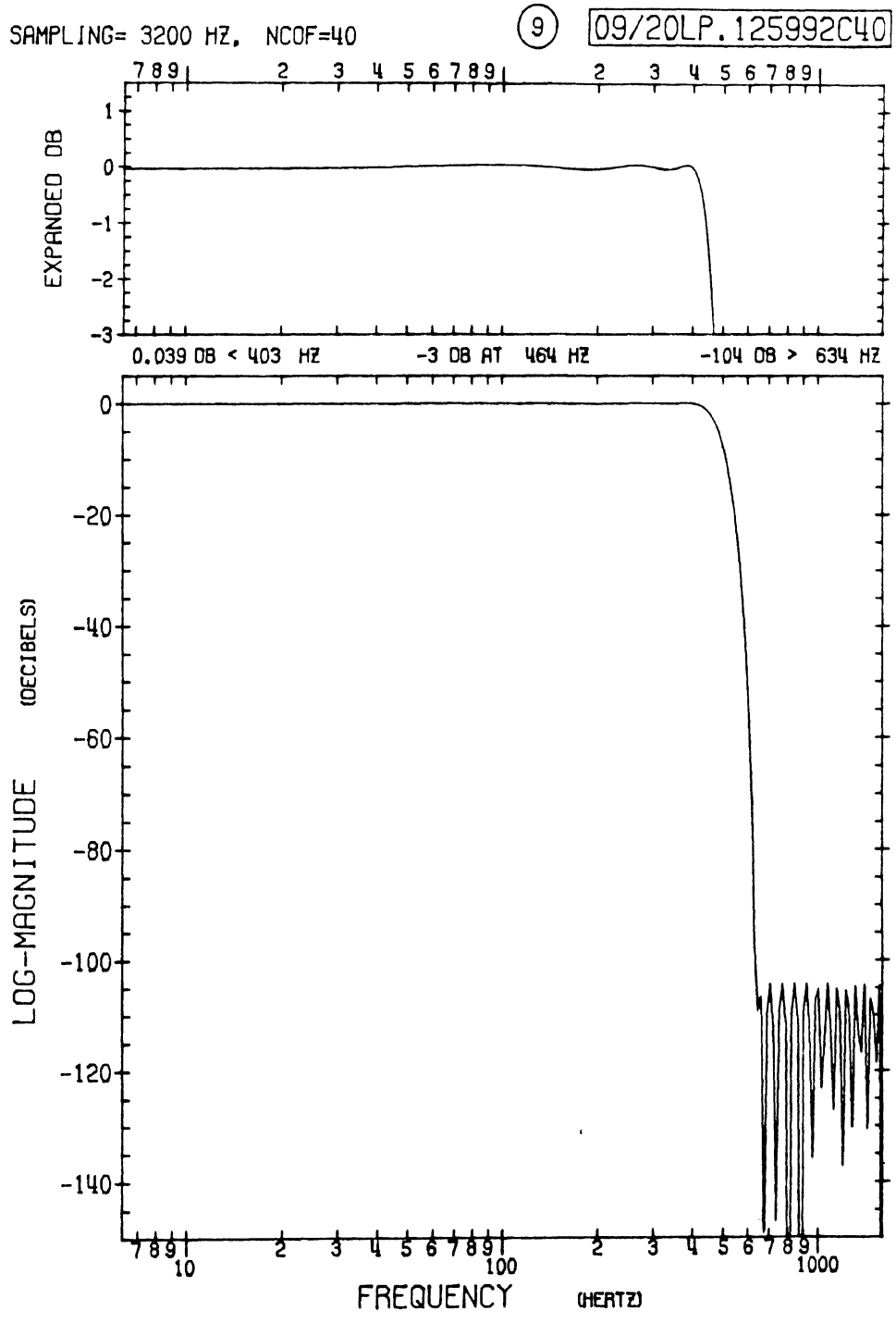

FIGURE 4. FREQUENCY RESPONSE OF FILTER #9 FOR 3200-HZ SAMPLING RATE.

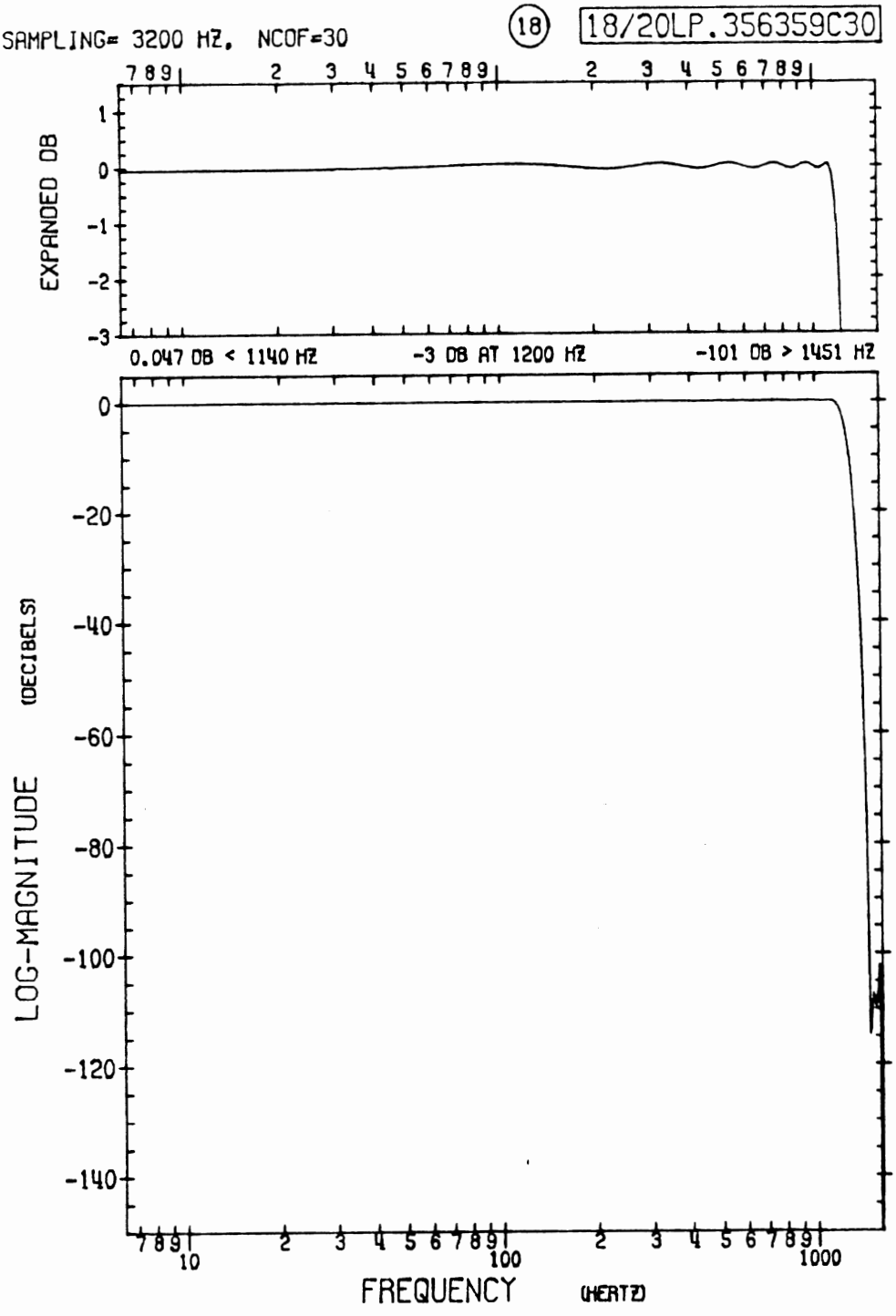

FIGURE 5. FREQUENCY RESPONSE OF FILTER #18 FOR 3200-HZ SAMPLING RATE.

FILTER IMPLEMENTATION

Digital filtering can be accomplished with a relatively high efficiency by employing the Fast Fourier Transform (FFT) algorithm together with a concept known as sectioning. Traditional methods of filtering involving a direct convolution procedure are computationally excessive in both time and space. The FFT serves to reduce computation time while sectioning eases computer memory requirements.

The central operation involved in filtering an input signal x(n) consists of convoluting x(n) with the filter impulse response h(n) producing an output signal y(n).

$$y(n) = x(n) * h(n) = \sum_{k=-\infty}^{\infty} x(k)h(n-k) \quad (1)$$

In application at HSRI, both the input signal and impulse response have finite nonzero duration. Specifically, there are integers M and N with M<N (usually M<<N) such that

$x(n)=0$ if $n<0$ or $n>N-1$
$h(n)=0$ if $n<0$ or $n>M-1$

The convolution in (1) then reduces to

$$y(n) = x(n) * h(n) = \sum_{k=0}^{N-1} x(k)h(n-k) \quad (2)$$

Based upon the number of nontrivial multiplications necessary, direct evaluation of y(n) as in (2) requires order NM time. Furthermore, the straightforward evaluation of (2) would require storing the entire nonzero portion of x(n) in computer memory. Hence, order N storage must be available.

A more efficient approach to filtering is based upon results of the Discrete Fourier Theory. With u(n) as a periodic sequence of period P, the Discrete Fourier Transform pair is given by

$$U(k) = \sum_{n=0}^{P-1} u(n) W_p^{kn} \quad (3)$$

$$u(n) = \frac{1}{P}\sum_{k=0}^{P-1} U(k) W_p^{-kn} \qquad (4)$$

where $W_p = e^{-2\pi i/P}$

For the implementation of high speed convolution, a centrally important result in the Discrete Fourier Theory is that pointwise multiplication in the frequency domain (3) corresponds to periodic or circular convolution in the time domain (4). That is, if $u_1(n)$ and $u_2(n)$ are periodic sequences of period P with $U_1(k)$ and $U_2(k)$ as their Discrete Fourier Transforms as in (3) then

$$\frac{1}{P}\sum_{k=0}^{P-1} U_1(k)U_2(k)W_p^{-kn} = \sum_{m=0}^{P-1} u_1(m)u_2(n-m) \qquad (5)$$

Since the FFT algorithm can compute either of the transformations (3) or (4) in order $P(\log_2 P)$ time, the periodic convolution on the right hand side of (5), denoted by $u_1(n) \circledast u_2(n)$, can also be computed in order $P(\log_2 P)$ time.

It must be recognized that the FFT algorithm applies only for periodic sequences. Furthermore, the above convolution which can be computed in order $P(\log_2 P)$ time is a periodic convolution, similar but by no means identical to the linear convolution $x(n)*h(n)$ in (2).

IMPLEMENTATION BY SECTIONING

By a suitable manipulation of the input signal x(n) and the impulse response h(n), FFT may be utilized and the linear convolution (2) extracted from a collection of periodic convolutions. To perform the convolution (2) with both time and space economy, the signal x(n) is first segmented into sections of length L>M. Each section is then viewed as one period defining a periodic sequence of period L. The value of the impulse response h(n) over the range [0,L-1] similarly defines a periodic sequence of period L. Derived sequences defined by the sections of x(n) are then circularly convolved with the periodic sequence defined from h(n). The portion of each circular convolution representing a linear convolution, the last L-M+1 values of a

representative period, is then extracted. Finally, the linear convolution extractions are pieced together to form the complete linear convolution (2).

The specific method of sectioning the signal x(n) is referred to as the overlap-save method, since each section overlaps the preceding section by M-1 points, and produces L-M+1 meaningful values of the linear convolution. With s_0 denoting the first section, s_1 the second, and so on, we have.

$$s_0 = \{x(-M+1), \ldots, x(L-M)\}$$
$$s_1 = \{x(L-2M+2), \ldots, x(2L-2M+1)\}$$
$$\vdots$$
$$s_j = \{x(jL-(j+1)M+(j+1)), \ldots, x((j+1)L-(j+1)M+j)\}$$
$$\vdots$$

(note that $x(-M+1)=x(-M+2)= \ldots =x(-1)=0$)

Each section s_j is then used to generate a periodic sequence $x_j(n)$ of period L characterized by its value over the single period [0,L-1].

$$x_0(n) = x(n-M+1) \qquad 0 \leq n \leq L-1$$
$$x_1(n) = x(n+L-2M+2) \qquad 0 \leq n \leq L-1$$
$$\vdots$$
$$x_j(n) = x(n+jL-(j+1)M+(j+1)) \qquad 0 \leq n \leq L-1$$
$$\vdots$$

Similarly, the impulse response h(n) generates a periodic sequence $\bar{h}(n)$ of period L characterized by its value over [0,L-1] as.

$$\bar{h}(n) = h(n) \qquad 0 \leq n \leq L-1$$
(note that $\bar{h}(M)=\bar{h}(M+1)= \ldots =\bar{h}(L-1)=0$)

Now since each of the sequences $x_0(n), x_1(n), \ldots, \bar{h}(n)$ is periodic with common period L, the circular convolutions

$$\left.\begin{array}{l} x_0(n) \circledast \bar{h}(n) \\ x_1(n) \circledast \bar{h}(n) \\ \vdots \\ x_j(n) \circledast \bar{h}(n) \\ \vdots \end{array}\right\} \quad (6)$$

can each be performed using the FFT algorithm in order L(log L) time. Finally, we construct the linear convolution (2) from the collection of circular convolutions (6). It can be seen that

$$\left.\begin{array}{lll} y(0) = x(0)*h(0) & = x_0(M-1) \circledast \bar{h}(M-1) \\ y(1) = x(1)*h(1) & = x_0(M) \circledast \bar{h}(M) \\ \vdots & & \\ y(L-M) = x(L-M)*h(L-M) & = x_0(L-1) \circledast \bar{h}(L-1) \\ y(L-M+1) = x(L-M+1)*h(L-M+1) & = x_1(M-1) \circledast \bar{h}(M-1) \\ y(L-M+2) = x(L-M+2)*h(L-M+2) & = x_1(M) \circledast \bar{h}(M) \\ \vdots & & \end{array}\right\} \quad (7)$$

Each circular convolution $x_j(n) \circledast \bar{h}(n)$ in (7) can be performed in order $L(\log_2 L)$ time and contains L-M+1 useful values of the linear convolution x(n)*h(n). Hence, the overall computing time behavior of the overlap-save method of FFT convolution is order $NL(\log L)/(L-M+1)$. By selecting L such that $M \ll L \ll 2^M$, the above computing time behavior approaches order $N(\log_2 L)$ which will in turn be less than order NM -- the behavior resulting from a direct evaluation of the linear convolution (2). Furthermore, since each circular convolution as in (6) requires only order L computer memory, the internal memory requirements are eased.

BIBLIOGRAPHY

1. R. E. Bogner and A. G. Constantinides, "Introduction to Digital Filtering." New York: John Wiley & Sons, 1975.

2. J. W. Cooley and J. W. Tukey, "An Algorithm for the Machine Calculation of Complex Fourier Series." Math. of Comput., vol. 19, 1965, pp. 297-301.

3. W. M. Gentlemen and G. Sande, "Fast Fourier Transforms - For Fun and Profit." 1966 Fall Joint Computer Conf. AFIPS Proc., vol. 29, Washington D.C.: Spartan, 1966, pp. 563-578.

4. J. H. McClellan, T. W. Parks, and L. R. Rabiner, "A Computer Program for Designing Optimum FIR Linear Phase Digital Filters." IEEE Trans. Audio Electroacoust., vol. AU-21, No. 6, 1973, pp. 506-525.

5. A. V. Oppenheim and R. W. Schafer, "Digital Signal Processing." Englewood Cliffs, New Jersey: Prentice-Hall, 1975.

6. L. R. Rabiner, "Approximate Design Relationships for Low-Pass FIR Digital Filters." IEEE Trans. Audio Electroacoust., vol. AU-21, No. 5, 1973, pp. 456-460.

3-D X-RAY TECHNIQUE

N. M. Alem

General

The diverse studies of impact and motion of human subjects and human analogues result in mechanical quantities described in reference frames which vary from one instrumentation method to another.

In order to ensure precise comparison of mechanical responses between subjects, it is necessary to refer all results to a "standard" anatomical frame which may be easily identified. On the other hand, it is impractical to require that transducers be aligned with this anatomical frame since this would create problems which may not be satisfactorily solved.

An alternative is to mount transducers in an arbitrary and convenient reference frame, then describe the transformation necessary to convert the data from this frame to the desired anatomical one.

The following sections describe a three-dimensional x-ray technique which has been developed at HSRI to obtain the orthogonal transformation matrix between the instrumentation and anatomical reference frames. The technique was developed for the HSRI measurement method of 3-D head motion, but may be applied to any general instrumentation hardware.

Anatomical Reference Frame

A widely adopted anatomical reference system for the human head is the one based on the skull's Frankfort plane, defined by four easily identifiable landmarks, and the head midsagittal plane, as shown in figure 1.

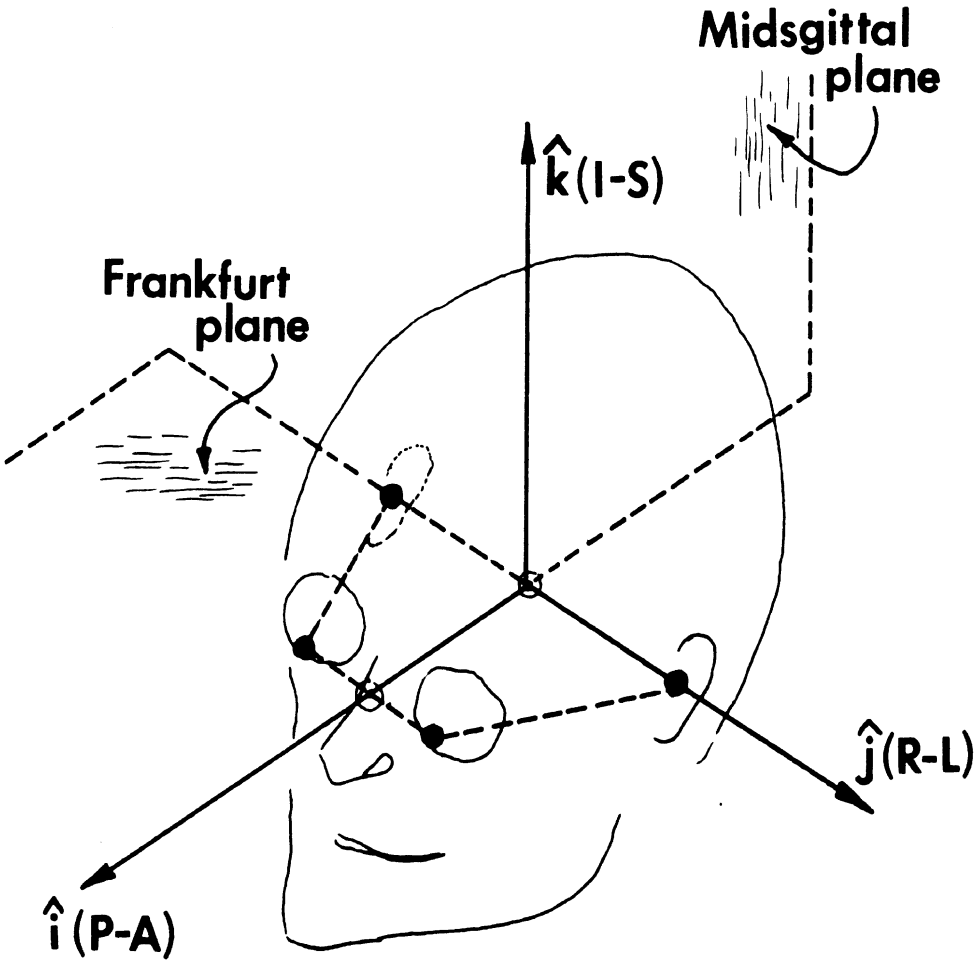

FIGURE 1. HEAD ANATOMICAL REFERENCE SYSTEM, BASED ON THE SKULL'S FRANKFORT AND MIDSAGITTAL PLANES.

The anatomical i-axis is defined along the intersection of the Frankfort and midsagittal planes in the posterior-to-anterior (P-A) direction. The j-axis is defined along the line joining the two superior edges of the auditory meati, in the right-to-left (R-L) direction. This j-axis, which lies in the Frankfort plane, is perpendicular to the midsagittal plane at the "anatomical center" which is taken as the origin of the anatomical frame. Finally, the k-axis is defined as the cross-product of the unit vectors of i- and j-axes, and therefore, will lie in the midsagittal plane perpendicular to the Frankfort plane, and will be in the inferior-to-superior (I-S) direction.

Thus, the anatomical reference frame (i,j,k) can be completely defined once the 4 anatomical landmarks are specified.

Instrumentation Reference Frame

The method used at HSRI to measure the 3-D motion of the head employs nine accelerometers mounted on the head in three clusters. Each cluster is a triaxial unit which measures the components of the acceleration vector at its center in 3 orthogonal directions, which are the same for the other two clusters. These orthogonal instrumentation directions are arbitrarily chosen for convenience of mounting, and are such that the centers Q1, Q2 and Q3 of the three triaxial clusters will lie on the axes E1, E2 and E3 of the instrumentation frame, at known distances R1, R2 and R3 from the origin P, as shown in figure 2.

Given the coordinates of the origin P, and those of two points Q1 and Q2, the unit vectors E1 and E2 are determined by normalizing the distances PQ1 and PQ2. The third unit vector E3 is then obtained by cross-multiplying E1 by E2. However, it is experimentally more practical to supply the coordinates of all three points Q1, Q2 and Q3, as well as the distances from them to the origin P, then compute the coordinates of other points necessary to define the instrumentation frame completely in the 3-D space.

Laboratory Reference Frame

It is desired to describe the instrumentaion (E1,E2,E3) in terms of the anatomical (i,j,k) unit vectors:

$$\begin{Bmatrix} E1 \\ E2 \\ E3 \end{Bmatrix} = [E] \begin{Bmatrix} i \\ j \\ k \end{Bmatrix} \qquad (1)$$

where [E] is an orthogonal transformation matrix made up with the 9 unknown direction cosines. This matrix may be determined by first expressing each of (E1,E2,E3) and (i,j,k) in terms of an arbitrary frame (I,J,K):

$$\begin{Bmatrix} E1 \\ E2 \\ E3 \end{Bmatrix} = [U] \begin{Bmatrix} I \\ J \\ K \end{Bmatrix} \quad \text{and} \quad \begin{Bmatrix} i \\ j \\ k \end{Bmatrix} = [V] \begin{Bmatrix} I \\ J \\ K \end{Bmatrix} \qquad (2)$$

then eliminating the (I,J,K) between the two expressions to obtain the matrix [E]:

$$[E] = [U]^{-1} [V] \qquad (3)$$

Since [U] and [V] are determined from coordinates of several points, the arbitrary frame (I,J,K) will simply be the laboratory frame in which these coordinated are measured. The x-ray method used at HSRI to measure these points automatically defines the laboratory frame.

Calibration Of Object Space

An x-ray image of an object is simply its shadow on a 2-D plane, generated by a near-point source of x-rays. The purpose of calibration is to obtain two of the 3-D laboratory coordinates, either (x,z) or (y,z), of the object point, given its 2-D film coordinates (u,v) and the third distance D along the missing coordinate.

A typical x-ray setup is simplified in the diagram of Figure 3. In this setup, the x-ray table is vertical, and the film cassette is located behind the table at a distance B. The distances from the table to the source and the object are A and D, respectively. For any single point, it is possible to develop relationships between the distance D, the film coordinates U and V, and the true coordinates X and Z.

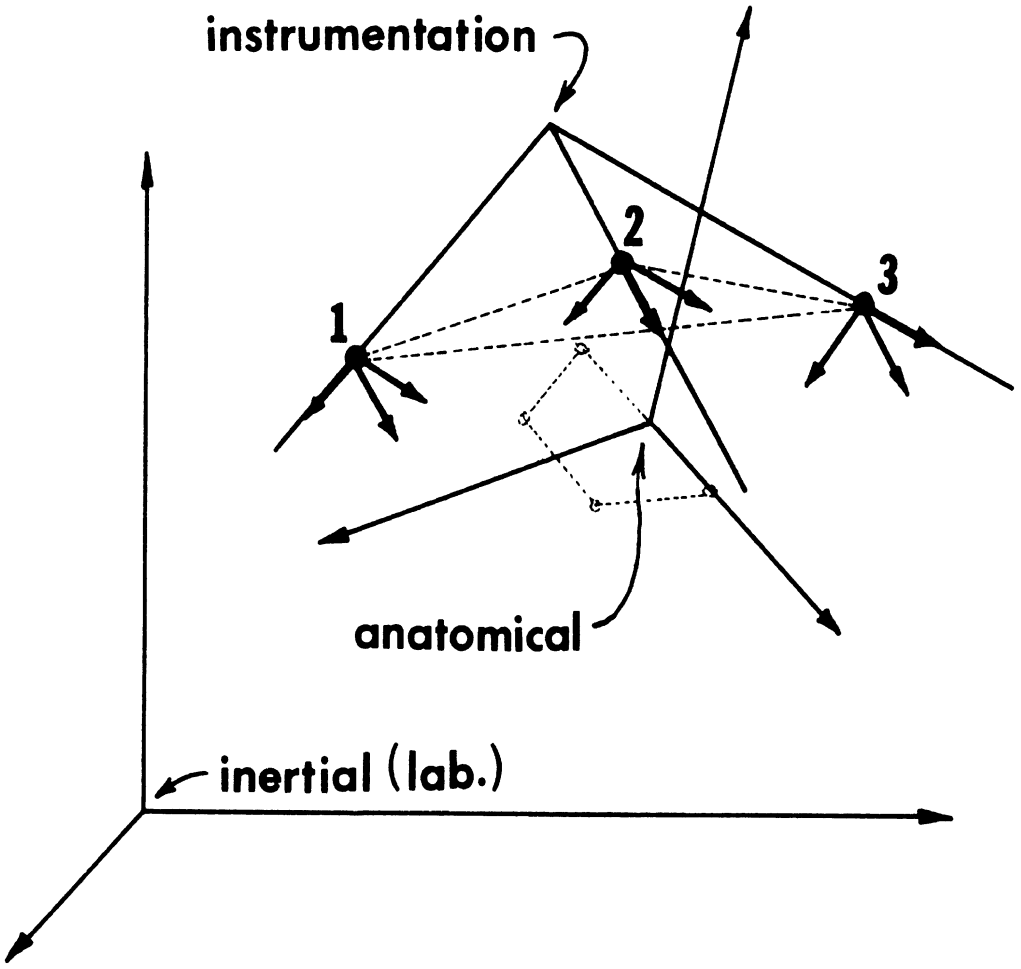

FIGURE 2. INSTRUMENTATION REFERENCE FRAME, AND THE LOCATION OF THE THREE TRIAXIAL ACCELEROMETERS FOR THE HSRI 3-D MOTION MEASUREMENT.

The film radial distance R is determined from the U and V measurements by

$$R = \sqrt{U^2 + V^2} \tag{4}$$

and the angle between R and the I-axis is given by

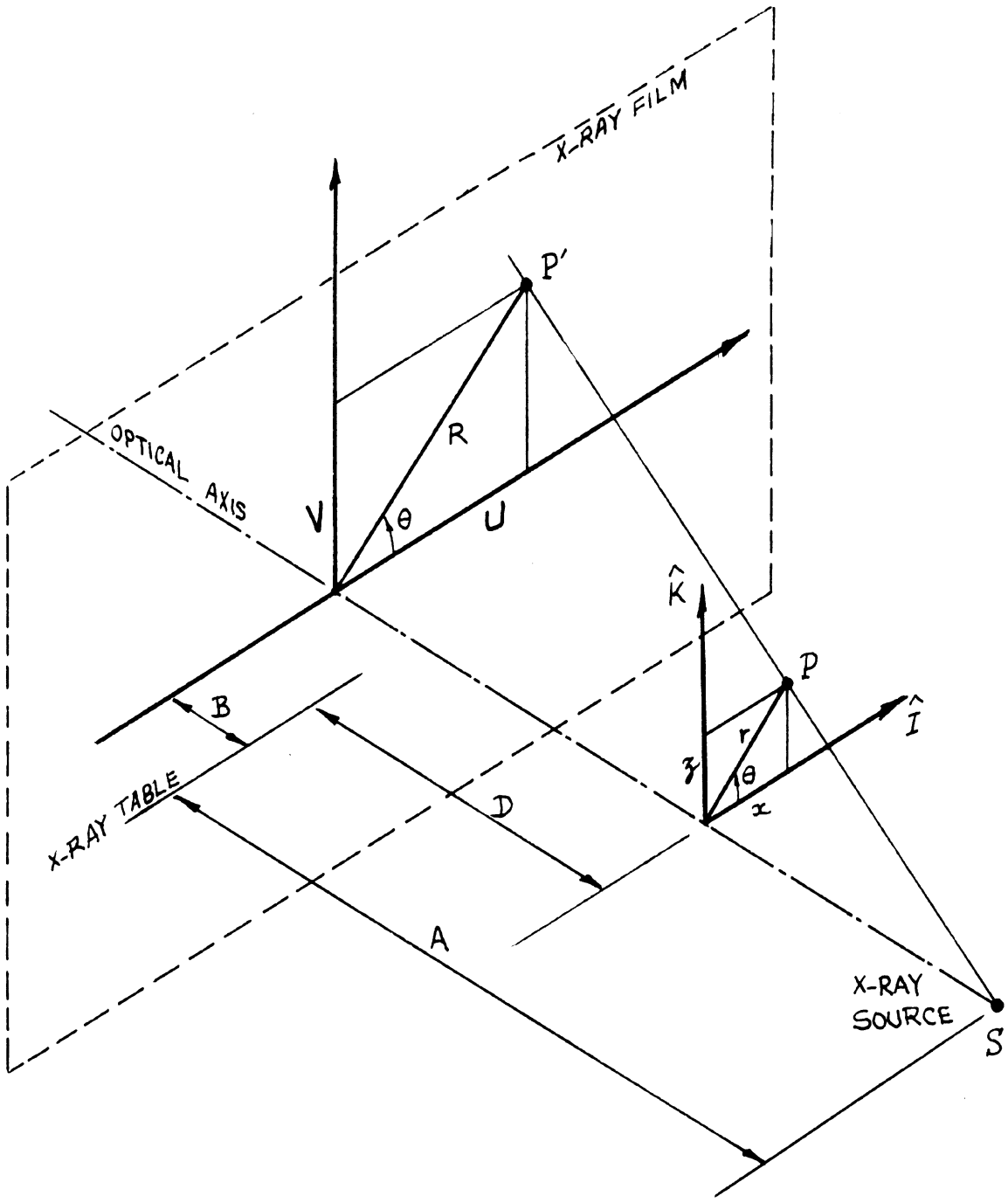

FIGURE 3. SIMPLIFIED DIAGRAM OF X-RAY SETUP.

3-D X-RAY TECHNIQUE

$$\theta = \tan^{-1} \frac{V}{U} \tag{5}$$

The true radial distance r, unknown at this stage, may be obtained from geometric properties. Thus,

$$\frac{r}{R} = \frac{A-D}{A+B} = \left[\frac{A}{A+B}\right] - \left[\frac{1}{A+B}\right] D \tag{6}$$

in which the groups of distances are constants and depend solely on the specific x-ray setup. Therefore,

$$r = [\alpha - \beta D] R \tag{7}$$

Assuming geometric similarities, the angle that the true r makes with the I-axis sould be the same as the one made by the film R, calculated by equation (5). The object-space coordinates x and z may therefore be determined from

$$\begin{aligned} x &= r \cos\theta \\ z &= r \sin\theta \end{aligned} \tag{8}$$

Calibrating the object-space means determining the constants α and β. This may be accomplished by accurately measuring the distances A and B. An alternative is to x-ray an array of targets whose radial distances and distances from the table are known, measure their film U and V to determine the film radial distances R, then perform a multiple regression analysis to determine the correlation constants α and β. This procedure was carried out and results are shown in Figure 4. It should be pointed out that these constants are specific to the HSRI x-ray table/source configuration.

From the magnitudes of α and β, it is clear that the target-table distance, to be measured during the x-raying, does indeed effect the accuracy of computation, but to a small extent. It was found that D may be measured to the nearest 1/2 inch without changing significantly the calculated coordinates.

X-Raying Procedure

The HSRI 9-accelerometer instrumentation for 3-D motion analysis of the head, is characterized by seven points, which determine the relationship between the anatomical reference frame and the instrumentation one. The coordinates of these points must be determined in an arbitrary

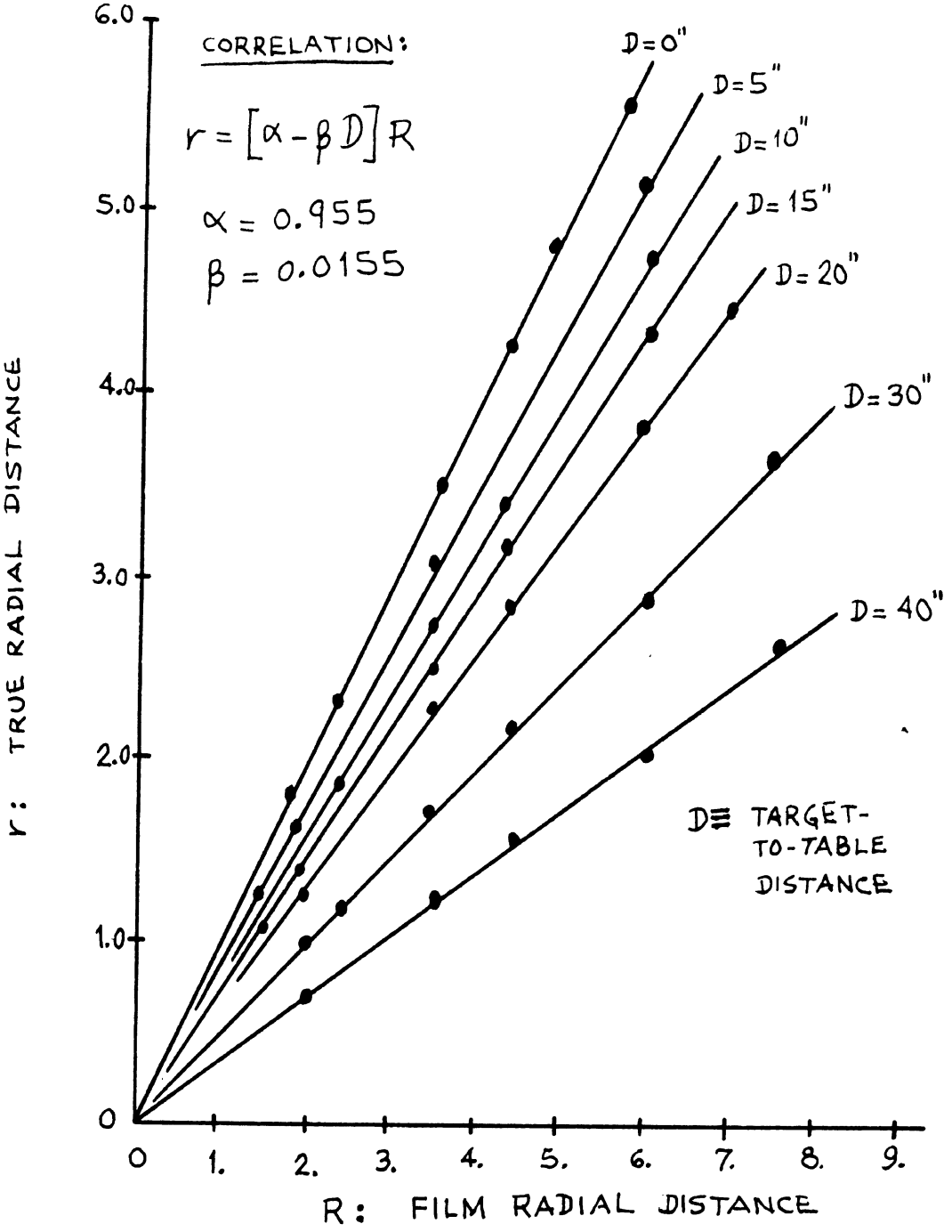

FIGURE 4. CALIBRATION OF HSRI X-RAY SETUP.

laboratory frame. The method is to mark them with seven distinguishable lead pellets then x-ray the targeted head to obtain two orthogonal radiographs which can then be analyzed as a stereo-pair.

Seven lead pellets are implanted at the three triaxial centers and at the four anatomical landmarks. These pellets must be visible and identifiable on both x-rays, and their coordinates on the film must be obtained. It is necessary therefore to be able to locate the origin of the film coodinate system, called the principal point, and defined as the trace of the central ray on the film. To accomplish this, an array of 4 lead pellets were installed on a plexi-glass plate which is machined to fit over the source unit's window, so that the central ray passes through the center of these points. Their images are then used to construct the principal point. The K-axis is determined by hanging a plumb weight with a soldering wire along the vertically positionned x-ray table. This leaves a line which would always be vertical, regardless of the orientation of the cassete. Thus, laboratory reference frames (I,K) and (J,K) may be accurately determined on the film.

Rather than place the instrumented head in two orthogonal x-ray fields aand obtain simultaneously the stero-pair, one x-ray field is sufficient to produce the pair of radiographs. The idea is to rotate the subject 90 degrees between takes, so that in effect, the laboratory frame is rotated, and two orthogonal radiographs are produced. During x-raying, the distances from the x-ray table to each of the seven targets are measured and recorded for later analysis. Since some pellets may not be visible, an estimate of the corresponding distance is made as accurately as possible.

The outcome of the experimental phase is a set of (X,Z,D) and (Y,Z,D) for the seven points. The next phase is to compute the true laboratory coordinates using the calibration constants obtained above, then use these points to reconstruct the anatomical and instrumentation matrices to determine their relative position. A typical example of these measurements is given in Figure 5.

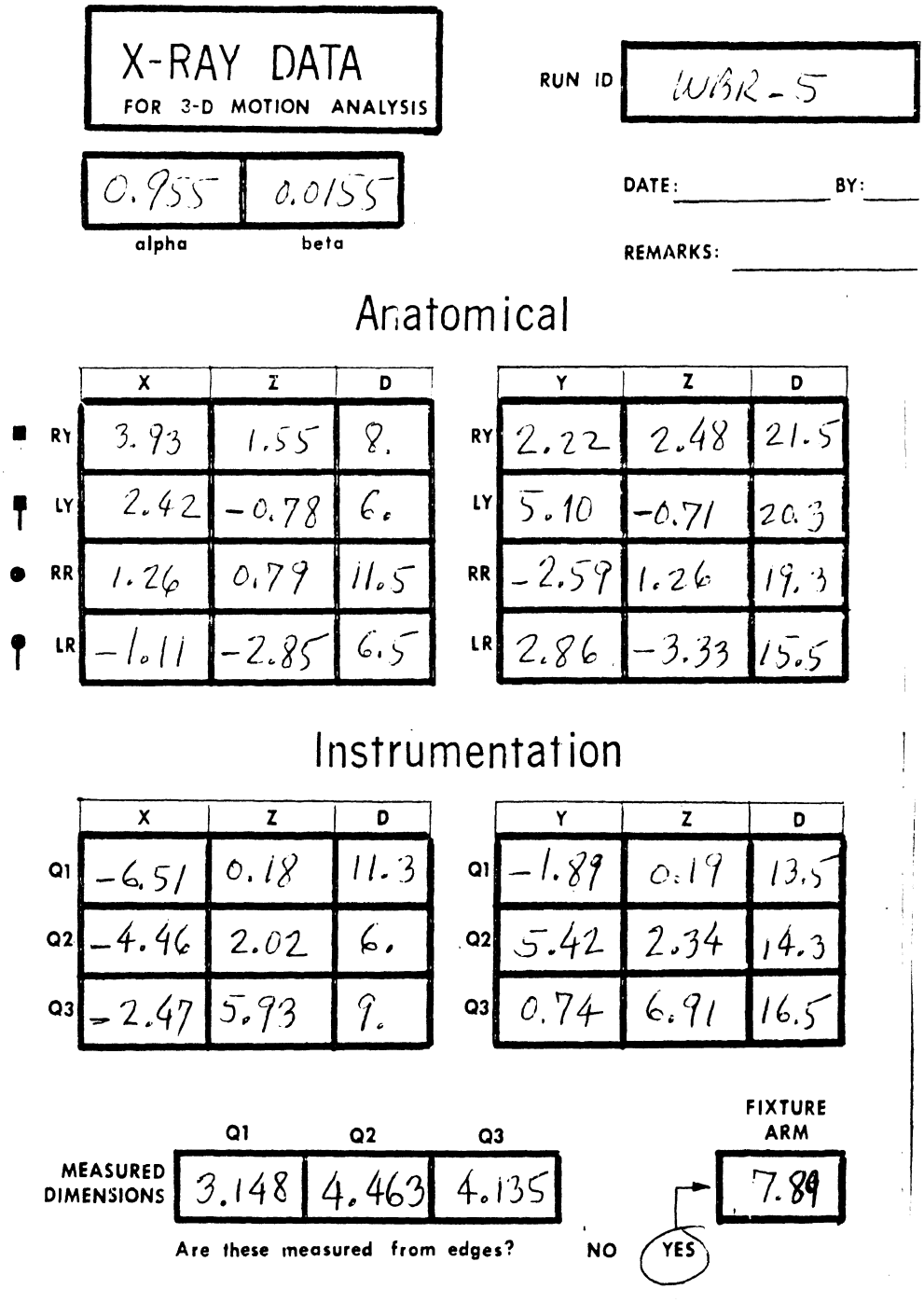

FIGURE 5. EXPERIMENTAL MEASUREMENTS FOR X-RAY ANALYSIS.

Anatomical Frame Reconstruction

The anatomical reference frame is completely defined in the laboratory frame, given the true (x,y,z) coordinates of the two superior edges of the auditory meati P1 and P2, and the two infraorbital notches P3 and P4 as shown in Figure 1.

The anatomical center C is defined as the mid-point between P1 and P2, and the anatomical j-axis is defined as the norm of the left-to-right distance from P2 to P1:

$$\hat{j} = \overrightarrow{P_1P_2}/|P_1P_2| \qquad (9)$$

Let M be the mid-point between P3 and P4. Then, the i-axis is defined as the norm of the posterior-to-anterior distance from C to M:

$$\hat{i} = \overrightarrow{CM}/|CM| \qquad (10)$$

Finally, the k-axis is defined as the cross-product of the unit vectors of i- and j-axes, and will be in the inferior-to-superior direction:

$$\hat{k} = \hat{i} \times \hat{j} \qquad (11)$$

Thus, the direction cosines of each unit vector are determined and the matrix [V] of equation (2) is completely defined. Since it is derived from experimental measurements, the elements of this matrix will carry some errors, and will be slighltly non-orthogonal. A correction scheme was developed to render this matrix orthogonal and is described in a later section.

Instrumentation Frame Reconstruction

The direction cosines of the three unit vectors , and of the instrumentation reference frame are easily determined once its origin P is located in laboratory frame.

Given the (x,y,z) coordinates of the 3 triaxial centers Q1, Q2 and Q3, and their distances R1, R2 and R3 from the origin P, it is proposed to compute the coordinates of P. Because of the quadratic nature of these distances, solution of the equations giving these distances as square-roots of sums of squares, yields two distinct locations of P, only one of which is correct. A solution based on geometric properties is therefore used to obtain a single location,

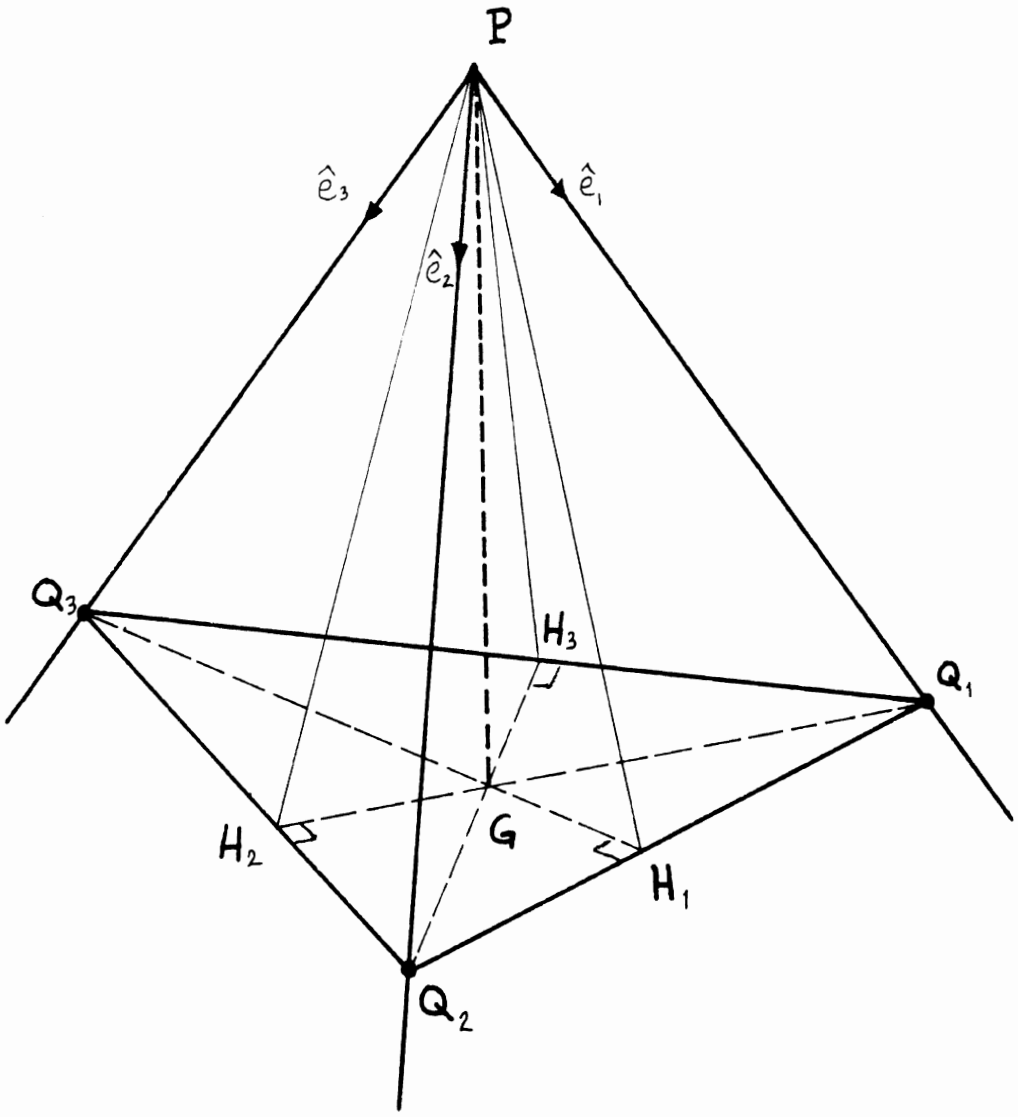

FIGURE 6. CONSTRUCTION OF ORIGIN P.
the correct one.

Consider the diagram of Figure 6, which depicts the instrumentation frame, its origin P and the three triaxial centers Q1, Q2 and Q3. The origin P must lie at the intersection of three spheres, centered at Q1, Q2 and Q3, with respective radii of R1, R2 and R3.

Consider spheres [Q1;R1] and [Q2;R3]. In order for P to exist, they must intersect along a circle whose center is H1, located on the line connecting Q1 and Q2, and whose radius is the distance from H1 to P. The third sphere [Q3;R3], which is orthogonal to each of the first two, must intersect the above circle at right angles; that is, the line from Q3 to P must lie in the plane of that circle, and must be tangent to it at point P.

Thus, the plane Q3-P-H1 is perpendicular to line Q1-Q2, and therefore, this line must be perpendicular to all lines contained in that plane; in particular, line Q1-Q2 is perpendicular to line Q3-H1. It may be concluded that line Q3-H1 is the height of the triangle Q1-Q2-Q3 at base Q2-Q1. Similar arguments lead to conclude that the other two heights of this triangle are Q1-H2 and Q2-H3. Since all three heights of any triangle intersect at a common point, this intersection is called point G.

Finally, since line Q1-Q2 is perpendicular to plane Q3-H1-P, it must also be perpendicular to all lines in this plane, and in particular, to line P-G. Similarly, lines Q2-Q3 and Q3-Q1 are perpendicular to line P-G. Therefore, it may be concluded that P-G is perpendicular to plane Q1-Q2-Q3 so that point G is the orthogonal projection of origin P on this plane.

With these geometric properties established, the problem of locating the origin P may be broken down in smaller problems of line-plane intersections. A single subroutine was written to solve this intersection problem, to be be called as needed.

Given an arbitray plane defined by a point (x_1, y_1, z_1) and the direction cosines of a normal vector (a_1, b_1, c_1), the normal form of the equation of the plane is given by

$$a_1(x-x_1) + b_1(y-y_1) + c_1(z-z_1) = 0 \qquad (12)$$

and given an arbitrary line defined by a point (x_2, y_2, z_2) and its direction cosines (a_2, b_2, c_2), the parametric form of the equation of the line is given by

$$x = x_2 + a_2 t \qquad y = y_2 + b_2 t \qquad z = z_2 + c_2 t \tag{13}$$

The intersection point (x,y,z) of the line with the plane must lie on both of them; therefore, it must satisfy both equations (12) and (13). Thus,

$$a_1[(x_2 + a_2 t) - x_1] + b_1[(y_2 + b_2 t) - y_1] + c_1[(z_2 + c_2 t) - z_1] = 0 \tag{14}$$

which may be solved for t to yield

$$t = \frac{a_1(x_1 - x_2) + b_1(y_1 - y_2) + c_1(z_1 - z_2)}{a_1 a_2 + b_1 b_2 + c_1 c_2} \tag{15}$$

The parameter t is precisely the distance, along the line, between the line's particular point and the intersection point. Once is is computed from (15), it is substituted back into (14) to yield the desired (x,y,z) coordinates of the intersection.

The computational procedure for locating origin P starts by locating H1 as the intersection of line Q1-Q2 with plane Q3-H1-P, both of which have known direction cosines and particular points. This is repeated for points H2 and H3.

Next, point G is located as the intersection of line Q3-H1 and plane Q1-H2-P. The location of G may alternately be obtained as the intersection of line Q1-H2 with plane Q2-H3-P, or as the intersection of line Q2-H3 with plane Q3-H1-P. The average of the three methods is taken to minimize experimental errors.

Finally, the direction cosines of line G-P are obtained from the cross-product of any two lines connecting Q1, Q2 and Q3. The proper order must be observed so that point P would be located on the correct side of Q1-Q2-Q3 plane. Thus, the direction cosines (u_1, u_2, u_3) of this unit vector are obtained from

$$\hat{u} = \left[\overrightarrow{Q_2Q_1} \times \overrightarrow{Q_1Q_3}\right] \Big/ \left|\overrightarrow{Q_2Q_1} \times \overrightarrow{Q_1Q_3}\right| \tag{16}$$

To complete the required information, the magnitude of line G-P must be computed. The length |GP| may be obtained by solving the right-angle triangle Q3-G-P, given points Q3

and G on one side of the 90-degree angle, and R3 as the hypothenus. This same magnitude may also be obtained from either triangle Q1-G-P or Q2-G-P. Again, all three methods are used and averaged to minimize experimental errors. The final step in locating origin P is to use the parametric equations of line G-P, given the magnitude |GP| and the line's directions cosines (u_1, u_2, u_3) computed from equation (16):

$$\begin{aligned} x_p &= x_c + |GP|\, u_1 \\ y_p &= y_c + |GP|\, u_2 \\ z_p &= z_c + |GP|\, u_3 \end{aligned} \qquad (17)$$

Once the origin P is located, and given the locations of the three triaxial centers, the direction cosines of the instrumentation unit vectors may be obtained by normalizing the distances P-Q1, P-Q2 and P-Q3. This determines completely the matrix [U] of equation (1). With the anatomical matrix [V] known, the laboratory reference frame may be eliminated as described in equation (3) to obtain matrix [E] necessary to convert all data from the instrumentation frame to the anatomical one.

Orthogonality Correction

The computational method described above has been programmed and typical output is shown in Figure 7. It is clear that the resulting matrices are not perfectly orthogonal. This is to be expected, since experimental readings always carry some error. The non-orthogonality may be eliminated by a perturbation scheme which is described below.

The scheme is based on the property that the product of an orthogonal matrix times its inverse is the unity matrix. Since the inverse of an orthogonal matrix is equal to its transpose, the orthogonality check is made on the product of the matrix times its transpose. The perturbation scheme forces this product to become the unity matrix.

Given the uncorrected matrix [E] of direction cosines:

X-RAY FILM ANALYSIS FEB 6, 1976 RUN ID: WBR-5

A=0.9550, B=0.0155

	READINGS OF X-Z PLANE X	Z	D	READINGS OF Y-Z PLANE Y	Z	D
P1- R.EYE:	3.930	1.550	8.00	2.220	2.480	21.50
P2- L.EYE:	2.420	-0.780	6.00	5.100	-0.710	20.30
P3- R.EAR:	1.260	0.790	11.50	-2.590	1.260	19.30
P4- L.EAR:	-1.110	-2.850	6.50	2.860	-3.330	15.50
Q1- ACC. :	-6.510	0.180	11.30	-1.890	0.190	13.50
Q2- ACC. :	-4.460	2.020	6.00	5.420	2.340	14.30
Q3- ACC. :	-2.470	5.930	9.00	0.740	6.910	16.50
P1,R2,R3 :	4.742	3.427	3.755			

	COORDINATES W.R.T. CAMERA X	Y	Z		COORDINATES W.R.T. CAMERA X	Y	Z
P1 :	3.266	1.380	1.415	Q1:	-5.077	-1.409	0.141
P2 :	2.086	3.266	-0.564	Q2:	-3.845	3.975	1.729
P3 :	0.979	-1.699	0.720	Q3:	-2.014	0.517	4.834
P4 :	-0.948	2.044	-2.407	P:	-5.428	1.625	3.727
C :	0.015	0.173	-0.844	CP:	-5.444	1.452	4.571

	ANATOMICAL FRAME (WRT CAMERA) <X>	<Y>	<Z>	ORTHOGONALITY CHECK		
<I> :	0.69465	0.66052	0.28489	1.0000	0.0	-0.0000
<J> :	-0.38188	0.67355	-0.63049	0.0	0.9970	0.0000
<K> :	-0.60907	0.32957	0.72099	-0.0000	0.0000	0.9994

	INSTRUMENT FRAME (WRT CAMERA) <X>	<Y>	<Z>	ORTHOGONALITY CHECK		
<E1>:	0.07463	-0.64419	-0.76122	1.0000	0.0363	0.0335
<E2>:	0.45680	0.67762	-0.57634	0.0363	1.0000	0.0455
<E3>:	0.90895	-0.29492	0.29468	0.0335	0.0455	1.0000

```
*****************************************
*                                       *
* RUN ID:WBR-5            FEB  6, 1976  *
*                                       *
* PQ1=  4.742, PQ2=  3.427, PQ3=  3.755 *
* CPI= -1.520, CPJ=  0.175, CPK=  7.090 *
*                                       *
* INSTRUMENTATION MATRIX WRT ANATOMICAL *
*          <I>       <J>       <K>      *
*                                       *
* <E1>:   -0.61006   0.01805  -0.79215  *
*                                       *
* <E2>:    0.60022   0.66319  -0.44713  *
*                                       *
* <E3>:    0.51728  -0.74823  -0.41542  *
*                                       *
*****************************************
```

PERTURBATIONS: E1,E2,E3
0.0245 0.0301 0.0294

ORTHOGONALITY CHECK

1.0000	0.0000	0.0000
0.0000	1.0000	0.0
0.0000	0.0	1.0000

FIGURE 7. TYPICAL "XRAY" PROGRAM OUTPUT.

$$[E] = \begin{bmatrix} [\hat{e}_1] \\ [\hat{e}_2] \\ [\hat{e}_3] \end{bmatrix} \tag{18}$$

the magnitudes of $\hat{e}_1$, $\hat{e}_2$ and $\hat{e}_3$ must be unity, if the matrix is to be orthogonal. Assuming that the deviations from unity are small, new unit vectors may be computed by normalizing the given ones. Thus,

$$\begin{aligned} \hat{e}_1^* &= \hat{e}_1 / |\hat{e}_1| \longrightarrow \hat{e}_1 \\ \hat{e}_2^* &= \hat{e}_2 / |\hat{e}_2| \longrightarrow \hat{e}_2 \\ \hat{e}_3^* &= \hat{e}_3 / |\hat{e}_3| \longrightarrow \hat{e}_3 \end{aligned} \tag{19}$$

The next step is cross-multiply each pair of the normalized vectors (3 possible combinations) to obtain 3 new unit vectors, which would be orthogonal to the pairs that produced them; i.e.,

$$\begin{aligned} \hat{e}_1^* &= [\hat{e}_2 / |\hat{e}_2|] \times [\hat{e}_3 / |\hat{e}_3|] \\ \hat{e}_2^* &= [\hat{e}_3 / |\hat{e}_3|] \times [\hat{e}_1 / |\hat{e}_1|] \\ \hat{e}_3^* &= [\hat{e}_1 / |\hat{e}_1|] \times [\hat{e}_2 / |\hat{e}_2|] \end{aligned} \tag{20}$$

Because of the non-orthogonality of the original matrix, the results of cross-multiplication would not be the same as the corresponding original unit vectors. Rather than seletct one or the other, the two sets of direction cosines are averaged, and the average is retained as a more accurate estimate of the true cosines. Thus,

$$\begin{aligned} \hat{e}_1 &= [\hat{e}_1^* + \hat{e}_1]/2 \\ \hat{e}_2 &= [\hat{e}_2^* + \hat{e}_2]/2 \\ \hat{e}_3 &= [\hat{e}_3^* + \hat{e}_3]/2 \end{aligned} \tag{21}$$

A check on the orthogonality of the new perturbed matrix is made by multiplying it by its transpose. If the deviation from the unity matrix is not acceptable, then the

```
ORIGINAL MATRIX                RUN ID: WBR-5          ORTHOGONALITY CHECK

-0.59052   0.01755  -0.80660                    0.99963   0.03604   0.03334
 0.60071   0.64534  -0.47043                    0.03604   0.99862   0.04682
 0.52055  -0.73154  -0.43835                    0.03334   0.04682   0.99827

                          PERTURBATIONS
    PERTURBED MATRIX          AMOUNT    CUMULATIVE
-0.59063  0.01755 -0.80675  0.1872E-03  0.1872E-03    1.0000    0.0361    0.0334
 0.60112  0.64579 -0.47075  0.6899E-03  0.6899E-03    0.0361    1.0000    0.0469
 0.52100 -0.73217 -0.43873  0.8633E-03  0.8633E-03    0.0334    0.0469    1.0000

    PERTURBED MATRIX          AMOUNT    CUMULATIVE
-0.60984  0.01803 -0.79232  0.2403E-01  0.2421E-01    1.0000    0.0004    0.0004
 0.60017  0.66309 -0.44733  0.2913E-01  0.2982E-01    0.0004    1.0000    0.0003
 0.51724 -0.74813 -0.41564  0.2832E-01  0.2918E-01    0.0004    0.0003    1.0000

    PERTURBED MATRIX          AMOUNT    CUMULATIVE
-0.61006  0.01805 -0.79215  0.2779E-03  0.2449E-01    1.0000    0.0000    0.0000
 0.60022  0.66319 -0.44713  0.2371E-03  0.3006E-01    0.0000    1.0000    0.0000
 0.51728 -0.74823 -0.41542  0.2501E-03  0.2943E-01    0.0000    0.0000    1.0000

    PERTURBED MATRIX          AMOUNT    CUMULATIVE
-0.61006  0.01805 -0.79215  0.6333E-07  0.2449E-01    1.0000    0.0000    0.0000
 0.60022  0.66319 -0.44713  0.5960E-07  0.3006E-01    0.0000    1.0000    0.0
 0.51728 -0.74823 -0.41542  0.5960E-07  0.2943E-01    0.0000    0.0       1.0000

    PERTURBED MATRIX          AMOUNT    CUMULATIVE
-0.61006  0.01805 -0.79215  0.6333E-07  0.2449E-01    1.0000    0.0000    0.0000
 0.60022  0.66319 -0.44713  0.0         0.3006E-01    0.0000    1.0000   -0.0000
 0.51728 -0.74823 -0.41542  0.8429E-07  0.2943E-01    0.0000   -0.0000    1.0000
```

FIGURE 8. PERTURBATION OF A TYPICAL NON-ORTHOGONAL MATRIX.

procedure is repeated to obtain a "more orthogonal" matrix. Typical output from the perturbation program is given in Figure 8.

It was found that 5 iterations were required for the worst case in which the off-diagonal terms were as high as 0.18. In all cases, none of the unit vectors were perturbed by more than 4 degrees in space, an amount which could conceivably be produced by measurement errors. It should finally be pointed out that the orthogonality of the final perturbed matrix does not imply that it is the true transformation; instead, this matrix remains an experimentally-produced one, and therefore, will carry some measurement error, be it orthogonal or not.

Translation Of Origins

The transformation matrix obtained above describes the rotation of the instrumentation frame relative to the anatomical one. The translation between the two frames may be described by specifying the components of the vector between their origin in the anatomical reference frame; i.e.,

$$\overrightarrow{CP} = d_1 \hat{i} + d_2 \hat{j} + d_2 \hat{k} \tag{22}$$

which may be computed from

$$\overrightarrow{CP} = \overrightarrow{OP} - \overrightarrow{OC} \tag{23}$$

then expressed in the anatomical frame. From the definitions of vectors OC and CP,

$$\overrightarrow{OC} = \left[\overrightarrow{OP_1} + \overrightarrow{OP_2}\right]/2 = \frac{x_1+x_2}{2}\hat{I} + \frac{y_1+y_2}{2}\hat{J} + \frac{z_1+z_2}{2}\hat{K} \tag{24}$$

$$\overrightarrow{OP} = x_p \hat{I} + y_p \hat{J} + z_p \hat{K} \tag{25}$$

therefore,

$$\overrightarrow{CP} = \begin{bmatrix}(x_p-x_c) & (y_p-y_c) & (z_p-z_c)\end{bmatrix}\begin{Bmatrix}\hat{I}\\ \hat{J}\\ \hat{K}\end{Bmatrix} \tag{26}$$

To obtain the components of CP in the anatomical frame,

the laboratory frame is eliminated to yield

$$\begin{bmatrix} d_1 & d_2 & d_3 \end{bmatrix} = \begin{bmatrix} (x_p - x_c) & (y_p - y_c) & (z_p - z_c) \end{bmatrix} [E]^T \quad (27)$$

Summary

The three-dimensional x-ray technique, described in the above sections, results in a complete description of the location and orientation f an arbitray instrumentation reference frame relative to a standard anatomical one. The procedure was developed for the head, but can easily be adapted to any body segment.

MEASUREMENT OF 3-D MOTION

N. M. Alem & G. L. Holstein

General

The general three-dimensional (3-D) motion of a rigid body (R.B.), described by its six degrees of freedom, may be determined by means of nine linear (translational) accelerometers which are properly mounted on the R.B. in three clusters. The nine accelerations are mathematically manipulated to produce the angular acceleration and velocity vectors of the R.B., its orientation in 3-D inertial (laboratory) space, the absolute translational acceleration, velocity and position vectors of an arbitrary point on the rigid body.

Each one of the three clusters is a triaxial accelerometer (or triax) which measures 3 orthogonal components of the acceleration vector of its "center." In general, these orhogonal instrumentation axes are arbitrarily chosen for convenience, and threfore, do not coincide with the "anatomical" reference frame in which the motion is to be described. It is assumed that the transformation matrix between the instrumentation and anatomical frames is known, so that the analysis is conducted on the anatomical components of the three acceleration vectors. Furthermore, it is assumed that the position vector of each triax center is known relative to an arbitrary point, which is taken as the origin of the anatomical reference frame.

In the following sections, the kinematic equations of motion will be developped, their solution will be presented, then validated with actual and hypothetical motions.

Kinematics Of Angular Motion

Consider the rigid body shown in figure 1. The anatomical reference frame ($\underline{i},\underline{j},\underline{k}$) is used to express the position vectors of the triax centers Q1, Q2 and Q3 relative to an arbitrary reference point Q0:

$$\underline{P1} = PI1\ \underline{i} + PJ1\ \underline{j} + PK1\ \underline{k}$$

$$\underline{P2} = PI2\ \underline{i} + PJ2\ \underline{j} + PK2\ \underline{k} \qquad (1)$$

$$\underline{P3} = PI3\ \underline{i} + PJ3\ \underline{j} + PK3\ \underline{k}$$

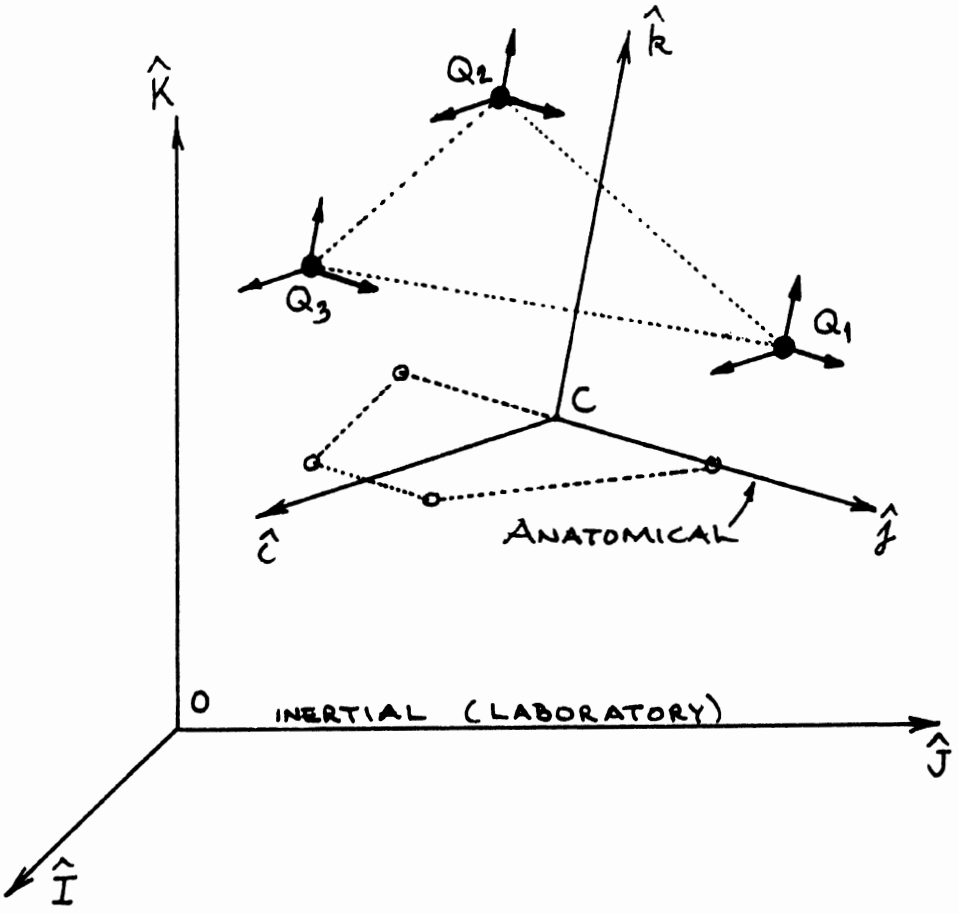

FIGURE 1. COORDINATE SYSTEMS AND THE NINE ACCELERATIONS USED IN 3-D MOTION ANALYSIS.

The measurement of nine accelerations defines the acceleration vectors at Q1, Q2 and Q3 which may be expressed in the anatomical frame:

$$\underline{A1} = AI1\ \underline{i} + AJ1\ \underline{j} + AK1\ \underline{k}$$

$$\underline{A2} = AI2\ \underline{i} + AJ2\ \underline{j} + AK2\ \underline{k} \qquad (2)$$

$$\underline{A3} = AI3\ \underline{i} + AJ3\ \underline{j} + AK3\ \underline{k}$$

The same acceleration vectors, given in equation (2), may be calculated from the kinematic equation of motion of a rigid body, given the translational acceleration vector of a body reference point and the angular acceleration (and velocity) vectors of the R.B.:

$$\underline{A1} = \underline{A} + \underline{U}\times\underline{P1} + \underline{W}\times\underline{W}\times\underline{P1}$$

$$\underline{A2} = \underline{A} + \underline{U}\times\underline{P2} + \underline{W}\times\underline{W}\times\underline{P2} \qquad (3)$$

$$\underline{A3} = \underline{A} + \underline{U}\times\underline{P3} + \underline{W}\times\underline{W}\times\underline{P3}$$

where $\underline{U}$, $\underline{W}$ and $\underline{A}$ are angular acceleration, velocity and translational acceleration vectors, respectively. These three vectors are unknown and must be determined as:

$$\underline{A} = AI\ \underline{i} + AJ\ \underline{j} + AK\ \underline{k} \qquad (4)$$

$$\underline{U} = UI\ \underline{i} + UJ\ \underline{j} + UK\ \underline{k} \qquad (5)$$

$$\underline{W} = WI\ \underline{i} + WJ\ \underline{j} + WK\ \underline{k} \qquad (6)$$

Vector-equation (3) represents 9 scalar equations, in which the unknowns are the components of equations (4), (5) and (6). Note however that the angular velocity is simply the integral of the angular acceleration, which means that there is a third-order redundancy in these equations.

Least-Squares Solution

The first step towards the solution of equation (3), is to write it in matrix form. The position vectors $\underline{P1}$, $\underline{P2}$ and $\underline{P3}$ are replaced by column matrices {P1}, {P2} and {P3} given by:

$$\{P1\} = \begin{Bmatrix} PI1 \\ PJ1 \\ PK1 \end{Bmatrix} \qquad \{P2\} = \begin{Bmatrix} PI2 \\ PJ2 \\ PK2 \end{Bmatrix} \qquad \{P3\} = \begin{Bmatrix} PI3 \\ PJ3 \\ PK3 \end{Bmatrix}$$

The acceleration vectors $\underline{A1}$, $\underline{A2}$ and $\underline{A3}$ are replaced by

$$\{A1\} = \begin{Bmatrix} AI1 \\ AJ1 \\ AK1 \end{Bmatrix} \qquad \{A2\} = \begin{Bmatrix} AI2 \\ AJ2 \\ AK2 \end{Bmatrix} \qquad \{A3\} = \begin{Bmatrix} AI3 \\ AJ3 \\ AK3 \end{Bmatrix}$$

The angular acceleration $\underline{U}$ and velocity $\underline{W}$ vectors are also replaced by the column matrices {U} and {W}:

$$\{U\} = \begin{Bmatrix} UI \\ UJ \\ UK \end{Bmatrix} \qquad \{W\} = \begin{Bmatrix} WI \\ WJ \\ WK \end{Bmatrix}$$

The cross-products, of the type $\underline{P}x\underline{U}$ and $\underline{W}x\underline{P}$, given in equation (3) are re-written by introducing the skew-symmetric matrices [W], [P1], [P2] AND [P3] defined by:

$$[W] = \begin{bmatrix} 0 & -WK & WJ \\ WK & 0 & -WI \\ -WJ & WI & 0 \end{bmatrix} \quad \text{and} \quad [P] = \begin{bmatrix} 0 & -PK & PJ \\ PK & 0 & -PI \\ -PJ & PI & 0 \end{bmatrix}$$

It may be shown that a cross-product of two vectors is equivalent to the product of the skew-symmetric matrix of the first, times the colmun matrix of the second. With these definitions and properties, equation (3) may be re-written in the following form:

$$\begin{aligned} &\{A\} - [P1]\{U\} + [W]\{\,[W]\{P1\}\,\} - \{A1\} = 0 \\ &\{A\} - [P2]\{U\} + [W]\{\,[W]\{P2\}\,\} - \{A2\} = 0 \qquad (7) \\ &\{A\} - [P3]\{U\} + [W]\{\,[W]\{P3\}\,\} - \{A3\} = 0 \end{aligned}$$

which may further be combined in a single equation:

$$\{a\} - [p]\{U\} + \{v\} = 0 \qquad (8)$$

where {a} and {v} are 9x1 column matrices, and [p] is a 9x3 matrix, defined as follows:

$$\{a\}=\begin{Bmatrix}\{A\}\\\{A\}\\\{A\}\end{Bmatrix} \quad [p]=\begin{bmatrix}[P1]\\[P2]\\[P3]\end{bmatrix} \quad \text{and} \quad \{v\}=\begin{Bmatrix}[W]\{[W]\{P1\}\}-\{A1\}\\[W]\{[W]\{P2\}\}-\{A2\}\\[W]\{[W]\{P3\}\}-\{A3\}\end{Bmatrix}$$

Equation (8) is a set of nine scalar simultaneous equations in six unknowns. The redundancy may be eliminated by realizing that, because of the experimental errors inevitably present in the nine acceleration measurements, the left-hand side of this equation is never exactly zero, but rather a small error 9x1 matrix {e}:

$$\{a\} - [p]\{U\} + \{v\} = \{e\} \qquad (9)$$

In order to minimize the measurement-induced errors, consider the sum of squares of these errors, given by the quadratic form $\{e\}'[c]\{e\}$, where $\{e\}'$ is the transpose of {e}, and [c] is the matrix of co-variances. It may be assumed that the errors are independant and have equal variances; then, the matrix [c] may be replaced by the unit matrix, and the quadratic form in question becomes $\{e\}'\{e\}$.

This square error will have a minimum when its partial derivatives with respect to the six unknowns are zero; i. e., when

$$d(\{e\}'\{e\})/d\{U\} = 0 \qquad (10)$$

$$d(\{e\}'\{e\})/d\{A\} = 0 \qquad (11)$$

where "d" denotes a partial differential operator. It turns out that it is not necessary to expand equation (11), since the same equations resulting from the expansion are obtained directly by another approach, as will be shown later.

Equation (10) may be expanded as

$$(d\{e\}'/d\{U\})\{e\} + \{e\}'(d\{e\}/d\{U\}) = 0$$

which may be shown to be equivalent to

$$2(d\{e\}'/d\{U\})\{e\} = 0 \qquad (12)$$

Using the prime (') to indicate the transpose of a matrix, the partial derivative of $\{e\}'$ with respect to {U} becomes:

$$d(\{a\} - [p]\{U\} + \{v\})' / d\{U\} = -[p]' \qquad (13)$$

which can be substituted in equation (12):

$$-[p]'(\{a\} - [p]\{U\} + \{v\}) = \emptyset$$

or the final form

$$-[p]'\{a\} + [p]'[p]\{U\} - [p]'\{v\} = \emptyset \qquad (14)$$

This final form involves {A} and {U} as unknowns. It is possible to follow a similar procedure by differentiating with respect to {A} to obtain another set of equations; however, the procedure is greatly simplified if the reference point Q0 is selected to be the centroid of Q1, Q2 and Q3. One such simplification is that the unknown acccelearation vector {A} is directly obtained from

$$\{A\} = (\{A1\} + \{A2\} + \{A3\}) / 3 \qquad (15)$$

Another simplification is that the first term of equation (14) drops out leaving only three unknowns:

$$[p]'[p] \{U\} - [p]' \{v\} = \emptyset \qquad (16)$$

which may be solved for {U} by pre-multiplying it by the inverse of the {U} factor, resulting in

$$\{U\} = [[p]'[p]] [p]' \{v\} \qquad (17)$$

This equation is a set of three simultaneous differential equations in which the unknowns are the angular velocity components WI, WJ and WK and their derivatives the acceleration components UI, UJ and UK. All other terms in this equation are either constant or known from accelerometer measurements. The solution may be obtained by numerical integration and the resulting angular accelerations and velocities are the best estimates, in the least-squares sense, of the true solution.

Angular Motion

Once the angular acceleration and velocity vectors are computed, the next phase is to define the orientation in inertial (laboratory) reference frame of the rigid body. This may be done by determining three Euler angles as functions of time. These angles define a direction cosines matrix which describes the rotation of the anatomical frame ($\underline{i},\underline{j},\underline{k}$) relative to an initial orientation coinciding with the laboratory frame ($\underline{I},\underline{J},\underline{K}$):

$$\{ \underline{i}\ \underline{j}\ \underline{k} \} = [E]\ \{ \underline{I}\ \underline{J}\ \underline{K} \} \qquad (18)$$

The three Euler angles are defined as follows: The first rotation is a yaw (PSI) about the initial $\underline{K}$-axis, resulting in an intermediate frame. The second rotation is a pitch (THETA) about the new $\underline{J}$-axis, resulting in yet another new frame. The last rotation is a roll (PHI) of this last frame about its $\underline{I}$-axis. This results in the final $(\underline{i},\underline{j},\underline{k})$ frame. To define the matrix [E], let

S1 = sin(PSI) S2 = sin(THETA) S3 = sin(PHI)

C1 = cos(PSI) C2 = cos(THETA) C3 = cos(PHI)

and let "*" denote a scalar multiplication; then,

$$[E] = \begin{bmatrix} C1*S2 & S1*C2 & -S2 \\ C1*S2*S3-S1*C3 & S1*S2*S3+C1*C3 & C2*S3 \\ C1*S2*C3+S1*S3 & S1*S2*C3-C1*S3 & C2*C3 \end{bmatrix} \qquad (19)$$

In order to solve for the three Euler angles, consider their time-derivatives, denoted by W1, W2 and W3. It may be shown that the angular velocity vector $\underline{W}$, obtained from the solution of equation (17), is the sum of three angular rate vectors which have magnitudes of W1, W2 and W3, and which may or may not be orthogonal:

$$\underline{W} = \underline{W1} + \underline{W2} + \underline{W3} \qquad (20)$$

Equation (20) may be projected on the three moving anatomical axes $(\underline{i},\underline{j},\underline{k})$ so that the anatomical components WI, WJ, and WK are written as sums of contributions from W1, W2 and W3:

$$\begin{Bmatrix} WI \\ WJ \\ WK \end{Bmatrix} = \begin{bmatrix} -S2 & 0 & 1 \\ C2*S3 & C3 & 0 \\ C2*C3 & -S3 & 0 \end{bmatrix} \begin{Bmatrix} W1 \\ W2 \\ W3 \end{Bmatrix} \qquad (21)$$

The unknowns in this equation are the Euler angles, represented by their sines and cosines, and their rates W1, W2 and W3, while the anatomical components WI, WJ and WK of the angular velocity are known. Solving for the unknowns yield the following differential equation:

$$\begin{Bmatrix} W1 \\ W2 \\ W3 \end{Bmatrix} = (1/C2) \begin{bmatrix} 0 & S3 & C3 \\ 0 & C3 & -S3 \\ 1 & S2*S3 & S2*C3 \end{bmatrix} \begin{Bmatrix} WI \\ WJ \\ WK \end{Bmatrix} \qquad (22)$$

Equation (22) may be numerically integrated to yield the three Euler angles and their rates. Note that no solution exists when C2=0, i.e., when the pitch THETA is exactly 90 degrees. This case, known as the "Gimbal lock," may be avoided by either switching to another set of Euler angles, or by a numerical algorithm which "jumps" over this critical value.

By solving for the Euler angles, the three rotational degrees of freedom are completely specified.

Translational Motion

The next and final phase of 3-D motion analysis is to determine the translational acceleration, velocity and position vectors of an arbitrary point on the R.B. with respect to the inertial laboratory ($\underline{I},\underline{J},\underline{K}$) reference frame. The first step is to determine the laboratory components XDD, YDD and ZDD of the acceleration vector of body-point B, then integrate them once to obtain the velocity components XD, YD and ZD, which may be integrated again to obtain the laboratory coordinates X, Y and Z of the desired body-point B.

Consider an arbitrary point B on the rigid body whose coordinates with respect to the moving anatomical frame are contant and known:

$$\underline{PB} = PBI\ \underline{i} + PBJ\ \underline{j} + PBK\ \underline{k} \qquad (23)$$

Given the angular accelration $\underline{U}$ of the R.B., its angular velocity $\underline{W}$, and the acceleration $\underline{A}$ of the reference point Q0 (taken as origin,) all expressed in the anatomical frame, the absolute acceleration of point B is given by:

$$\underline{AB} = \underline{A} + \underline{U}x\underline{PB} + \underline{W}x\underline{W}x\underline{PB} \qquad (24)$$

When this equation is expanded, the components ABI, ABJ and ABK of the acceleration $\underline{AB}$, along the anatomical frame, are determined, so that

$$\underline{AB} = ABI\ \underline{i} + ABJ\ \underline{j} + ABK\ \underline{k} \qquad (25)$$

This same vector may be written in terms of the laboratory ($\underline{I},\underline{J},\underline{K}$) reference frame as

$$\underline{AB} = XDD\ \underline{I} + YDD\ \underline{J} + ZDD\ \underline{K} \qquad (26)$$

where XDD, YDD and ZDD are to be determined. To compute these unknowns, recall that, since the Euler angles have been determined, the transformation matrix [E] given by equation (19) is completely determined; thus, the unit vectors $\underline{i}$, $\underline{j}$ and $\underline{k}$ may be expressed in terms of the $\underline{I}$, $\underline{J}$ and $\underline{K}$ vectors, using equation (18). Substituting these expressions in equation (25) yields

$$\begin{Bmatrix} XDD \\ YDD \\ ZDD \end{Bmatrix} = \{\ ABI\ ABJ\ ABK\ \}\ [E] \qquad (27)$$

Once the time histories of XDD, YDD and ZDD have been calculated, the absolute velocities XD, YD and ZD may be obtained by simple integrations. Finally, these are in turn integrated to give the laboratory coordinates X, Y and Z of the body-point B in question.

With this, the three translational degrees of freedom of the rigid body are completely specified.

Input Requirements

The 3-D analysis presented in the previous sections is carried out at HSRI by the computer program "NINACC" which calls several subroutines to perform the various phases of the analysis. The current version of "NINACC" is interactive with the user who can control the progress of the analysis from a computer terminal.

Input to the program is prepared ahead of run time and stored on disk and digital tape files. At run time, the program prompts the user to specify the locations of the various input data, and after reading it, asks for verification and/or modification. The input data may be divided according to the method and source of preparation into three groups.

GROUP 1: The first group of data is required to transform the acceleration data from the instrumentation reference frame to the anatomical one. It consists of the 9-element orthogonal transformation matrix, the anatomical coordinates of the origin of the instrumentation frame, the locations of the three triaxial accelerometers centers in the instrumentation frame, and the anatomical coordinates of an arbitrary body-point whose translational motion is to be studied.

GROUP 2: This group consists of 4 sets (3 components each) of the initial values of the anatomical angular velocity, the inertial (laboratory-referred) Euler angles, the inertial translational velocity of the body-point of interest, and the corresponding position.

GROUP 3: This group is the time-histories of 9 accelerometers readings. These are originally analog transducer outputs which have been converted to digital signals. It is necessary to ensure that the analog-to-digital conversion process and the filtering of the signals (analog and digital) do not introduce any phase shift between one signal and the others.

The first two groups are usually obtained from high-speed movies and x-ray films. The methods used must produce three-dimensional orthogonal components of velocities and positions. Such methods have been developped at HSRI and their applications have produced satisfactory results.

Programming Considerations

The 3-D analysis program "NINACC" calls special subroutines to perform the various phases of input, computations, and output. These subroutines are listed below, along with brief descriptions of the functions they perform.

1. NINACC — Controls the calling sequence.

2. X9RCON — Reads the two groups of constants described in the pervious section.

3. X9RACC — Reads the digitized signals of 9 accelerometers.

4. X9PREP — Transforms all data into the anatomical frame; prepares the constant matrix of equation (17); computes the acceleration of the reference point Q0, given by equation (15); outputs the raw 9 acceleration readings.

5. C91000 — Calls "SXHPCG" to integrate the angular accelerations given by equation (17), which calls at each time step "C9FCT" to compute the right-hand side of the equation, integrates one time step, then returns the integrated values to "C91OUT" to record them; outputs the time-histories of angular motion when integration is completed.

6. X92000 — Calls "SHPCG" to integrate the Euler rates, given by equation (22), which in turn calls "C92FCT" and "C92OUT"; outputs the Euler rates and angles when integration is completed.

7. X93000 — Selects a body-point with user's help; calculates the anatomical accelerations of that point; calculates the inertial components using equation (27); calculates the Gadd Severity Index (GSI) and the Head Injury Criterion (HIC) numbers; outputs the results of calculations; and repeats this procedure for another body-point.

8. X94000 — Integrates the inertial accelerations of the last body-point selected above, using "SXHPCG", "X94FCV" and "X94OUV"; integrates the resulting velocities using "SXHPCG", "9X4FCP" and "9X4OUP"; outputs the translational velocities and positions.

The numerical integration routine "SXHPCG" called above is a modified version of the IBM routine "HPCG". The modifications were necessary to force output at specified and equal intervals of time, and to simplify the list of input arguments. The numerical method used for integeration is best decribed by quoting from the "HPCG" description, given in the IBM System/360 Scientific Subroutine Package, Version III, publication number GH 20-0205-4:

> "These subroutines use Hamming's modified predictor-corrector method for the solution of general initial-value problems. ...to obtain an approximate solution of a general system of first-order ordinary differential equations with given initial values. It is a stable fourth-order integration procedure that requires the evaluation of the right-hand side of the system only two times per step. This is a great advantage compared to other methods of the same order of accuracy, especially the Runge-Kutta method, which requires the evaluation of the right-hand side four times per step. Another advantage is that at each step the calculation procedure gives an estimate for the local truncation error; thus, the procedure is able, without significant amount of calculation time, to chose and change the step size h. On the other hand, Hamming's predictor-corrector method is not self-starting; that is, the functional values at a single previous point are not enough to get the functional values ahead. Therefore, to obtain the starting values, a special Runge-Kutta procedure followed by one iteration step is added to the predictor-corrector method."

Except for the SSP routine "HPCG," all subroutines were developped at HSRI and coded in Fortran-IV to be run on MTS, the Michigan Terminal System. Therefore, many input/output subroutines are system-dependant and are designed to process data generated at HSRI and make use of MTS support routines; However, the final output is saved on unlabeled magnetic tape in card image (EBCDIC characters,) and may be read and post-processed at any computer installation.

Validation: Hypothetical Motion

The 3-D motion measurement method, described in the previous sections, may be validated by comparing the calculated motion against what is known to be the true one. The procedure is to generate nine acceleration readings resulting from a precisely known motion, and "feed" them to the analysis program "NINACC" which will predict the 3-D

motion. It is difficult to generate a precisely known general 3-D motion in the laboratory; however, it is simpler to simulate such a motion where all 6 degrees of freedom are variable functions of time. These may be prescribed by closed-form mathematical functions, which are at least twice-differentiable.

This section describes a validation procedure in which a hypothetical motion is imposed on a hypothetical rigid body, by specifying closed-form functions for the 3 rotations and 3 translations. The 3-D analysis is performed in reverse order to generate exact time-histories of various quantities that the "NINACC" will generate. Knowing the exact motion, the readings of nine hypothetical accelerometers are simulated by computing the acceleration vectors at their centers. These "readings" are then used as input to "NINACC" analysis program to compute the motion, which is finally compared to the exact one.

The mathematical function selected to describe each of the six degrees of freedom has the general form:

$$S(t) = S_m \left[\sin 2\pi f_1 t - \sin 2\pi f_2 t \right]$$

where f_1 and f_2 are frequencies (Hertz) of the two sinusoidal components, and S_m is the amplitude (inches or radians) of either component. This form is continuous, and has a continuous first time-derivative (velocity) given by

$$\dot{S}(t) = 2\pi S_m \left[f_1 \cos 2\pi f_1 t - f_2 \cos 2\pi f_2 t \right]$$

This velocity is also continuous, and has an acceleration which is zero at t=0, given by

$$\ddot{S}(t) = -4\pi^2 S_m \left[f_1^2 \sin 2\pi f_1 t - f_2^2 \sin 2\pi f_2 t \right]$$

To simulate a general 3-D motion, 6 amplitudes and 12 frequencies must be specified. The simulation presented in this validation is based on the values given in table 1, which completely specify the rigid body motion. To generate the 9 acceleration readings, the distances R1, R2 and R3 of the triaxial centers to the origin were given as 3.0, 4.0 and 5.0 inches, respectively. Finally, a sampling rate of 1600. Hertz was specified to generate tabular time-histories of these signals. This rate must be at least twice the highest frequency contained in the digitized signals.

	TRANSLATIONS			ROTATIONS		
	X	Y	Z	YAW	PITCH	ROLL
Amplitude:	25.	7.	20.	20.	15.	25.
1st Freq.:	2.0	1.0	4.0	12.	7.0	8.0
2nd Freq.:	3.5	5.0	2.5	4.0	13.	0.5

Table 1. Amplitudes (Inches or Degrees) and Frequencies (Hertz) of the Six Degrees of Freedom of the Simulated 3-D Motion.

Once the positions, velocities and accelerations of the 3 translations and 3 rotations have been specified, as in table 1, the various time-histories are computed and saved in appropriate files for later comparisons. Thus, the translational positions and velocities of the origin, in the inertial (laboratory) frame, are saved as shown in figure 2. Given the Euler angles and the inertial translational accelerations of the origin, its anatomical components may be computed, and both types are saved in one file, which is plotted in figure 3. The Euler angles and their rates, shown in figure 4, are saved in a third file. These are used to compute the angular velocities and accelerations which are also saved and plotted in figure 5. Finally, given the complete description of motion, and the distances R1, R2 and R3, the "readings" of the 9 accelerometers are computed, and are shown in figure 6.

Given the 9 accelerometer "readings" and their locations and orientations on the rigid body, the "NINACC" program was called to perform the 3-D motion analysis. The program then produced 4 output files containing the various groups of variables describing the 3-D motion. These files were plotted and compared to the exact time-histories described in the previous paragraph. The various plots were so similar that it was not possible to distinguish graphically between the exact and calculated ones. Therefore, plots of the calculated motion are not shown here. Instead, the differences between calculated and exact motions were calculated point-by-point and plotted in figures 7, 8, 9 and 10.

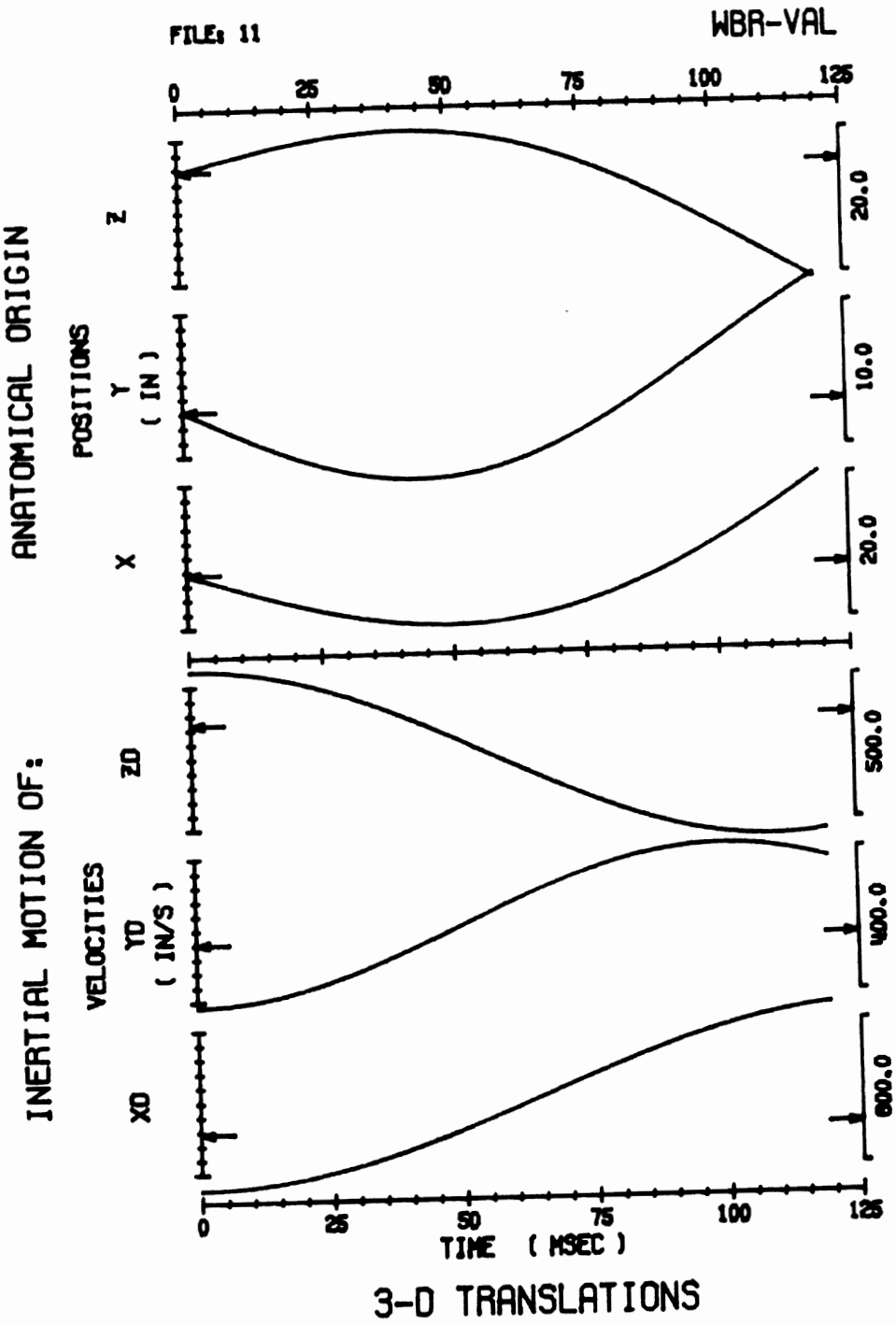

FIGURE 2. TRANSLATIONAL POSITIONS AND VELOCITIES OF THE ORIGIN OF THE SIMULATED 3-D MOTION.

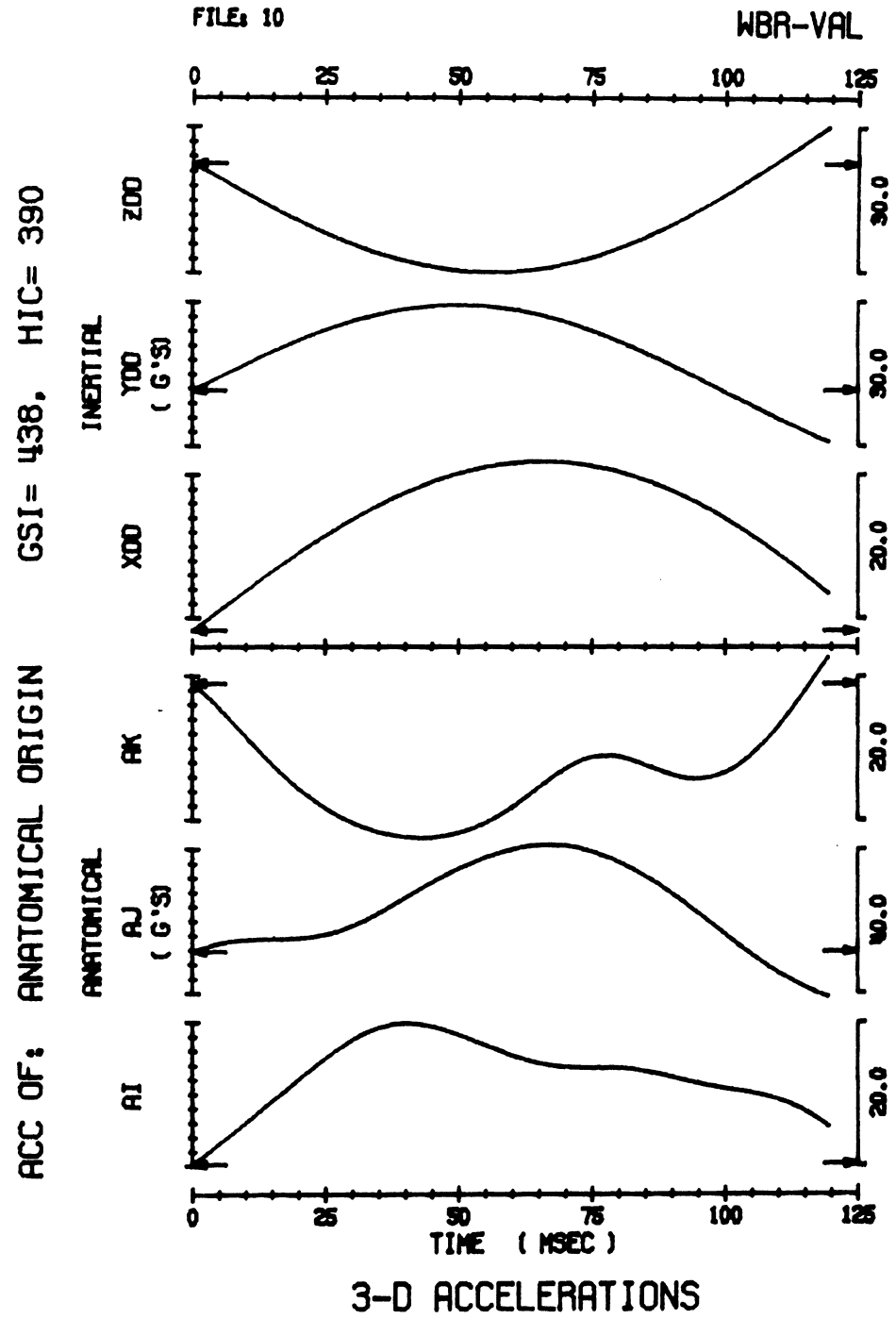

FIGURE 3. HYPOTHETICAL TRANSLATIONAL ACCELERATIONS OF ORIGIN IN INERTIAL(FIXED) AND ANATOMICAL(MOVING) FRAMES.

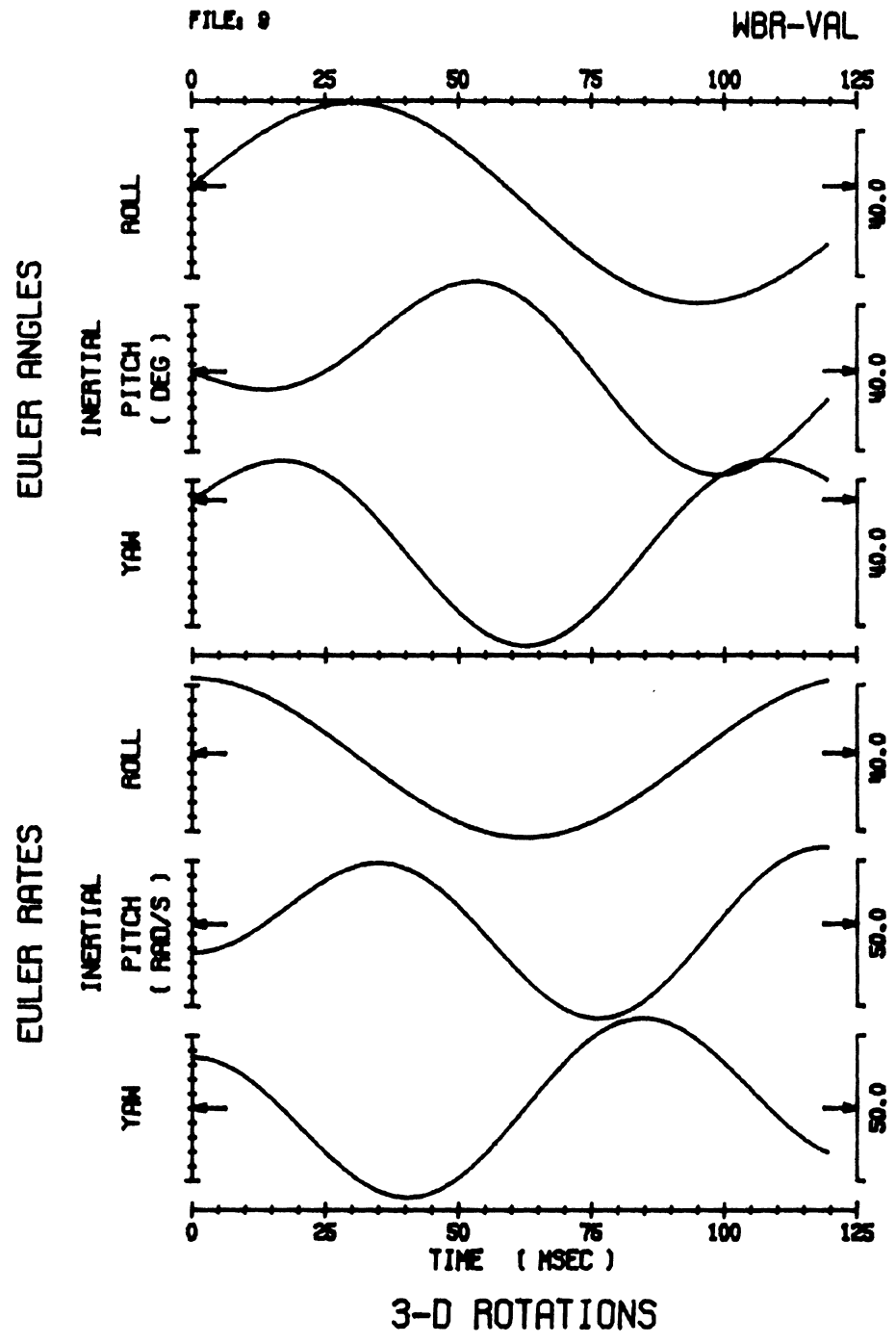

FIGURE 4. EULER ANGLES AND THEIR RATES FOR THE HYPOTHETICAL 3-D MOTION, GIVEN IN INERTIAL FRAME.

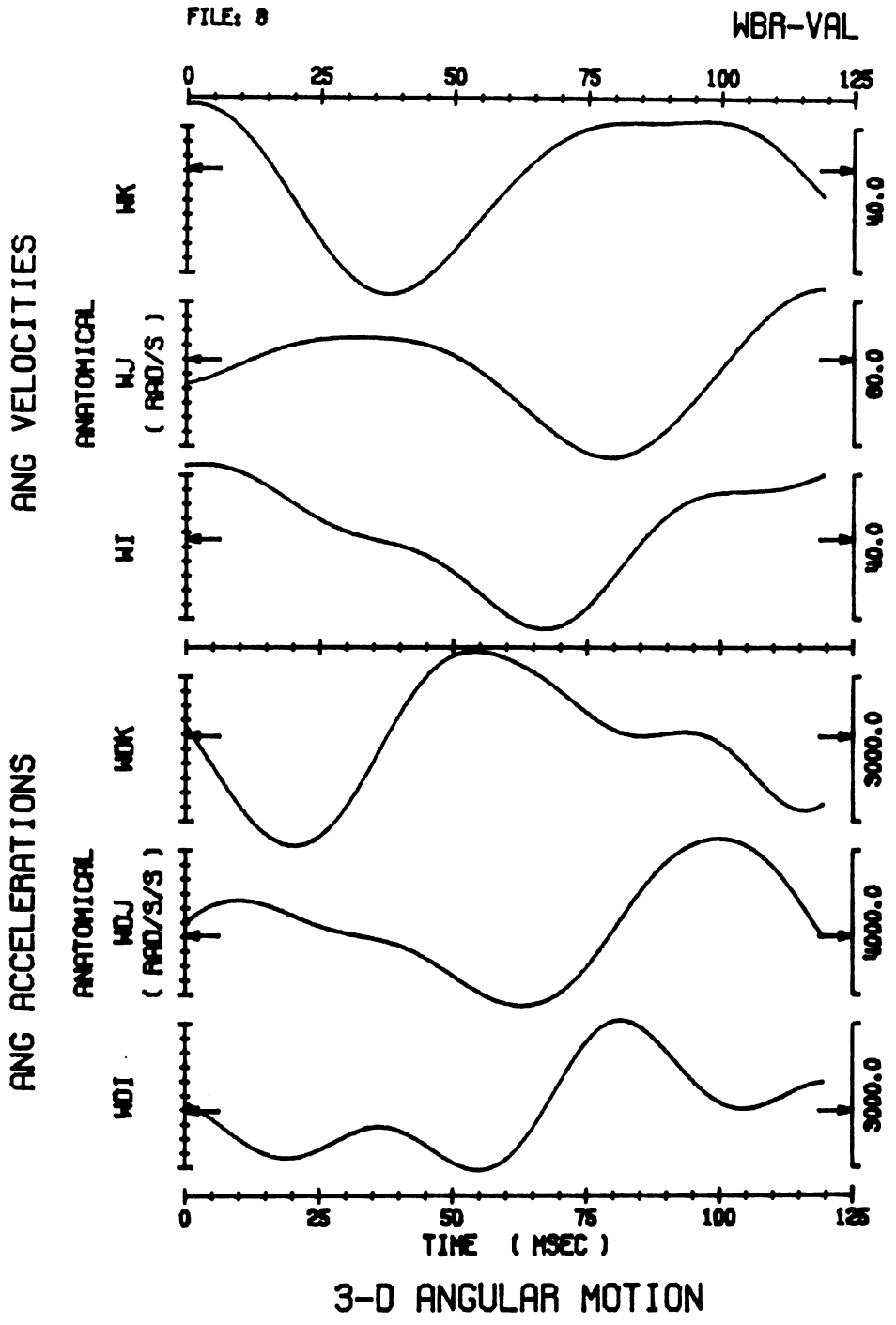

FIGURE 5. HYPOTHETICAL ANGULAR VELOCITIES AND ACCELERATIONS, ALONG THE MOVING ANATOMICAL FRAME.

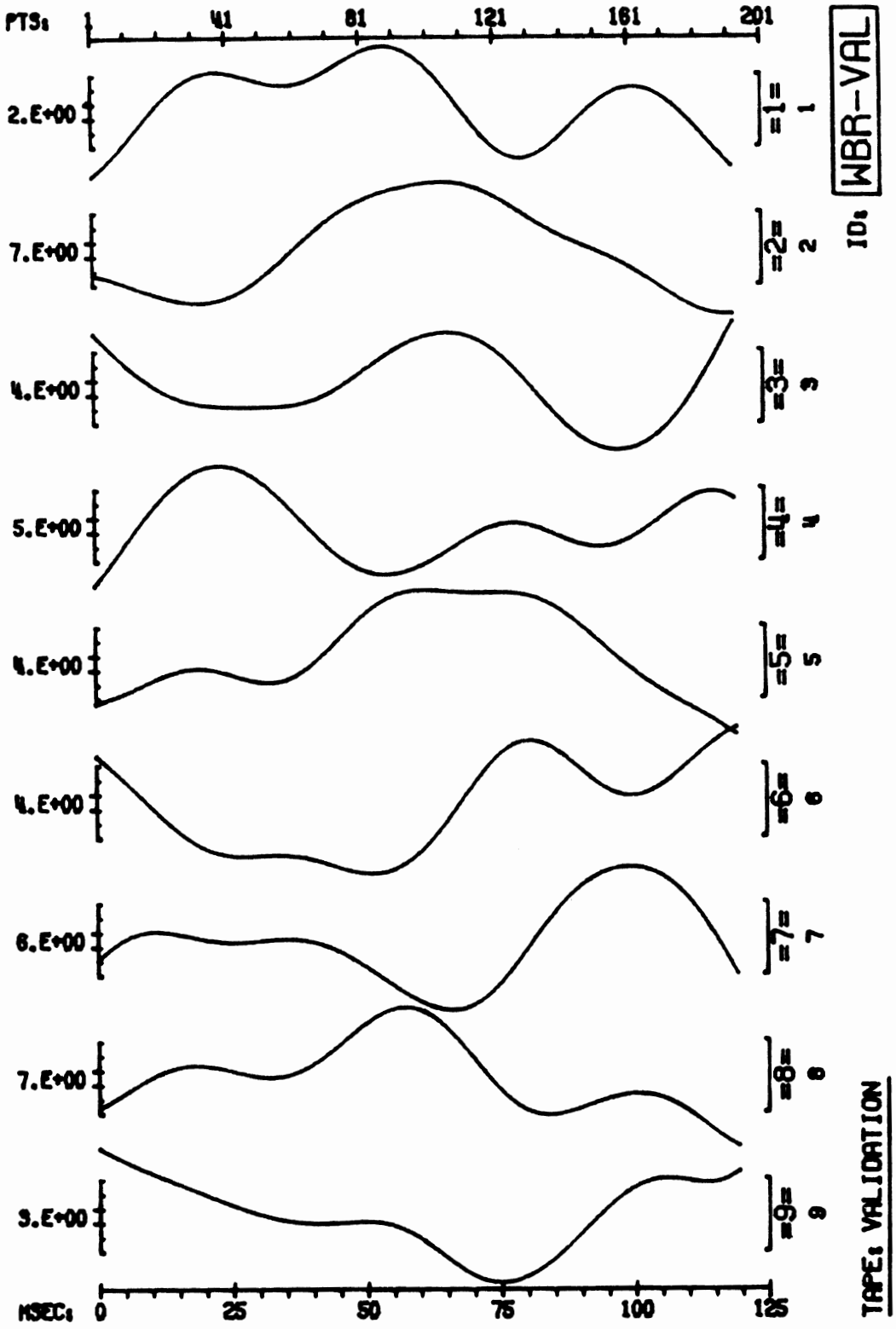

FIGURE 6. SIMULATED READINGS OF NINE ACCELEROMETERS USED AS INPUT TO "NINACC" TO COMPUTE THE 3-D MOTION.

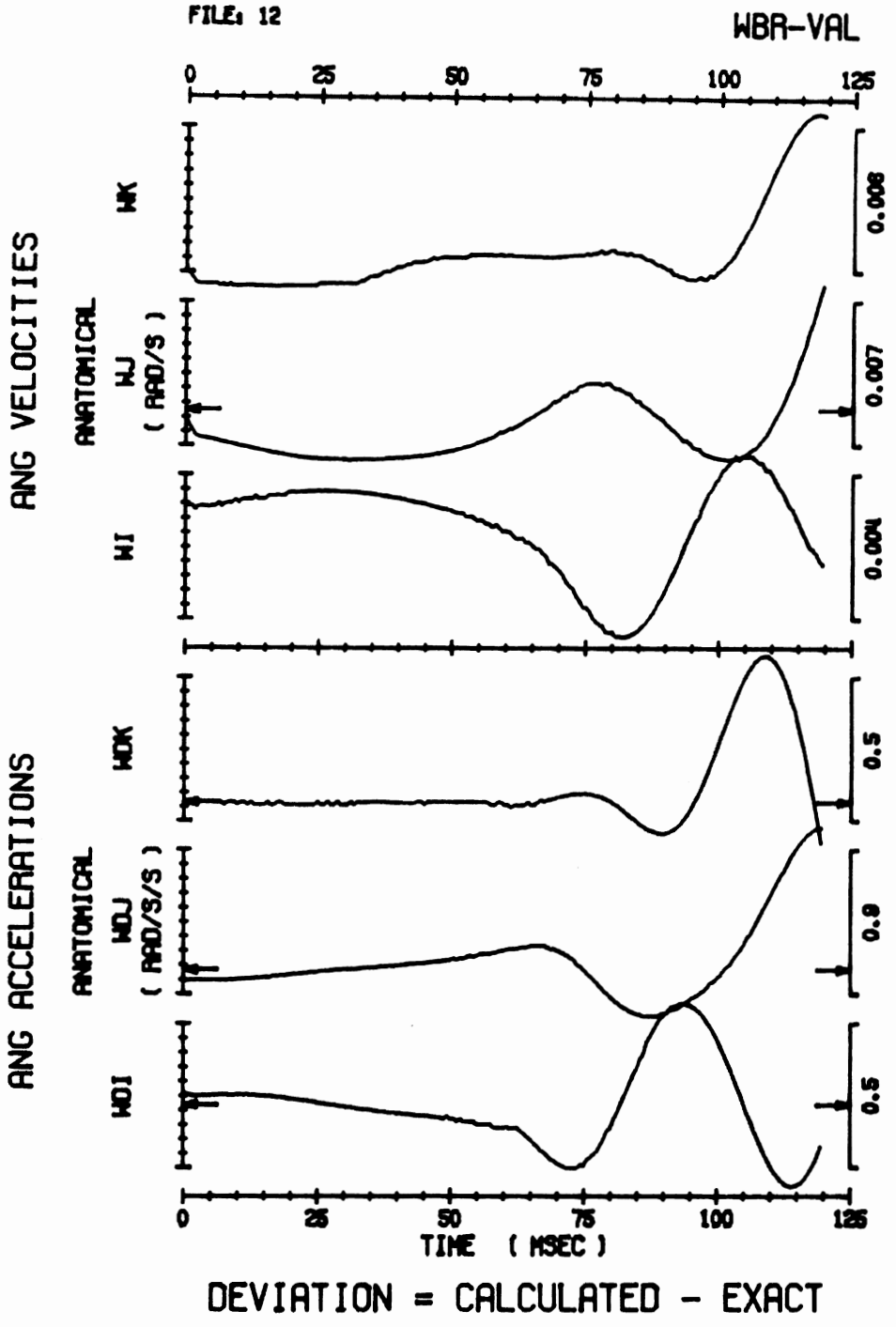

FIGURE 7. DEVIATIONS OF "NINACC" OUTPUT FROM THE EXACT MOTION GIVEN IN FIGURE 5.

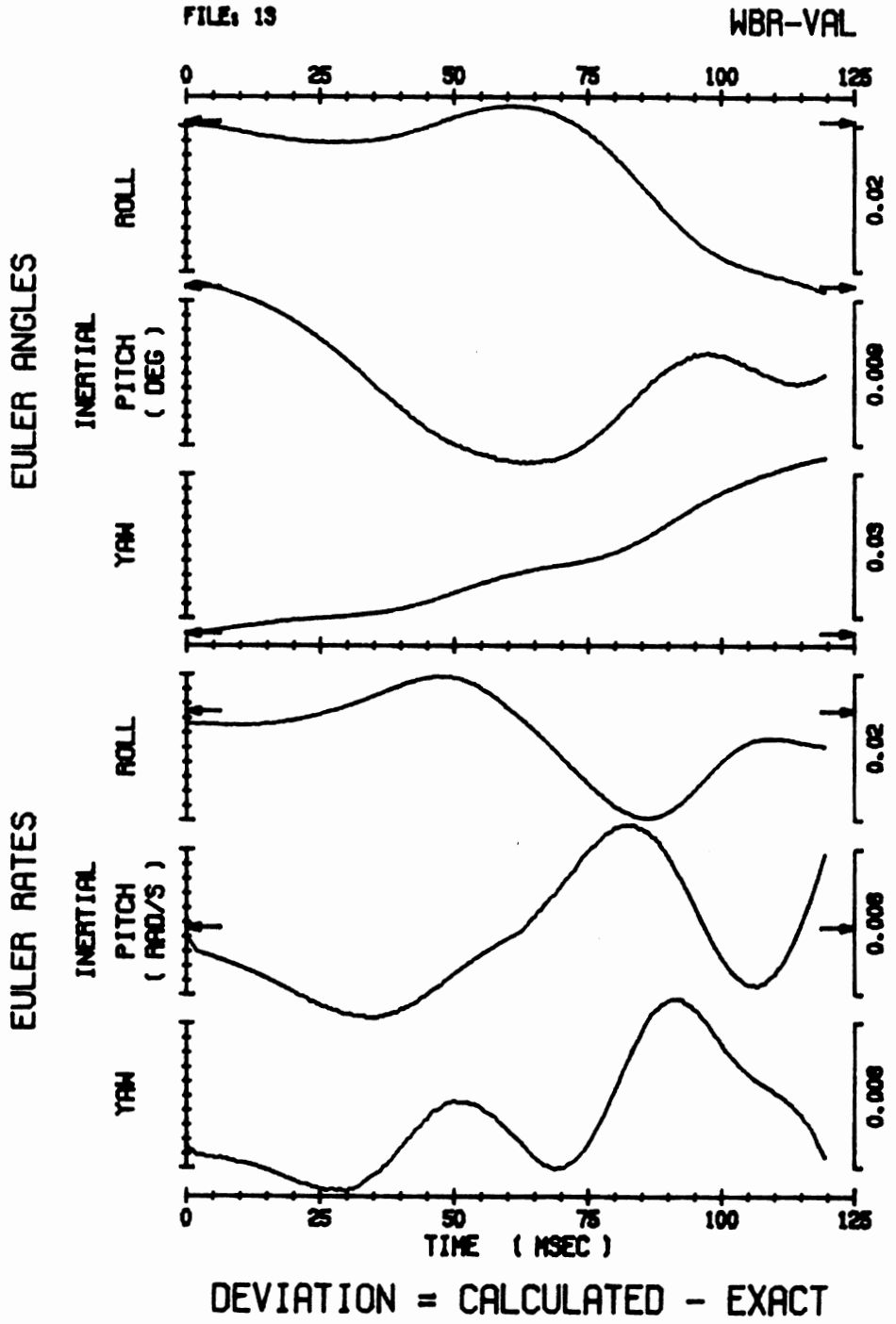

FIGURE 8. DEVIATIONS OF "NINACC" OUTPUT FROM THE EXACT MOTION GIVEN IN FIGURE 4.

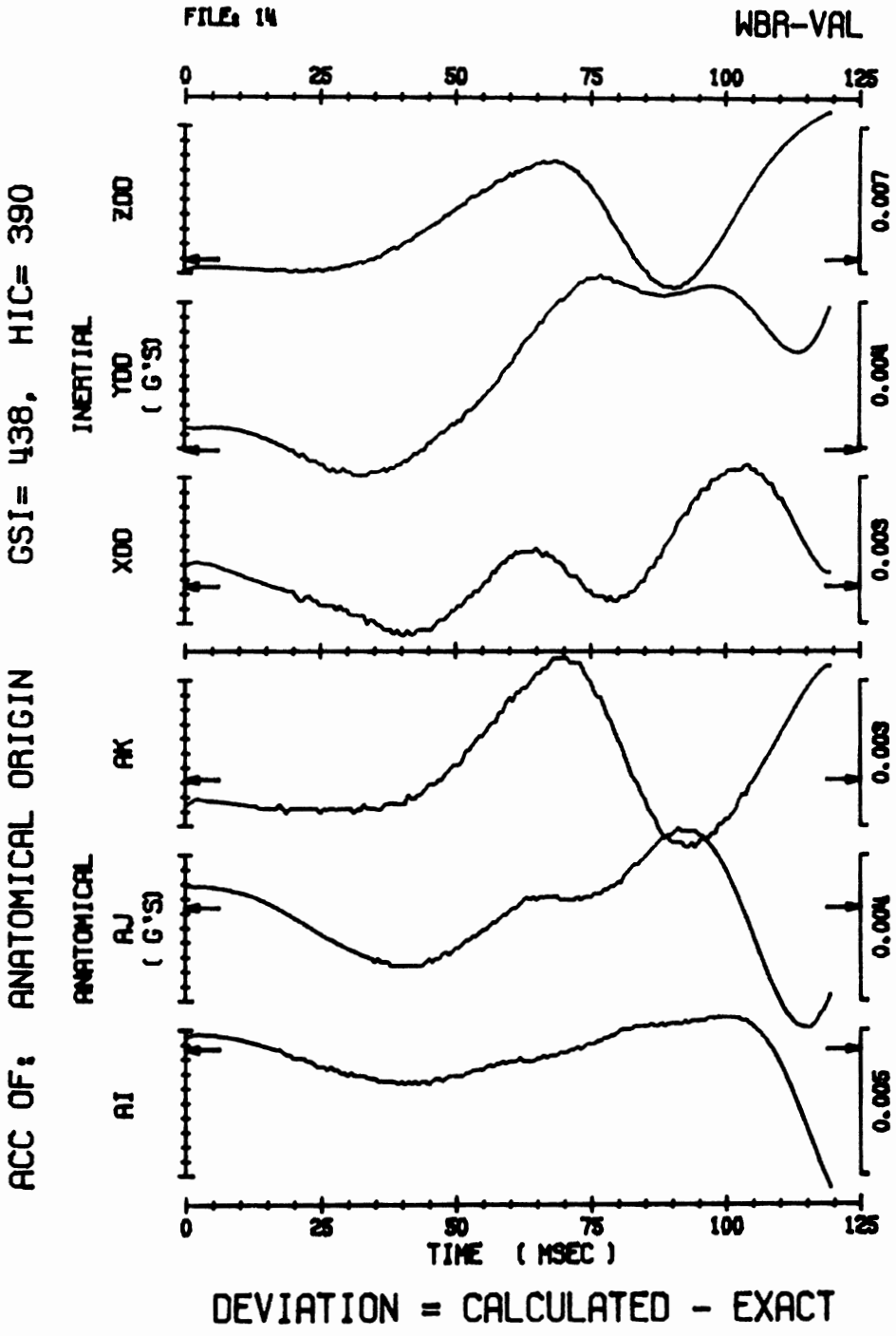

FIGURE 9. DEVIATIONS OF "NINACC" OUTPUT FROM THE EXACT MOTION GIVEN IN FIGURE 3.

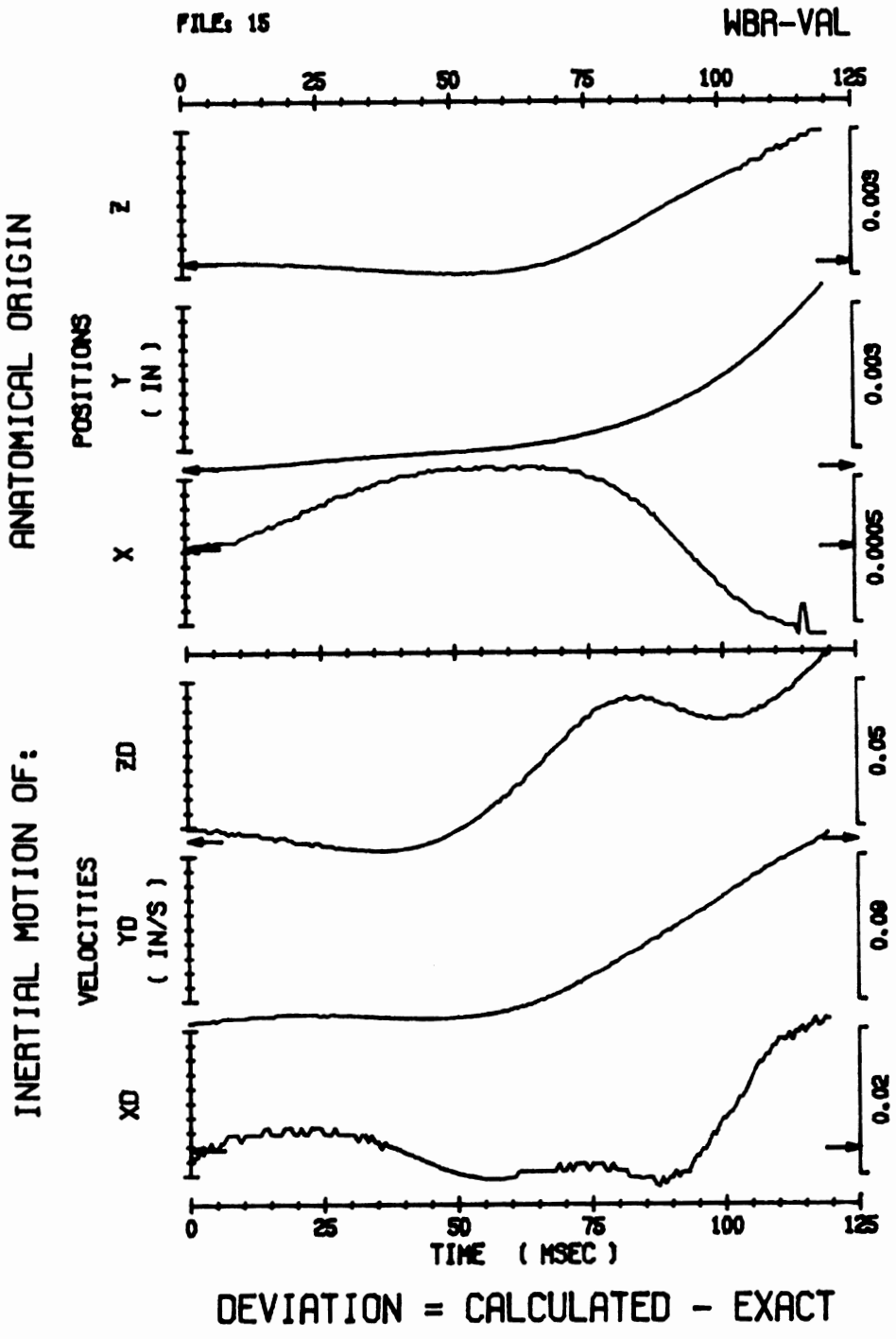

FIGURE 10. DEVIATIONS OF "NINACC" OUTPUT FROM THE EXACT MOTION GIVEN IN FIGURE 2.

The above hypothetical example represents a 3-D motion with magnitudes of the same order as those encountered in a typical non-impact head motion. In this example, the deviations of the angular accelerations were of the order of 2. rad/s over magnitudes of the order of 3000. rad/s. The ratio of these two numbers may be used as a quantitative measure of the relative accuracy of the analysis, which is of the order of 0.07% for the angular accelerations. Similarly, the orders of accuracy are 0.10% for angular velocities, 0.08% for Euler angles, 0.07% for translational accelerations, 0.10% for velocities, and finally, 0.10% for displacements.

Such accuracies are not typical of engineering measurements because no experimental errors were involved in generating the acceleration readings. The above-descibed deviations result solely from two source: truncation errors due to the finite length of a computer word, and the approximation (round-off) errors in the numerical integration procedure. These are negligeable when compared to the experimental errors associated with actual measurements in real experimental situations.

Validation: Experimental Motion

In order to produce a precisely known, yet general, 3-D rigid body motion in a laboratory, elaborate mechanisms must be constructed to vary simultaneously the six degrees of freedom in a controlled fashion. For validation purposes, it is much simpler to let an instrumented rigid body undergo an unknown general motion and measure the acceleration vector at an arbitrary body-point using a triaxial accelerometer; then, using the 9-accelerometer package, predict the acceleration vector at the same point and in the same moving directions.

Such an experiment was included in a full Whole Body Response sled run, test number 77B001, which was conducted to measure the 3-D motion af an embalmed cadaver head. In addition to the 9-accelerometer package, the head was instrumented with a triaxial accelerometer which was mounted inside the head at the base of the skull, and the brain was substituted by a jelly-like substance. The location and orientation of the triax relative to the head anatomical reference frame were determined using the HSRI 3-D x-ray

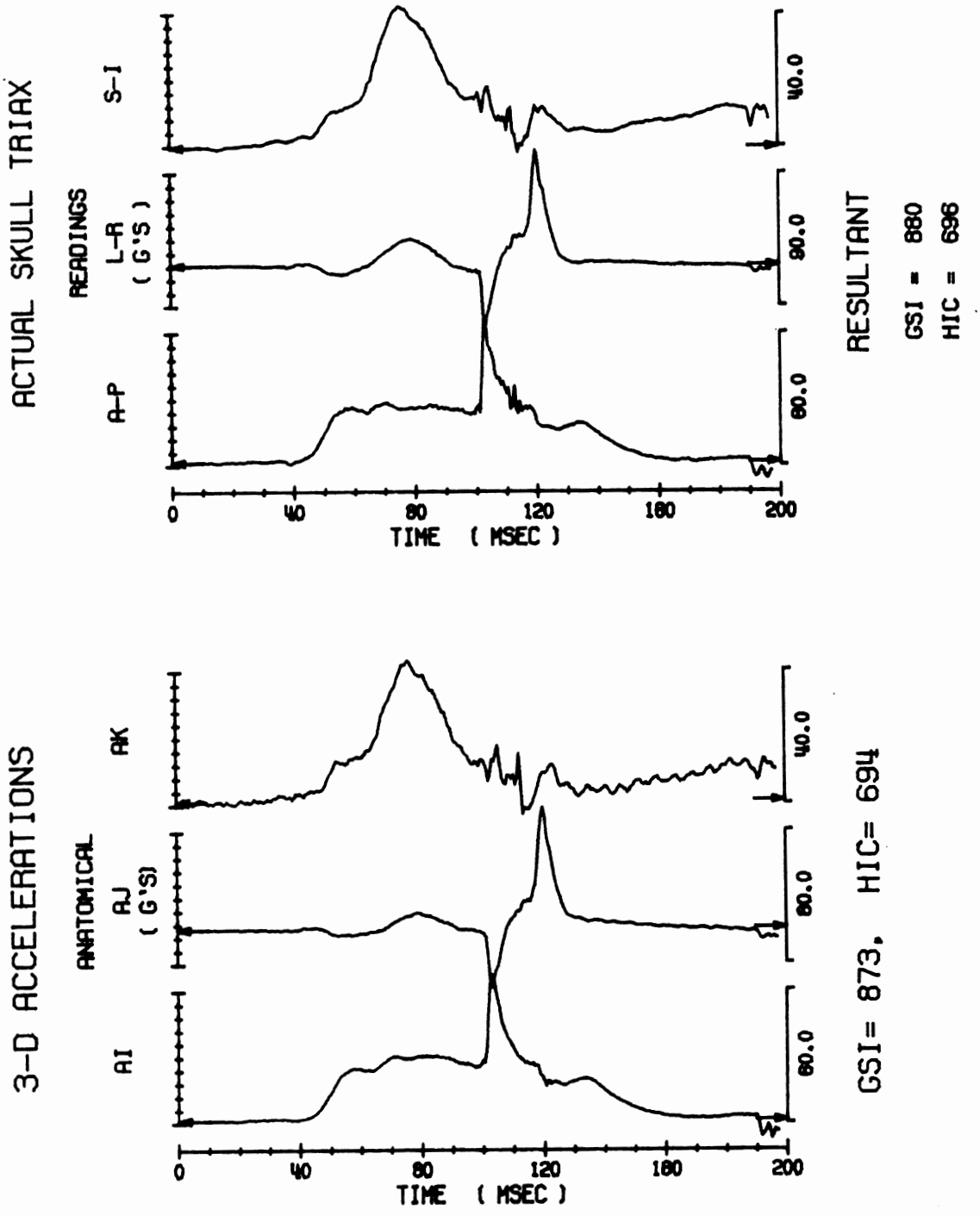

FIGURE 11. ACCELERATIONS AT THE BASE OF THE SKULL, TEST 77B001. TOP 3 CURVES ARE MEASURED DIRECTLY. BOTTOM ONES ARE COMPUTED BY "NINACC."

technique, described elsewhere in this Appendix. After the test was conducted, the 12 transducer signals were digitized and the "NINACC" program was run to predict the acceleration components along the sensitive axes of the triax, and at its center.

These accelerations are shown in figure 11. The top three curves are directly measured with the triaxial accelerometer; the bottom three are indirectly computed by "NINACC" using the 9 acceleration signals. The agreement between the two sets of curves is striking; however, the deviations between the actual and computed ones are significantly larger than those obtained in the hypothetical example of the previous section. Quantitative evaluation of these deviations may be best summarized by computing the HIC and GSI of both resultants. The HIC numbers were 696 for the actual resultant, and 694 for the calculated one. The GSI's were 880 and 873 for the actual and calculated resultants, respectively.

These deviations may be attributed to the errors commited during mounting, x-ray analyses, transducer calibrations and other phases of signal processing. Therefore, is may be concluded that the accuracy of the 3-D motion analysis method is limited by the transducers themselves and the expermimental techniques used to generate the required input to "NINACC."

Limitations Of The Method

An in-depth investigation of the accuracy of this and other 3-D motion measurement methods is underway at HSRI. Some of the influencing factors are discussed briefly in this section. The accuracy of any analysis based on experimental measurements depends mainly on the errors commited during the instrumentation of the experiment. These errors may be divided into 4 major groups, according to their sources and types.

TYPE 1 MISALIGNMENT & MISLOCATION. These errors are due largely to the mechanical mounting of the accelerometers and to the 3-D methods for measuring their locations and orientations, relative to the anatomical frame. Another source of this type of errors is the physical seperation between the seismic masses of the 3 uniaxial elements, which are used to approximate a single triaxial accele-

rometer. A third source is the manufacturing process where the alignment is usually not quaranteed to be better than within Ø.5 degrees. Finally, the cross-axis sensitivity of the sensing element, an inherent property, result in errors which may be shown to be equivalent to misalignment arrors.

TYPE 2 MIS-CALIBRATION. Most calibration procedures cannot guarantee perfect accuracies in converting volts into physical units. Errors could be made at any point in the measurement chain which includes transducers, signal conditionners, tape recording and playback amplifiers, A-to-D converting unit, and the analog and digital filtering processes.

TYPE 3 NOISE. The transducers' signals contain high frequency components which do not result from rigid body motion per se. These could be internal to the signal processing equipments, such as amplifier noise and cross-talk between channels, or external from mechanical vibrations of the mounts at some of their resonnant frequencies. Most of this noise can be filtered out; however, the lower harmonics and other lower frequencies may be at or below the actual motion's frequencies. In this case, the noise cannot be filtered out without altering the real signal; thus, the noise-to-signal ratio becomes an important factor in the accurate measurement of 3-D motion. If these noise-related errors are random-like in nature, then their effects on the accuracy is minimized by the least-squares method presented earlier.

TYPE 4 ZERO-BIAS. This type of errors result from misadjustment of the equipment during calibration, testing, recording, playback and A/D conversion processes. Although this type of error can be delt with by forcing the pre-test portion of the digitized signal to zero, and adjusting the remaining portion accordingly, the problem is not completely solved since a drift in on amplifier can cause an unknown and variable zero shift. Furthermore, an exact 3-D analysis must take into account the acceleration of gravity, which is neglected when all signals are zero-adjusted. This may be tolerated if the motion being measured

produces accelerations which are much higher than that of gravity. Otherwise, the initial orientation of each accelerometer, relative to the gravity field, must be known in order to correct for gravity.

It is difficult to point out one source of error that is most damaging to the accuracy of 3-D motion analysis; however, it is safe to state that experimental errors are inevitable, and to conclude that one can only attempt to minimize their effects, first in the laboratory by careful instrumentaion, then during analysis by using a least-squares technique.

Summary

By proper measurements of 9 linear accelerometers embedded in the moving rogid body, the six degrees of freedom of 3-D motion may be completely determined, at the acceleration, velocity and displacement levels. The equations of motion are derived by minimizing the error of measurement, in the least-squares sense. The accuracy of computed motion is limited by the accuracy of the experimental measurements, and the signal processing techniques used to prepare the input to the analysis program.

BIBLIOGRAPHY

1. J. A. Bartz and F. E. Butler, "Three-Dimensional Computer Simulation of a Motor Vehicle Crash Victim, Phase 2 - Validation Study of the Model." Calspan Technical Report No. VJ-2978-V-2, 1972, pp. B-340 - B-343.

FAST ALGORITHM FOR COMPUTING "HIC"

G. L. Holstein & N. M. Alem

Background

The current Federal Motor Vehicle Safety Standard 208 (FMVSS 208) requires that the Head Injury Criterion (HIC) be used to evaluate the severity of impact to the head of a passenger in an automobile crash [1]. The HIC is a weighted impulse criterion which requires the knowledge of the resultant translational acceleration of the head's center of gravity as a function of time. Because of the complexity of its definition [5], the HIC is best obtained with the aid of a digital computer.

Even with the speed of digital computers, numerical evaluation of the HIC is a lengthy and costly proposition, if approached in a straightforward manner. However, a clever use of HIC properties reduces computation time. Some of these properties were explored by Chou and Nyquist [3] for half-sine, triangular, trapezoidal and square acceleration pulses.

The objectives of this presentation are to further explore these properties, introduce new ones, offer formal proofs to all these properties, and then finally, use them to outline a fast and efficient algorithm for computing the HIC of a given resultant acceleration pulse.

Introduction

Prior to the use of HIC as required in FMVSS 208, the severity of impact to the head was determined by the Gadd Severity Index (GSI). For a given resultant acceleration

profile of duration T, the GSI is defined by

$$GSI = \int_0^T A(t)^{2.5}\,dt \tag{1}$$

where Ø and T are the beginning and end of the acceleration pulse in seconds, and A(t) is the pulse itself given in standard g units.

The definition of HIC for the same A(t) is somewhat similar to that of the GSI. For any two time instants u and v in the interval [Ø,T] such that

$$0 \leq u < v \leq T \tag{2}$$

let H(u,v) be a function defined by

$$H(u,v) = \left[\frac{\int_u^v A(t)\,dt}{(v-u)}\right]^{2.5}(v-u) \tag{3}$$

HIC is then defined as the maximum value of H(u,v) over its domain of definition (2), i.e. the maximum of H(u,v) calculated for all possible (u,v) combinations, subject to the constraint (2). That is

$$HIC = \max H(u,v)\ ;\ 0 \leq u < v \leq T \tag{4}$$

The HIC, then, is a function of the acceleration pulse A(t), and may alternately be written as HIC(A). To facilitate the writing of subsequent mathematical expressions, other functions and notations are introduced. Thus, let S(t) be the "severity function" defined by

$$S(t) = \int_0^t [A(x)]^{2.5}\,dx \tag{5}$$

so that the GSI of A(t) is simply the value of S(t) for t=T; i.e.

FAST ALGORITHM FOR COMPUTING "HIC"

$$GSI = S(T) \tag{6}$$

Also, let V(t) be the "velocity function" defined by

$$V(t) = \int_0^t A(x)\, dx \tag{7}$$

so that the function H(u,v) may be written simply as

$$H(u,v) = \left[\frac{V(v) - V(u)}{(v-u)}\right]^{2.5} (v-u) \tag{8}$$

If the acceleration A(t) were given as a continuous analog signal, it would be impossible, in general, to compute HIC(A) since H(u,v) must be computed for an infinite number of (u,v) combinations. In practice, however, A(t) is given as a finite collection of N samples, defined for N discrete time instants, $\emptyset = t1 < t2 < \ldots < tN = T$, usually equally spaced over the [Ø,T] interval. The actual HIC of the continuous signal may then be approximated by

$$HIC_N(A) = \max_{1 \le j < k \le N} H(t_j, t_k) \tag{9}$$

which approaches the true HIC as N approaches infinity. A straightforward computation of $HIC_N(A)$ requires N(N-1)/2 evaluations of H(u,v) with an equal number of comparisons of the resulting values. It is possible to reduce computation time, while retaining the accuracy of approximation, by taking advantage of the mathematical properties of the HIC expression. These properties are developed below.

PROPERTIES OF THE HIC

It is assumed in the following sections that the function A(t) is a nonnegative continuous function of time on the interval [Ø,T]. The functions H(u,v), S(t), and V(t) are then defined from A(t) as above. Three fundamental properties are presented below. The first one has already been discussed in [3], but is included here for the sake of completeness.

Property I: A(t) And Limits Of Integration

If H(u,v) achieves its maximum value at the time pair (u*,v*), where u* is greater than zero and v* is less than T, then A(t) has the same value at u* as at v*. Furthermore, this common value is precisely 3/5 of the average value of A(t) over the interval [u*,v*]. That is

$$A(u^*) = A(v^*) = \frac{3}{5}\left[\frac{V(v^*) - V(u^*)}{(v^* - u^*)}\right] \qquad (10)$$

This property, derived in reference [3], has two important consequences which are derived below as corollaries.

COROLLARY 1. The common value of A(t) at the times u* and v* must be less than or equal to 3/5 of the global maximum, AMAX, of A(t). That is

$$A(u^*) = A(v^*) \leq \frac{3}{5}\,AMAX \qquad (11)$$

The inequality may be derived by applying the Mean Value Theorem which assures us that there exists a point t* in the closed interval [u*,v*] such that A(t*) is equal to the average of A(t) over this interval. But clearly, A(t*) must be less than or equal to AMAX, the global maximum of A(t). Combining these two facts with (10) yields the desired corollary.

COROLLARY 2. Let D be any upper bound for v*-u* and B be any nonnegative lower bound for HIC(A). Then the common value of A(t) at u* and v* must be greater than or equal to 3/5 of the ratio B/D raised to the 2/5 power. That is

$$A(u^*) = A(v^*) \geq \frac{3}{5}\left[\frac{B}{D}\right]^{\frac{2}{5}} \qquad (12)$$

From the assumption $0 \leq B \leq HIC(A)$, we have

$$0 \leq B \leq \frac{\left[V(v^*) - V(u^*)\right]^{5/2}}{(v^* - u^*)^{3/2}}$$

By raising both sides to the 2/5 power, and by isolating the expression representing the average of A(t) over [u*,v*], we obtain

$$\left[\frac{B}{v^* - u^*}\right]^{2/5} \leq \frac{V(v^*) - V(u^*)}{v^* - u^*}$$

which may be combined with equation (10) to yield

$$A(u^*) = A(v^*) \geq \frac{3}{5}\left[\frac{B}{v^* - u^*}\right]^{\frac{2}{5}}$$

But since D≥v*-u*, the above inequality reduces to the second corollary given in (12).

PROPERTY II: Upper Bound Of HIC

> If A(t) is restricted to any sub-interval [t1,t2] of its domain [0,T], the HIC of A(t) for this sub-interval, denoted by HIC(A,t1,t2), must be less than or equal to the function $A(t)^{2.5}$ integrated over the sub-interval. Furthermore HIC(A,t1,t2) can equal the later integral if and only if A(t) is constant in value over the sub-interval [t1,t2]. That is
>
> $$HIC(A,t1,t2) \leq S(t2) - S(t1) \qquad (13)$$
>
> with equality if and only if A(t) is constant over [t1,t2].

Since A(t) restricted to the sub-interval [t1,t2] remains a continuous nonnegative function, it will clearly be sufficient to establish this property in the special case where [t1,t2] coincides with [0,T]. The proof is based upon Holder's Inequality [4] which states that given numbers p

and q such that $p>1$ and $1/p + 1/q = 1$, together with functions E and F defined on an interval [a,b] such that $|E|^p$ and $|F|^q$ have finite Lebesgue integrals over [a,b], then

$$\left| \int_a^b E(t)F(t)\,dt \right| \leq \left[\int_a^b |E(t)|^p dt \right]^{\frac{1}{p}} \cdot \left[\int_a^b |F(t)|^q dt \right]^{\frac{1}{q}} \qquad (14)$$

with equality if and only if $|E|^p / |F|^q$ is constant almost everywhere in [a,b].

To apply Holder's Inequality, fix two points u and v such that $0 \leq u < v \leq T$, and let

$p=5/2$, $q=5/3$, $a=u$, $b=v$
$E(t)=A(t)$ for all t in [u,v]
$F(t)=(v-u)^{-3/5}$ for all t in [u,v]

Then substitute these expressions into (14) to obtain

$$\left| \int_u^v A(t)(v-u)^{-\frac{2}{5}} dt \right| \leq \left[\int_u^v |A(t)|^{\frac{5}{2}} dt \right]^{\frac{2}{5}} \cdot \left[\int_u^v (v-u)^{-1} dt \right]^{\frac{3}{5}} \qquad (15)$$

with equality if and only if $|A(t)|$ is constant almost everywhere in [u,v].

By observing that $\int_u^v (v-u)^{-1} dt = 1$

and recalling that A(t) is a nonnegative function, and using the previously defined functions V(t) and S(t), inequality (15) may be restated as

$$\frac{V(v) - V(u)}{(v-u)^{3/5}} \leq \left[S(v) - S(u) \right]^{2/5} \qquad (16)$$

Both sides of (16) may be raised to the 5/2 power to obtain

$$\left[\frac{V(v)-V(u)}{v-u}\right]^{\frac{5}{2}}(v-u) \leq S(v)-S(u) \qquad (17)$$

Since A(t) is continuous and nonnegative over [u,v], and since it is well known that two continuous functions which are equal almost everywhere on an interval are in fact identical, it is easily seen that |A(t)| is constant almost everywhere in [u,v] if and only if A(t) is constant in [u,v].

Thus with the function H(u,v) as defined in (3), and for an arbitrary pair (u,v) such that $0<u<v<T$ we have

$$H(u,v) \leq S(v)-S(u) \qquad (18)$$

with equality if and only if A(t) is constant over the sub-interval [u,v].

But, since A(t) is nonnegative, we have $S(v)-S(u)\leq S(T)$ for any $0\leq u<v\leq T$. Therefore, from (18), the HIC of A(t) over [0,T], which is precisely the maximum of H(u,v), is subject to

$$HIC(A) \leq S(T) \qquad (19)$$

It is clear that equality holds in (19) if the function A(t) is constant in value over [0,T]. Conversely, if the equality were to hold, then it may be concluded that A(t) must be constant over the interval [0,T]. That is if

$$HIC(A) = S(T) \qquad (20)$$

then A(t) must be constant over the interval [0,T]. To prove this converse, let u* and v* be a pair in the domain of definition for H(u,v) such that

$$H(u^*,v^*) = HIC(A) \tag{21}$$

Combining (20) and (21) gives

$$H(u^*,v^*) = S(T) \tag{22}$$

But, since $S(v^*)-S(u^*) \leqslant S(T)$, we have from equation (22)

$$H(u^*,v^*) \geqslant S(v^*)-S(u^*) \tag{23}$$

which may be combined with (18) to give

$$H(u^*,v^*) = S(v^*)-S(u^*) \tag{24}$$

and A(t) is constant over the sub-interval [u*,v*].

This equation may be combined with (22) resulting in

$$S(v^*)-S(u^*) = S(T) \tag{25}$$

Since $0 \leqslant u^* < v^* \leqslant T$, there are two possible cases that must be delt with. The first case is when u*=0 and v*=T, in which case it may be seen from (24) that A(t) is constant over [0,T]. The second case is when u*>0 or v*<T; then, equation (25) forces the continuous and nonnegative A(t) to be zero outside the [u*,v*] interval. Therefore, A(t) must also be zero inside this interval, since it is continuous over all of [0,T] and constant over the subinterval [u*,v*]. It may therefore be concluded that in either case, A(t) must be constant over the entire [0,T] interval, if the GSI and the HIC are to be equal.

PROPERTY III: Resolution Of HIC

Since the A(t) is given as a digital signal consisting of N points, usually sampled at equal intervals of time, it is conceivable that the actual HIC occurs for time instants which fall between the sampling times. The question arises then as to the possible difference between the true HIC and the approximation obtained at discrete time points for which A(t) is given.

Specifically, if H(u,v) is evaluated at two arbitrary points, (u1,v1) and (u2,v2), in its upper triangular domain, then how does the magnitude of H(u1,v1)-H(u2,v2) relate to the distance in the plane between the two points (u1,v1) and (u2,v2). The following property deals with this question.

> The absolute difference between the value of H(u,v) at one point in its domain and another cannot be greater than $3/\sqrt{2}$ times AMAX, the global maximum of A(t) over [0,T], raised to the 2.5 power times the distance in the plane between the two points. That is, given any two points (u1,v1) and (u2,v2) in the domain of H(u,v), then

$$\left| H(u_1,v_1) - H(u_2,v_2) \right| \leq \frac{3}{\sqrt{2}} AMAX^{2.5} \left\| (u_1-u_2 \, , \, v_1-v_2) \right\| \qquad (26)$$

> where $\| \; \|$ is the 2-norm function, e.g. $\|(x,y)\| = \sqrt{x^2+y^2}$.

To prove this property, notice first that H(u,v) has continuous first partial derivatives given by

$$\left.\frac{\partial H}{\partial u}\right|_{(u,v)} = -2.5\left[\frac{V(v)-V(u)}{v-u}\right]^{1.5} A(u) + 1.5\left[\frac{V(v)-V(u)}{v-u}\right]^{2.5} \qquad (27)$$

and

$$\left.\frac{\partial H}{\partial v}\right|_{(u,v)} = 2.5\left[\frac{V(v)-V(u)}{v-u}\right]^{1.5} A(v) - 1.5\left[\frac{V(v)-V(u)}{v-u}\right]^{2.5} \qquad (28)$$

Let (u1,v1) and (u2,v2) be any two points in the triangular domain of definition of H(u,v). Then, applying the Mean

Value Theorem for functions of several variables [2], we know that there exists a point (u0,v0) on the line segment determined by (u1,v1) and (u2,v2) such that

$$H(u_1,v_1) - H(u_2,v_2) = \left.\frac{\partial H}{\partial u}\right|_{(u_0,v_0)} (u_1-u_2) + \left.\frac{\partial H}{\partial v}\right|_{(u_0,v_0)} (v_1-v_2) \quad (29)$$

The Cauchy Inequality [2] may then be applied to equation (29) to yield

$$\left|H(u_1,v_1)-H(u_2,v_2)\right| \leq \left\|\left(\left.\frac{\partial H}{\partial u}\right|_{u_0,v_0}, \left.\frac{\partial H}{\partial v}\right|_{u_0,v_0}\right)\right\| \cdot \left\|(u_1-u_2,\ v_1-v_2)\right\| \quad (30)$$

The right-hand side of (30) consists of two terms, both of which are "norms" or "distances". To conclude the proof, the norm of the partial derivative pair will be shown to be no greater than $3/\sqrt{2}$ $AMAX^{2.5}$. In fact it will be shown that for any pair (u,v) in the domain of H(u,v) we have

$$\left\|\left(\left.\frac{\partial H}{\partial u}\right|_{(u,v)}, \left.\frac{\partial H}{\partial v}\right|_{(u,v)}\right)\right\| \leq \frac{3}{\sqrt{2}} AMAX^{2.5} \quad (31)$$

Fixing u and v such that $0 \leq u < v \leq T$, we know by the Mean Value Theorem that there exists a t0 in the closed interval [u,v] such that

$$\frac{V(v)-V(u)}{v-u} = A(t0)$$

Then (27) and (28) may be rewritten as

$$\left.\frac{\partial H}{\partial u}\right|_{(u,v)} = -2.5\left[A(t0)\right]^{1.5} A(u) + 1.5\left[A(t0)\right]^{2.5} \quad (32)$$

$$\left.\frac{\partial H}{\partial v}\right|_{(u,v)} = 2.5\left[A(t0)\right]^{1.5} A(v) - 1.5\left[A(t0)\right]^{2.5} \quad (33)$$

But since A(t) is nonnegative, it is clear from (32) that

$$\left.\frac{\partial H}{\partial u}\right|_{(u,v)} \leq 1.5\ AMAX^{2.5} \tag{34}$$

Now define an auxiliary function Y(x), for $x \geq 0$, as

$$Y(x) = -2.5\, x^{1.5} AMAX + 1.5\, x^{2.5} \tag{35}$$

It is clear that

$$Y(A(to)) \leq -2.5\,[A(to)]^{1.5} A(u) + 1.5\,[A(to)]^{2.5} \tag{36}$$

By solving $Y'(x)=0$, we obtain for $x \geq 0$ the following inequality:

$$-AMAX^{2.5} \leq Y(x) \tag{37}$$

which may be combined with (32) and (36) to yield:

$$-AMAX^{2.5} \leq \left.\frac{\partial H}{\partial u}\right|_{(u,v)} \tag{38}$$

and combining this with (34) yields:

$$\left| \left.\frac{\partial H}{\partial u}\right|_{(u,v)} \right| \leq 1.5\ AMAX^{2.5} \tag{39}$$

A similar argument may be applied to the partial derivative of H(u,v) with respect to v to show that it is bounded by the same upper limit:

$$\left| \left.\frac{\partial H}{\partial v}\right|_{(u,v)} \right| \leq 1.5\ AMAX^{2.5} \tag{40}$$

Combining inequalities (39) and (40) we establish the truth of (31), and consequently Property III is proven.

As a result of this property, the HIC of A(t) may be

approached from below as closely as desired by increasing the digital sampling frequency. Thus if $0=t1<t2<\ldots<tN=T$ is an equi-spaced partition of the interval $[0,T]$ of step size d, and $HIC_N(A)$ is defined as in (9), then

$$HIC(A) - HIC_N(A) \leq \frac{3}{\sqrt{2}} AMAX^{2.5} d \qquad (41)$$

Outline Of Algorithm

Given the resultant acceleration pulse A(t) as a set of N points sampled at equal intervals of time, the overall strategy in computing the HIC of A(t) is to calculate a crude lower estimate, and then judiciously refine this estimate.

PHASE 1 of the algorithm serves to compute the velocity V(t) and severity S(t) functions, as defined respectively by equations (7) and (5), for all N points. Immediately, the GSI of the pulse is available as the value of S(t) at the last point. The global maximum of A(t), AMAX, is also computed during this phase of the algorithm.

PHASE 2 serves to obtain a crude low estimate of the HIC. This is done by reducing the number of points which define the pulse. It was found that a full search for the maximum of H(u,v) can be tolerated, if the total number of points in the A(t) is not larger than 21 samples. The number of combinations of (u,v) pairs is then 21(21-1)/2 or approximately 200 pairs. In practice, however, the number of samples which define the acceleration pulse is more likely to be about 300 points, which corresponds to a total of 300(300-1)/2 or about 45000 (u,v) pairs. Therefore, the crude estimate of HIC is obtained by selecting 21 points of A(t), equally spaced over the pulse duration, then computing the H(u,v) for all combinations to search for the maximum. This maximum is compared with H(0,T), and the higher value, HMAXG, is retained as the crude low estimate of the actual HIC.

PHASE 3 of the algorithm serves to define an acceleration band in which the equality (10) could hold. It is specifically assumed that the HIC occurs at a time pair (u*,v*) such that $0<u^*<v^*<T$. With AMAX from PHASE 1,

Corollary 1 of Property I gives an upper bound, RMAX, above which (1Ø) could not possibly hold. The lower bound in this band is obtained by invoking Corollary 2 of Property I, given by (12). HMAXG, from PHASE 2, is used as the nonnegative lower bound for the HIC. Initially, T is used as the upper bound for v*-u*. The lower bound, RMIN, below which (1Ø) could not hold, is then computed. RMIN is then used to search for a subinterval [T1,T2] of [Ø,T], such that u* and v* are both contained within [T1,T2]. Invoking Corollary 2 again, T2-T1 is used as an upper bound for v*-u*, resulting in an improved estimate RMIN.

It may be shown that this lower bound, RMIN, cannot be less than 3/5 of the average value of A(t) over the entire pulse duration. The band for which equality (1Ø) can hold is illustrated in Figure 1.

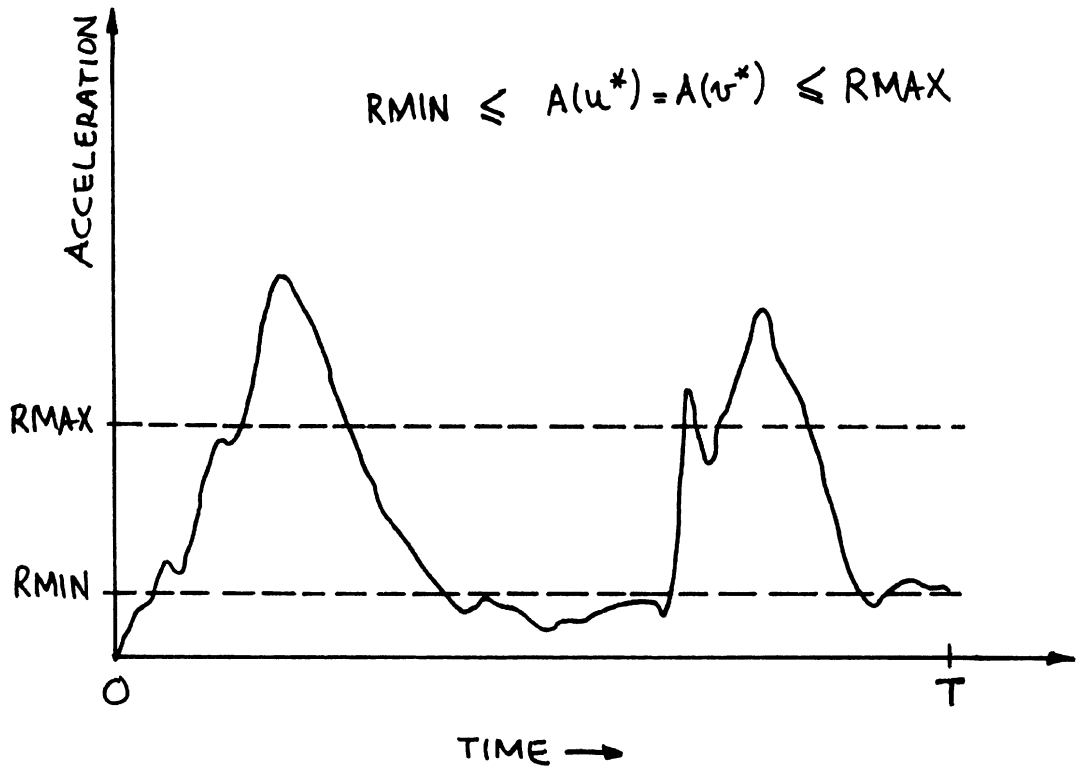

FIGURE 1. ACCELERATION BAND WHERE THE HIC WILL OCCUR.

PHASE 4 serves to determine regions in the domain of H(u,v) where refinement of the estimate HMAXG will take place. By invoking Property II, regions where H(u,v) cannot exceed HMAXG are eliminated.

The procedure is to eliminate the right portion of the pulse in which u cannot lie together with the left portion in which v cannot lie, as shown in Figure 2. First, a time instant, T1MAX, is computed such that GSI-S(T1MAX)>HMAXG and GSI-S(t)$\leqslant$HMAXG for any time t>T1MAX. Then by Property II, H(u,v)$\leqslant$GSI-S(t)$\leqslant$HMAXG for any T1MAX<t$\leqslant$u<v$\leqslant$T. It must be concluded then, that H(u,v) can be larger than HMAXG only if u is less than or equal to T1MAX. A similar argument, using a time limit T2MIN such that S(T2MIN)>HMAXG and S(t)$\leqslant$HMAXG for any t<T2MIN, will show that H(u,v) can be larger than HMAXG only if v is greater than or equal to T2MIN.

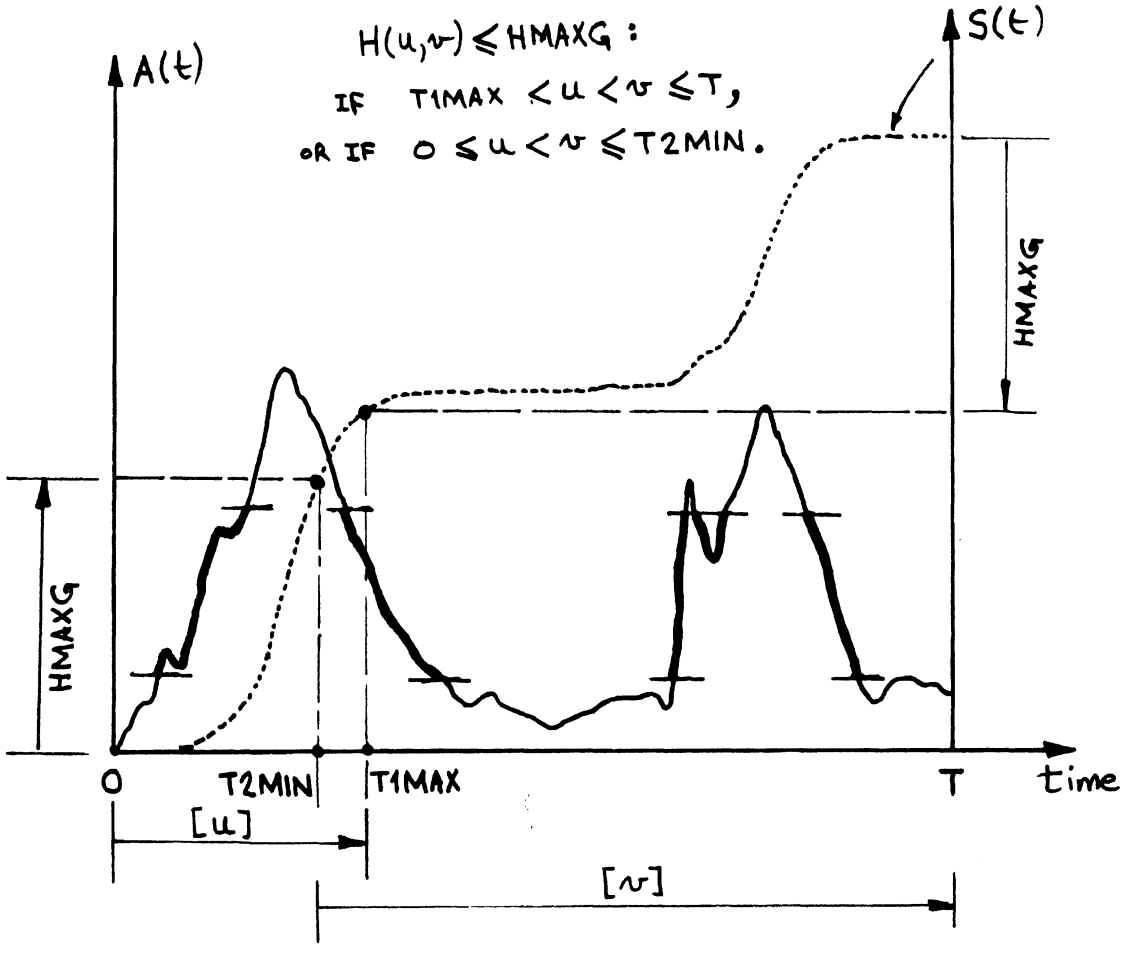

FIGURE 2. REFINEMENT REGIONS IN DOMAIN OF H(U,V).

The final "reduced" pulse consists of the regions defined in PHASE 4, restricted further by the band defined in PHASE 3. The result of these elimination procedures is a great savings in the number of necessary evaluations of the function H(u,v). The HIC is then obtained by scanning only these valid regions.

Program Listing

The following is a listing of subroutine "HICGSI" and an auxiliary partitioning subroutine "PARTN". These routines were written at HSRI in Fortran-IV and require no additional subroutines for their execution.

```
C     ---------------------------------
      SUBROUTINE HICGSI(A,N,DT,HIC,GSI)
C     ---------------------------------
C
C     INPUT:   A(I) - RESULTANT ACCELERATION (G'S)
C              N    - NUMBER OF SAMPLES
C              DT   - SAMPLING INTERVAL (SECONDS)
C     OUTPUT:  HIC  - HEAD INJURY CRITERION
C              GSI  - GADD SEVERITY INDEX
C
C
      DIMENSION A(3600),V(3600),S(3600),IX1(100),IX2(100)
C
      V(1)=0.0
      S(1)=0.0
      AMAX=A(1)
      AL=A(1)
      A25L=AL*AL*SQRT(AL)
      F=0.5*DT
      DO 10 I=2,N
      AR=A(I)
      A25R=AR*AR*SQRT(AR)
      V(I)=V(I-1)+(AL+AR)*F
      S(I)=S(I-1)+(A25L+A25R)*F
      IF(AR.GT.AMAX) AMAX=AR
      AL=AR
      A25L=A25R
   10 CONTINUE
      GSI=S(N)
C
      HMAXG=0.0
      NIP=N-1
      NIG=20
      IF(NIG.GT.NIP) NIG=NIP
      NSKP=NIP/NIG
      MNI=NSKP
      MXI=NIG*NSKP
      MNJ=1
      MXI1=MXI+1
      DO 30 I=MNI,MXI,NSKP
      MXJ=MXI1-I
```

```
      DVMAX=0.0
      DO 20 J=MNJ,MXJ,NSKP
      DV=V(I+J)-V(J)
      IF(DV.GT.DVMAX) DVMAX=DV
   20 CONTINUE
      DTG=I*DT
      AVE=DVMAX/DTG
      H=AVE*AVE*SQRT(AVE)*DTG
      IF(H.GT.HMAXG) HMAXG=H
   30 CONTINUE
      IF(NIG.EQ.NIP) GO TO 150
C
      T=NIP*DT
      AVE=V(N)/T
      H=AVE*AVE*SQRT(AVE)*T
      IF(H.GT.HMAXG) HMAXG=H
C
      RMAX=0.6*AMAX
      RMIN=0.6*(HMAXG/T)**0.4
      IT1=1
      IF(A(1).GE.RMIN) GO TO 50
      DO 40 I=2,N
      IF(A(I).LT.RMIN) GO TO 40
      IT1=I-1
      GO TO 50
   40 CONTINUE
   50 IT2=N
      IF(A(N).GE.RMIN) GO TO 70
      DO 60 I=1,NIP
      IF(A(N-I).LT.RMIN) GO TO 60
      IT2=N-I+1
      GO TO 70
   60 CONTINUE
   70 D=(IT2-IT1)*DT
      RMIN=0.6*(HMAXG/D)**0.4
C
      IT1MAX=NIP
      DELT=GSI-HMAXG
      DO 80 I=2,NIP
      IF(S(I).LT.DELT) GO TO 80
      IT1MAX=I-1
      GO TO 90
   80 CONTINUE
   90 IT2MIN=2
      DO 100 I=2,N
      IF(S(I).LE.HMAXG) GO TO 100
      IT2MIN=I
      GO TO 110
  100 CONTINUE
```

```
C
  110 CALL PARTN(A,1,IT1MAX,RMIN,RMAX,IX1,NX1,NPT1,IFL)
      IF(IFL.EQ.1.OR.NPT1.EQ.0) GO TO 150
      CALL PARTN(A,IT2MIN,N,RMIN,RMAX,IX2,NX2,NPT2,IFL)
      IF(IFL.EQ.1.OR.NPT2.EQ.0) GO TO 150
      IF(IX1(1).GE.IX2(NX2)) GO TO 150
C
      LMAX=IX2(NX2)-IX1(1)
      LMIN=1
      IF(IX1(NX1).LT.IX2(1)) LMIN=IX2(1)-IX1(NX1)
      NSKP1=1
      NSKP2=1
      IF(NPT1*NPT2.LE.500) GO TO 120
      NSKP1=NPT1/20
      NSKP2=NPT2/20
      IF(NSKP1.LT.1) NSKP1=1
      IF(NSKP2.LT.1) NSKP2=1
      MXSKP=.005/DT
      IF(MXSKP.LT.1) MXSKP=1
      IF(NSKP1.GT.MXSKP) NSKP1=MXSKP
      IF(NSKP2.GT.MXSKP) NSKP2=MXSKP
C
  120 H4MAX=HMAXG**0.4
      DO 130 I=LMIN,LMAX
      S(I)=(I*DT)**(-0.6)
  130 CONTINUE
      DO 140 I=1,NX1,2
      NB1=IX1(I)
      NE1=IX1(I+1)
      DO 140 J=NB1,NE1,NSKP1
      VJ=V(J)
      DO 140 K=1,NX2,2
      NB2=IX2(K)
      NE2=IX2(K+1)
      DO 140 L=NB2,NE2,NSKP2
      IF(J.GE.L) GO TO 140
      H4=(V(L)-VJ)*S(L-J)
      IF(H4.GT.H4MAX) H4MAX=H4
  140 CONTINUE
C
      HIC=H4MAX**2.5
      RETURN
C
  150 HIC=HMAXG
      RETURN
C
      END
```

FAST ALGORITHM FOR COMPUTING "HIC"

```
C     ------------------------------------------------
      SUBROUTINE PARTN(A,NB,NE,RMN,RMX,IX,NIX,NPT,IFL)
C     ------------------------------------------------
      DIMENSION A(3600),IX(100)
      IFL=0
      NPT=0
      NIX=0
      ISWL=0
      IF(A(NB).LE.RMN.OR.A(NB).GE.RMX) GO TO 10
      ISWL=1
      NIX=1
      IX(1)=NB
C
   10 NBP=NB+1
      DO 40 I=NBP,NE
      ISWC=0
      IF(A(I).LE.RMN) GO TO 20
      IF(A(I).GE.RMX) GO TO 20
      ISWC=1
   20 IF(ISWC.EQ.ISWL) GO TO 40
      NIX=NIX+1
      IF(NIX.LE.100) GO TO 30
      IFL=1
      RETURN
   30 IX(NIX)=I-ISWL
      IF(ISWL.EQ.1) NPT=NPT+IX(NIX)-IX(NIX-1)+1
      ISWL=ISWC
   40 CONTINUE
C
      IF(ISWL.EQ.0) RETURN
      NIX=NIX+1
      IX(NIX)=NE
      NPT=NPT+NE+1-IX(NIX-1)
      RETURN
      END
```

References

1. Department of Transportation NHTSA Docket Number 69-7, Notice 19, Occupant Crash Protection - Head Injury Criteria, S6.2 of FMVSS 208.

2. R. G. Bartle, "The Elements of Real Analysis." New York: John Wiley & Sons, 1964, pp. 61,62,230,233,239.

3. C. C. Chou and G. W. Nyquist, "Analytical Studies of the Head Injury Criterion (HIC)." SAE Automotive Engineering Congress, Detroit: 1974.

4. M. R. Spiegel, "Real Variables, Lebesgue Measure and Integration." Schaum's Outline Series, New York: McGraw-Hill, 1969, p. 115.

5. J. Versace, "A Review of the Severity Index." Ford Technical Report, No. S-71-43, Ford Motor Co., 1971.